Dissertation

Supercooled liquids and glasses: dynamics, dynamic heterogeneity, and stability

Submitted by

Hannah Staley

Department of Physics

In partial fulfillment of the requirements

For the Degree of Doctor of Philosophy

Colorado State University

Fort Collins, Colorado

Summer 2016

Doctoral Committee:

Advisor: R. Mark Bradley
Co-Advisor: Grzegorz Szamel

Martin Gelfand
David Aristoff

Abstract

Supercooled liquids and glasses: dynamics, dynamic heterogeneity, and stability

We used molecular dynamics simulations to study supercooled liquids and glasses. Supercooled liquids are liquids that have been cooled below their freezing temperature. We start the thesis with an introduction on supercooled liquids.

We studied several different model glass-formers and compared them by scaling all data to the point where the Stokes-Einstein relation was violated. The Stokes-Einstein relation holds for many liquids, but breaks down at some temperature for most supercooled liquids. In all the systems we studied, we examined dynamic heterogeneity as quantified by the dynamic susceptibility, χ_4, and the dynamic correlation length, ξ_4. When dynamics are heterogeneous, a liquid breaks up into regions of particles with correlated mobility. The susceptibility is related to the number of particles in such a region, and the dynamic correlation length is related to the size of a region. We broke up our model glass-formers into the categories of strong glass-formers and fragile glass-formers. A strong glass-former has a viscosity, which obeys the Arrhenius relationship, while a fragile glass-former has super-Arrhenius behavior. We compared the systems by relating them at the temperature where the Stokes-Einstein relation was violated. We found that when variables are rescaled to their values at the Stokes-Einstein violation temperature, T_s, the fragile glass-formers all behaved in the same way, and we created plots where the data in all the systems followed the same curve. In the fragile glass-formers, we also found that clusters of correlated particles became compact below T_s. We studied one strong glass-former, and found that it did not match the fragile

glass-former curves. However, the Stokes-Einstein violation temperature still appears to be significant in that system, since it appears to mark a change in shape of clusters of correlated particles. However, the clusters did not become compact.

We examined the stability of a glass that was created by cooling at different rates. We investigated mechanical stability by measuring the energy and shear modulus of the glass. We also studied the kinetic stability upon heating the glass by examining the average overlap function, a dynamic correlation function. The average overlap function measures how much correlation the positions of particles have with their initial positions after a certain amount of time. We used a stability ratio, S, to probe kinetic stability. Stability is higher in glasses that were prepared by cooling at a slower rate. The different measures of stability have different relationships with initial cooling rate, and we determined that kinetic stability is the best measure of stability.

Acknowledgements

We gratefully acknowledge the support of NSF (National Science Foundation) grant CHE 1213401.

For Chapter 3 and Chapter 2, we used the CSU (Colorado State University) ISTeC (The Information Science & Technology Center) Cray HPC (High Performance Computing) System supported by NSF Grant CNS-0923386.

Thanks to my group of Dr. Flenner and Professor Szamel. They introduced me to the subject matter, and helped me become better at research, presentation, and critical thinking.

Thanks to Matthew Hogan and Nic Kuon for proofreading this work and for their helpful comments.

I would like to thank Mark Ediger for his discussions with me on Chapter 4 throughout the progress of that work.

This dissertation is typset in LaTeX using a document class designed by Leif Anderson.

Table of Contents

List of Tables

List of Figures

List of Symbols

Acronyms

Acronym	Description
a-Si	amorphous silicon
BD	brownian dynamics
BKS	Beest, Kramer, and van Santen (their model)
c-Si	crystalline silicon
CP	Coslovich and Pastore (their model)
CPU	central processing unit
CSU	Colorado State University
fcc	face-centered cubic (crystal structure)
FIRE	fast inertial relaxation engine (for energy minimization)
GPU	graphics processing unit
HARD	hard spheres
HARM	harmonic spheres
HPC	high performance computing
HOOMD-blue	Highly Optimized Object-oriented Many-particle Dynamics - Blue Edition
IMC	indomethacin
ISTeC	The Information Science & Technology Center
KA	Kob and Andersen (the binary Lennard-Jones system created by them)
LAMMPS	Large-Scale Atomic/Molecular Massively Parallel Simulator

MCT	mode coupling theory
MMT	methyl-m-toluate
Ni	nickel (element)
NMR	nuclear magnetic resonance
NREL	National Renewable Energy Laboratory
NSF	National Science Foundation
NVE	microcanonical ensemble, i.e. a constant N, V, and E simulation
NVT	canonical ensemble, i.e. a constant N, V, and T simulation
P	phosphorus (element)
RFOT	random first-order transition theory
TNB	trisnaphthylbenzene
VFT	Vogel-Fulcher-Tamman (law), eq. 1.6
WCA	Weeks-Chandler-Andersen (model)

Greek symbols

Symbol	**Description**
α	a parameter used in eq. 4.16; α relaxation (or decay), which is the final part of a correlation function
β	an exponent for stretched exponential decay, eq. 1.16; $\beta = 1/(k_B T)$; β relaxation (or decay), which is the initial part and plateau region of a correlation function
γ	exponent in mode coupling fit, eq. 1.3

δ_{nm}	the Kronecker delta function
$\delta(t-t')$	the Dirac delta function
ϵ	depth of the potential well
ζ	a constant in the exponent in Section 2.4.2 and Figure 4.10(these are unrelated)
η	viscosity, eq. 3.8
$\vec{\eta}$	random noise, see eq. 2.4
θ	an angle; an exponent in eq. 1.36
Θ	Heaviside step function
μ	shear modulus
μ_i	chemical potential at a site i in eq. 1.32
ν	a constant in eq. 1.41
ξ	a length scale in RFOT, see eq. 1.36
ξ_4	the four-point dynamic correlation length found from four point functions, (we use a fit to the four point structure factor)
ξ_{fac}	the length between excitations in dynamic facilitation theory
ρ	particle number density, $\rho = N/V$; mass density, $\rho = m/V$; density functions from eqs. 1.26 and 1.27
σ	collision diameter
$\sigma^{\alpha\beta}$	element of the stress tenstor, otherwise known as the pressure tensor
τ	a relaxation time in Section 1.5.3
τ_0	a constant, eq. 1.6
τ_α	the α relaxation time, eq. 1.11 and eq. 1.13
τ_i	a constant in eq. 3.6

τ_i'	a constant in eq. 3.6
τ_{NH}	time parameter of an NVT Nosé Hoover thermostat
τ_p	time of the peak of the susceptibility
τ_s	the out of equilibrium relaxation time
ϕ	volume fraction, eq. 2.30
ϕ_c	mode coupling volume fraction
ϕ_o	onset volume fraction for glassy dynamics
χ_4	four point dynamic susceptibility
χ_c	the c derivative of F_s or F_o, where $\chi_c = \partial F_s/\partial c$, as in eq. 2.21 (applies to other variables besides c)
ψ	a friction coefficient, see eq. 2.4

Symbols

Symbol	**Description**
a	a distance
$\mathbf{a}$	acceleration
A	area; a constant in Section 2.4.2; a fitting constant to the stability ratio fit
$\mathscr{A}$	a measurable quantity
A_1	a fitting parameter from a fit to inverse diffusion coefficient from Figure 1.6
A_{IPL}	a constant in eq. 2.2
A_q	a fitting constant in eq. 1.31
B	a constant in Section 2.4.2; a fitting constant to the stability ratio fit

$\mathscr{B}$	a measurable quantity
c	concentration of a particle type, as in eq. 2.21; concentration of regions of mobile particles
c_g	concentration of mobile sites at a temperature T_g
C	specific heat
C_V	specific heat per particle
d	number of spatial dimensions
D	diffusion coefficient; a measure of fragility in eq. 1.6 and in eq. 1.37 (different)
D_r	rotational diffusion coefficient
E	total (internal) energy
E_0	a constant activation energy
E_1	activation energy from a fit to inverse diffusion coefficient from Figure 1.6
E_a	activation energy, as in eq. 1.5
E_i	a constant like activation energy in eq. 3.6
E_{IS}	inherent structure energy
f	a constant intensive parameter in an ensemble, see eq. 1.22
F	a constant extensive parameter in an ensemble, see eq. 1.22
F, $\mathbf{F}$	force, force between particles
$F(q;t)$	intermediate scattering function
$F(\rho_i)$	free energy function of eq. 1.33
F_o	average overlap function, eq. 1.12
F_s	self intermediate scattering function
g, $g(r)$	pair correlation function, eq. 1.1

G_4	four point correlation function of eq. 1.19
G_s	self van Hove function, eq. 4.11
h	height
H	hamiltonian
k, $\mathbf{k}$	wave vector
k_B	Boltzmann constant
K	kinetic energy; a scaling constant appearing in Figure 2.2; fragility index in eq. 1.7
K_f	frustration of eq. 1.41
$K(q;t)$	memory function of eq. 1.29
$K_{MCT}(q;t)$	the estimated memory function of eq. 1.30
l	an integer in eq. 4.4
L	length
m	mass
n_i	number of statistically independent configurations; number of particles at a site i in eq. 1.32
n_{IPL}	a constant exponent in eq. 2.2
N	number of particles
N_b	number of nearest neighbor particles in eq. 4.3
$N_{metastable}$	number of metastable states (in the Kauzmann paradox) in Section 1.2.1
p, $\mathbf{p}$	momentum
P	pressure; power, used in the FIRE algorithm
$P(x)$	probability distribution of some variable x, see eq. 4.12

q, $\mathbf{q}$	wave vector
$\bar{q}_l$	locally averaged parameter of eq. 4.4
q_{lm}	function of eq. 4.3
$\bar{q}_{lm}$	parameter of eq. 4.5
q_m	the overlap function of eq. 4.7
q_s	the average overlap function, eq. 4.7
Q_6	the order paramer of eq. 4.6
r	distance, radial distance, radius
r, $\mathbf{r}$	position of a particle
r_c	cutoff radius
R	size of a rearranging region in eq. 1.36
R_D	length of region of unfrastrated order, eq. 1.41
s	the s ensemble described in Section 4.1
S, $S(q)$	static structure factor
S	stability ratio
S_4	four-point structure factor
S_c	configurational entropy (in the Kauzmann paradox) in Section 1.2.1, or in eq. 1.36
S_{exc}	excess entropy (in the Kauzmann paradox) in Section 1.2.1
t	time
t_{trans}	transition time
t_w	waiting time
T	temperature

T_*	constant in eq. 1.7
T^*	the temperature where the theory of geometric frustration predicts a transition
T_0	the theoretical true glass transition temperature
T_c	the mode coupling temperature
T_g	the glass transition temperature
T_i	the temperature below which relaxation time has a super-Arrhenius fit in eq. 3.6
T_j	a fitting parameter in eq. 3.6
T_K	the Kauzmann temperature
T_m	the melting temperature
T_o	the onset temperature of glassy dynamics
U	potential energy
v, $\mathbf{v}$	velocity
V	volume
$V_{\alpha\beta}$	potential energy between particles of type α and β
V_{nm}	potential energy between particles n and m
$\tilde{V}_{\mathbf{q-k},\mathbf{k}}$	a function in eq. 1.30
V_{sp}	specific volume, $V_{sp} = V/m$
$w_n(a;t)$	a weight function that depends on a
$w_n(t)$	a weight function
$w(t)$	the average of the weight function $w_n(t)$
W	thermodynamic potential of eq. 1.32
x	x coordinate in the Cartesian coordinate system; a distance as in Δx in eq. 4.17
x_1	concentration of particle type 1, as in eq. 2.21

x_t	a time multiple for $P[\log_{10}(\delta r); x_t \cdot \tau_s]$
$\mathcal{X}$	correction terms to the full susceptibility
y	y coordinate in the Cartesian coordinate system
Y	surface tension in eq. 1.36
Y_{lm}	a spherical harmonic function in eq. 4.3
z	z coordinate in the Cartesian coordinate system; an exponent in eq. 1.18

Other symbols

Symbol	**Description**
$\langle\rangle$	(brackets) an ensemble or time average
∞	infinity
∇	del, $\nabla = \left(\frac{\partial}{\partial x}, \frac{\partial}{\partial y}, \frac{\partial}{\partial z}\right)$
∂	partial derivative, as in $\partial f/\partial x$
$\dot{\mathbf{r}}$	(dot) a time derivative
$\hat{\mathbf{v}}$	(hat) a direction, i.e. a unit vector in the direction of $\mathbf{v}$
$\delta\mathscr{A}$	from eq. 1.22
δC	error in the specific heat
δr	a displacement, see eq. 4.12
$\langle \delta r^2 \rangle$	mean square displacement, eq. 1.14
$\delta \mathbf{r}_n(t)$	a difference, given by $\delta \mathbf{r}_n(t) = \mathbf{r}_n(t) - \mathbf{r}_n(0)$
$\delta \mathbf{r}_{nm}(0)$	a difference, given by $\delta \mathbf{r}_{nm}(0) = \mathbf{r}_n(0) - \mathbf{r}_m(0)$
δt	time step

Δ	change in
$\Delta\xi_4$	a difference, given by $\Delta\xi_4 = \xi_4^0 - \xi_4^{\pi/2}$

Subscripts and superscripts

Symbol	**Description**
1	particle type 1, as in m_1; thermostat 1, as in p_{η_1}
2	particle type 2, as in m_2; thermostat 2, as in p_{η_2}
α	in the α direction, which can be the x, y, or z directions; particle type 1 or 2; alpha relaxation, as in τ_α
β	in the β direction, which can be the x, y, or z directions; particle type 1 or 2
δr	the weight function is $\delta\mathbf{r}_n^\perp$ of eq. 4.19
a	the a value in the overlap function
B	Boltzmann, as in k_B
c	configurational, as in S_c; MCT, as in T_c or ϕ_c
cos	the weight function is the real part of the intermediate scattering function
ens	measured in a given ensemble, such as NVT or NVE
f	a constant intensive parameter in an ensemble, see eq. 1.22
F	a constant extensive parameter in an ensemble, see eq. 1.22
i	the number in the chain of thermostats in the Nosé Hoover chain method; particle i, as in $\mathbf{r}_{ij}$; a lattice site in eq. 1.32
j	the number in the chain of thermostats in the Nosé Hoover chain method; particle j, as in $\mathbf{r}_{ij}$

l	integer, as in q_{lm}
m	integer, as in q_{lm}; particle m, as in $\mathbf{r}_{nm}$
n	particle n, as in $\mathbf{r}_{nm}$
N	number of timesteps a simulation has run
o	onset, as in T_o or ϕ_o
ov	the weight function is the overlap function
s	value corresponds to the Stokes-Einstein violation value
sh	the shift to a potential

Units

Symbol	**Description**
Å	Angstrom, $1\text{Å} = 10^{-10}m$, (a measure of distance)
cm	centimeter 1000cm = 1m (a measure of distance)
g	gram (a measure of mass)
K	Kelvin (a measure of temperature)
m	meter (a measure of distance)
P	poise, $1\text{P} = 1\text{g} \cdot \text{cm}^{-1} \cdot \text{s}^{-1}$ (a measure of viscosity)
Pa	pascal, $1\text{Pa} \cdot \text{s} = 10\text{P}$ (a $\text{Pa} \cdot \text{s}$ is a measure of viscosity)
s	second (a measure of time)

CHAPTER 1

Introduction

In this chapter, I introduce the subject of glasses and supercooled fluids, from modeling them to measuring their structure and dynamics. I describe some of the unique features of supercooled liquids seen at low temperatures. I also describe some theories about supercooled liquids and the glass transition.

Chapter 2 is about my first project, where I simulated and analyzed one of the glass-formers that appeared in the paper by Flenner, Staley, and Szamel [1]. We studied universal behavior of dynamic heterogeneity in several fragile glass-forming systems.

In Chapter 3, I discuss a network glass-former, which is a strong system, unlike the systems studied in Chapter 2. This chapter is based a paper by Staley, Flenner, and Szamel [2]. We examined whether a network forming glass has the same universal features we saw in the glasses of Chapter 2.

In Chapter 4, I examined cooling a glass at different rates and measuring its stability. This work lead to a paper by myself, Flenner, and Szamel [3]. We researched which measure of stability was best for comparing different simulations.

In Chapter 5, I summarize and draw conclusions about the work I presented in the previous chapters and discuss some directions for future work.

See page v for a list of symbols we use in this work.

1.1. Motivation

Glasses are found everywhere, yet if and at what temperature the glass transition occurs remains unsolved, or, at least, highly debated. The word glass refers to any solid amorphous material. In a solid, we can measure elastic moduli, and in a liquid we can measure viscosity, since the system can flow. Another way to think about solidity is to measure a relaxation/rearrangement time, τ_α, which is the typical time for a system to return to equilibrium after a disturbance. Around the temperature where a crystal melts, the relaxation time of a liquid is around a few picoseconds [4], while at the glass transition temperature, T_g, below which the system is considered a glass, the relaxation time is around 100 s. At slightly lower temperatures the relaxation time increases rapidly. Of course, if the relaxation time is still around 100 s, you could measure viscosity if you were patient enough. This choice of T_g is arbitrary. It based on what is convenient to measure in experiments. For relaxation times greater than 100 s, the system is considered solid. Notice that the relaxation time at the glass transition is about 14 orders of magnitude larger than for a liquid. A glass is also an amorphous material, meaning that it does not have the lattice structure of a crystal. Glasses do have regions of local order, but these regions do not match up periodically.

Glasses have been used for a long time, but new applications continue to appear. For example, glasses can be used in the pharmaceutical industry to improve oral delivery of pills [5]. For pills to be taken orally they have to dissolve, but some crystalline drug candidates are insoluble. There is interest in making amorphous oral pills, since the glassy forms of pills have been seen to be more soluble than the crystalline forms [6]. Companies are appearing that make metallic glasses. LiquidMetal Technologies [7] is a company that creates corrosion resistant metallic glasses with high strengths (higher yield strength and tensile strength than

high-strength titanium). They have made casings for smart phones, parts in electronics like chassis and hinges, and medical instruments. Glasses are also being used in the field of solar energy. Solar cells can be made from amorphous silicon (a-Si) as well as crystalline silicon (c-Si). Solar cells made from c-Si can have efficiencies up to 27.6%, while amorphous silicon solar cells have reached 13.6%, according to the latest chart by the National Renewable Energy Laboratory (NREL) [8] on research cell efficiency. However, a-Si solar cells can be made much more cheaply than c-Si solar cells. Industries making pharmaceuticals, metallic glasses, and solar cells, as well as many other industries have succeeded in creating glasses with many desirable properties out of a range of molecules.

While glasses can be used and created in many ways, they are not well understood, and neither is the glass transition. When we cool a liquid below the equilibrium melting/freezing temperature and avoid the phase transition to a crystal, we get a supercooled liquid. If we continue cooling at a rate fast enough to avoid crystallization, then the supercooled liquid will become a glass. The temperature where the supercooled liquid becomes a glass is called the glass transition temperature, T_g. We will examine some definitions for T_g in Section 1.2, but for now T_g can be thought of as the temperature below which the material begins to look solid, meaning its relaxation time is at least 100 s. Even though T_g marks an experimental "glass transition", it is not a true phase transition temperature. One way to see that T_g does not mark a true phase transition is that T_g depends on how the glass was created, and another is that T_g has many different definitions, which result in slightly different temperatures. Different theories have different ideas about where the true glass transition temperature is and if there even is one.

Researchers are still making progress on learning about glasses. Industries continue to create new glassy materials and improve old ones. The nature of the ideal glass transition remains an open question that theorists continue to ponder, and experimenters and computer simulators continue to try to examine. New ways to make glasses in computer simulations and experiments and new ideas for interpreting data get the field closer to understanding glasses and the glass transition.

1.2. Supercooled liquids and glasses

A crystal is an ordered rigid material, a liquid is a disordered fluid, and a glass is any rigid material that doesn't have the long range order of a crystal [9]. The pair correlation function, $g(r)$, gives the probability of finding a particle at a certain distance from another particle, and it can show whether a material is amorphous/disordered or crystalline/ordered. The pair correlation function is

$$g(r) = \frac{1}{\rho}\left\langle \frac{1}{N}\sum_{n}^{N}\sum_{m\neq n}^{N}\delta(\mathbf{r} - [\mathbf{r}_m(0) - \mathbf{r}_n(0)])\right\rangle, \tag{1.1}$$

where $\rho = N/V$ is the number density, N is the number of particles, V is the volume, δ is the Dirac delta function, and $\mathbf{r}_n(t)$ is the position of particle n at time t. The brackets, $\langle\rangle$, mean an ensemble average. (An ensemble average is an average over systems that have the same macroscopic properties as the current system [10]. It is equivalent to an average over time, as long as the average does not change with time [10].) Figure 1.1 shows the pair correlation function in a single component Lennard-Jones system. The system was created as an fcc (face-centered cubic) crystal, and $g(r)$ is shown for an fcc crystal, a liquid, and a glass. The pair correlation function for the glass has peaks at the same positions as the

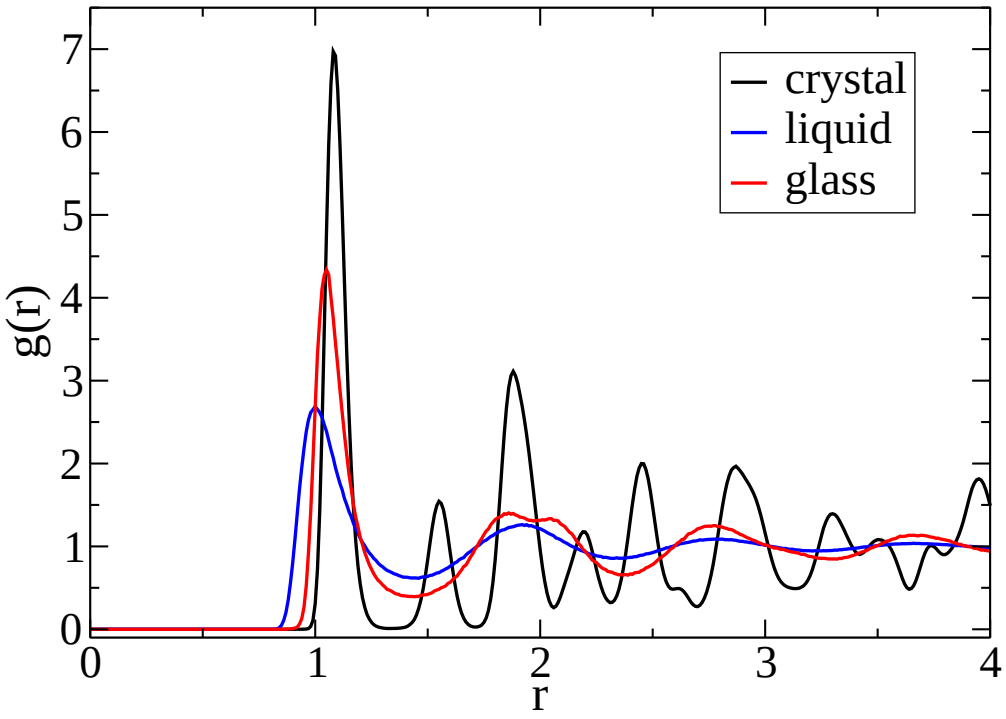

FIGURE 1.1. The pair correlation function in a Lennard-Jones single particle model at a number density of $\rho = N/V = 1.1$. This system melts around $T = 1.6$. The curves show the system as a crystal at a temperature of $T = 0.2$, as a liquid at a temperature of 3.0, and as a glass at $T = 0.5$ upon a sudden quench to $T = 0.5$ from $T = 3.0$.

liquid, but the peaks are a little more pronounced, and the second peak from the left has split a little. The curve for the fcc crystal shows many more peaks than the curves for the liquid or the glass. The peaks for the crystallized system are also in different positions than for either of the amorphous systems and they are bigger. A glass has the disorder of a liquid, but it is also solid [4].

A glass is never in equilibrium, meaning that its properties change in time. If a system is not in equilibrium, it is aging and its history matters. Consider aging a glass, after a liquid is suddenly cooled to a temperature below T_g. The system will try to equilibrate, but it will never reach equilibrium on an experimental timescale. The system will always depend on the time since the quench, t_w, i.e. its age. Indeed many measurements are functions of

t_w. Some properties of a system change very little, like the volume. The relaxation time, on the other hand, will increase as t_w increases, and it will eventually be too long to find in measurements. We will investigate how a glass is made (i.e. its history) affects its stability in Section 1.4, which discusses vapor deposited glasses.

Most liquids can form glasses if they are cooled fast enough. Figure 1.2 shows the specific volume V/m, where m is mass and V is volume, as a function of temperature T, for a system at constant pressure P that is being cooled at different rates. The fastest cooling leads to glass 1 in the figure, the next slowest cooling leads to glass 2, and a very slow cooling leads to a crystal instead of a glass. The system begins as a liquid. It is first cooled at a fast rate, avoiding crystallization, and becoming a supercooled liquid. Upon further cooling it becomes a glass, called glass 1 in Figure 1.2. In Figure 1.2, the glass transition temperature T_g is defined as the temperature where the curves of specific volume as a function of temperature of the supercooled liquid and the glass intersect. This definition of T_g doesn't match our first definition of T_g, which was defined as the temperature where the relaxation time was 100 s. When the system is cooled at a slightly slower rate, it again avoids forming a crystal, and falls out of equilibrium at a slightly lower temperature, becoming glass 2. When the system is cooled at a slow enough rate, it forms a crystal, as shown in the lowest curve of Figure 1.2. If a liquid is cooled past its melting temperature T_m and it doesn't crystallize, it remains a fluid and is called a supercooled liquid. Both the cooling paths for supercooled liquids for crystals can be seen in Figure 1.2. If the cooling of the supercooled liquid is continued, then the supercooled liquid will become a glass at T_g, the glass transition temperature. T_g is usually about 2/3 of T_m [4]. The laboratory T_g depends on the system's relaxation time, τ_α, the typical time over which particles rearrange. The laboratory T_g occurs when τ_α is

more than 100 s [9]. (We will define the relaxation time more precisely in Section 1.2.3.) Below T_g, a system doesn't flow on most experimental timescales, and thus below T_g the system appears solid. A liquid or a supercooled liquid has a viscosity that can be measured in an experiment or simulation of reasonable length. Reasonable length is hard to define, as it depends on how long a researcher is willing to run an experiment. Whereas, in a solid we measure the shear modulus. Figure 1.2 shows that in a constant pressure experiment, when a glass forms the volume of a system shrinks more slowly than in a liquid state. The extrapolations from the liquid state no longer apply, and the system falls out of equilibrium. When a liquid transforms to a glass its structure is maintained in the glass. Particles are stuck in the configuration they had when the system fell out of equilibrium. This freezing process is accompanied by changes in the heat capacity and other system properties like the thermal expansion coefficient.

For most definitions of T_g, how the glass is prepared can actually change the value of T_g, although very weakly. Figure 1.2 shows a different definition of T_g. In this figure, T_g occurs when the system falls out of equilibrium. In Figure 1.2, the point where the system falls out of equilibrium is where there is a change in the thermal expansion coefficient. The transition from a liquid to a crystal, on the other hand, is a first order phase transition. This type of transition is accompanied by a discontinuity in the first derivative of the free energy as a function of temperature. Notice that, in Figure 1.2, specific volume drops suddenly and discontinuously when a crystal is formed. If we avoid crystallization and cool to a glass, on the other hand, the specific volume as a function of temperature is continuous, as is its derivative. The figure demonstrates that changing cooling rate will change T_g, with slower cooling rates resulting in a lower T_g.

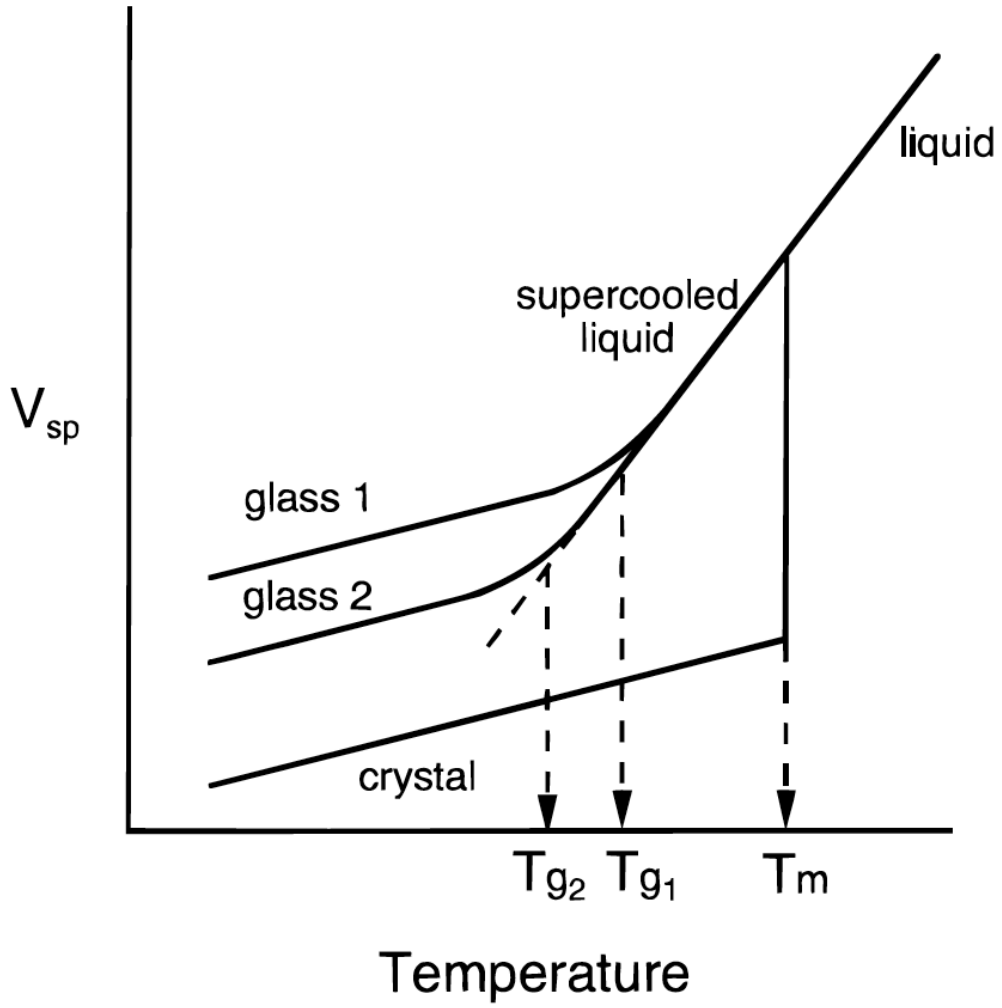

FIGURE 1.2. Specific volume $V_{sp} = V/m$ versus temperature T. T_m is the melting point of the crystal. T_g is the glass transition temperature, which is protocol dependent. When a liquid is cooled it may go through the glass transition at temperature T_{g_1}. If it is cooled more slowly then it will instead have a glass transition at temperature T_{g_2} Reprinted with permission from M. D. Ediger, C. A. Angell, and S. R. Nagel, J. Phys. Chem.-US **100**, 13200 (1996). Copyright 1996 American Chemical Society.

Besides the melting temperature T_m and the glass transition temperature T_g, there are a few other temperatures that are important to supercooled liquids. The onset temperature T_o for supercooling is often measured instead of T_m, since it is difficult to crystallize some glass-formers. Indeed T_o and T_m are not necessarily equivalent. Another temperature of interest is where dynamics become so slow that particle movement is dominated by rearrangements

of a few particles at a time. This temperature is known as the temperature where activated dynamics begins. Finally, an often referenced temperature is the mode-coupling temperature T_c from mode-coupling theory.

The onset temperature T_o for supercooled dynamics is the temperature below which liquids show features of supercooled liquids. There are several different methods for finding the onset temperature. One way of defining T_o is to find the temperature where particles are first visibly stuck in cages of their nearest neighbors. This behavior can be seen in correlation functions like the self intermediate scattering function and the mean square displacement, which will be discussed in Section 1.2.3. Brumer and Reichman [11] came up with a different way of finding the onset temperature using the inherent structure energy, which can be thought about in terms of the energy landscape. Goldstein [12] presented an energy landscape picture of equilibrium supercooled liquids. The energy landscape is given by the potential energy $U(\mathbf{r}_1, ..., \mathbf{r}_N)$ of a system of N particles. Thus, the energy landscape has $3N$ dimensions. The energy landscape can be pictured as a series of hills and valleys. Figure 1.8 gives a one dimensional representation of the landscape. The valleys represent favorable states for the system, where it can minimize energy. The hills represent barriers the system must cross to get to another valley (favorable state). The system moves to different valleys by particle rearrangements. Consider a system that has a position in some valley in the landscape. The inherent structure energy of the system is the energy at the bottom of that valley. One way to define the onset temperature T_o is to investigate average inherent structure energy as a function of temperature. As temperature is lowered in a liquid, at some temperature, the average inherent structure energy begins to sharply decrease. This temperature is known as the onset temperature. Elmatad, Chandler, and Garrahan [13]

found the onset temperature using a fit for relaxation time τ as a function of temperature where data from 58 glass formers collapsed onto a single curve shaped like a parabola, given by

$$\log(\tau/\tau_o) \simeq (J/T_o)^2(T_o/T-1)^2, T_o > T > T_x \tag{1.2}$$

where J is a fitted energy scale and τ_o is a fitted time. The upper bound for this fit is the onset temperature, T_o, a fit parameter to the parabolic equation. The lower bound is the temperature T_x, below which Elmatad *et al.* predicted a change in dynamics, and the fit does not apply.

Another important temperature in the cooling of a glass is the mode-coupling temperature, T_c, from mode-coupling theory (MCT), which will be briefly introduced in Section 1.5.1. MCT predicts that the relaxation time has an algebraic divergence at a temperature T_c, which is above T_g [14]. This divergence is described by eq. 57 of Ref. [15], which gives

$$\tau_\alpha \sim (T-T_c)^{-\gamma}, \tag{1.3}$$

where T_c and γ often come from fitting to supercooled temperatures below the onset temperature T_o. For many simple glass formers that we use, T_c and γ can be solved for, but the results from calculations disagree with the fit results. However many systems, including computer simulations, can be equilibrated below T_c, which is above T_g. Note that it is difficult to equilibrate computer simulations below T_c. Figure 1.3 shows relaxation time as a function of temperature for a model system created by Coslovich and Pastore [16], which we will call the CP system. It will be studied in Chapter 3. We equilibrated the system at each temperature and found the relaxation time. The mode-coupling temperature for this system of $T_c = 0.31$

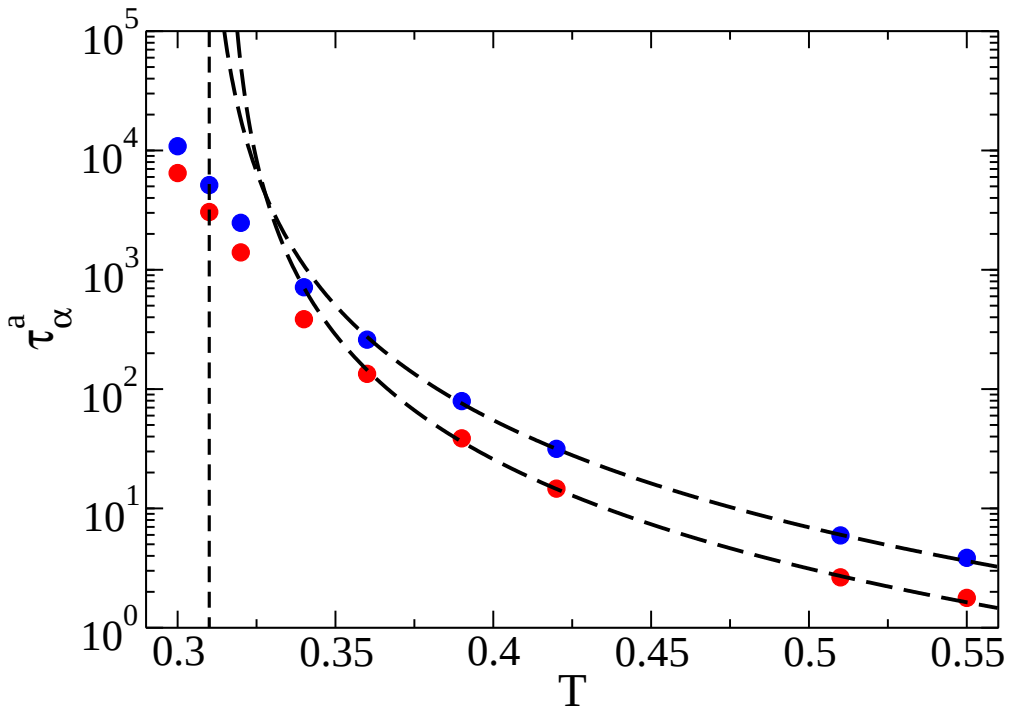

FIGURE 1.3. Relaxation time, τ_α^a, versus temperature, T, in the CP system, showing the divergence at the mode-coupling temperature, $T_c = 0.31$. Note that in this system we examined the average overlap function at two distances, a, in the average overlap function. Thus the relaxation time is marked with an a. The thin dashed line is the mode-coupling temperature, and the thick dashed lines are the fits to data using eq. 1.3.

is marked as a dashed vertical line in Figure 1.3. In the CP system, we found the mode coupling temperature from a fit to supercooled temperatures below the onset temperature, using eq. 1.3. Note that in this system we examined relaxation time for two different length scales, using the average overlap function, eq. 1.13, a time correlation function, which will be discussed in Section 1.2.3. We note that other simulations have results that agree with ours [17]. From Figure 1.3, we observe that T_c is not the temperature where relaxation time diverges, as it first appears from the fit to higher temperatures. Equilibrating supercooled glasses below T_c is often necessary to get important information on a supercooled liquid.

Another temperature of interest is the temperature where activated dynamics first appear. It can be defined by the energy landscape. Recall that the energy landscape can be

thought of as a series of hills and valleys. The hill represent energy barriers. Activated dynamics occur below temperatures where the thermal energy of the system is on the order of the energy barrier heights [18]. At high temperatures a system can change states easily, since its energy is around the level of the energy barriers. At lower temperatures, the system gets stuck in an energy well. When the system is in a particular potential energy well for a long period of time, it is in a metastable state [19]. However, even a deeply supercooled liquid can still hop between potential energy minima. The hops are equivalent to the system relaxing to a new configuration, and they involve the rearrangements of just a few particles at a time [12]. The hops between metastable states are called activation events. Many researchers have searched for the temperature where activated dynamics first appears. Some researchers suggest that T_c could be a candidate for a crossover temperature to activated processes [20].

Cooling a supercooled liquid down from the melting temperature, T_m, to the glass transition temperature, T_g, is accompanied by the dynamics slowing down by many orders of magnitude. This slow down can be seen in the increase in the relaxation time or the increase in the shear viscosity, η [4], where η is a measure of the resistance of a fluid to outside shear stresses/forces. In experiments, the relaxation time at T_m is usually about 14 orders of magnitude smaller than at T_g [4], whereas computer simulations, using ordinary cooling, can access only about 5 of the 14 orders of magnitude of increase of the relaxation time seen in experiments [9].

The increase in viscosity is an important signature of the glass transition, and viscosity changes much more in a supercooled liquid over a short temperature range than in a liquid. In liquids, at temperatures above T_m, there is not nearly as much slowing down of the

viscosity. In liquid water for example, which is liquid from 273.15 K to 373.15 K at standard pressure, the viscosity can be modeled by

$$\eta = 2.414 \times 10^{-4} * 10^{247.8/(T-140)}, \tag{1.4}$$

for water from 273.15 K to 373.15 K [21]. In eq. 1.4, η is in units of poise ($\mathrm{P} = \mathrm{g} \cdot \mathrm{cm}^{-1} \cdot \mathrm{s}^{-1}$), and T is in units of K. Over the standard liquid range of 273.15 K to 373.15 K, the viscosity goes from 1.75 $\mathrm{g/m \cdot s}$ to 0.279 $\mathrm{g/m \cdot s}$, dropping less than an order of magnitude. Recall that, below the melting point, T_m, the viscosity of supercooled liquids drops around fourteen orders of magnitude before the glass transition occurs. Water demonstrates that the viscosity of liquids changes much less than the viscosity of a typical supercooled liquid does.

Besides the interesting slow down in dynamics of a supercooled liquid in comparison to a liquid, the relaxation times and viscosities of different supercooled liquids have very different temperature dependences. Angell [22] came up with a way of classifying supercooled liquids based on the temperature dependence of their viscosities. He created a plot, now called an Angell plot, of viscosity, η, or relaxation time, τ_α, as a function of T_g/T. In this plot, T_g is defined to be the temperature where the viscosity reaches 10^{13} poise. The plot divided glasses into strong and fragile glasses. Strong glasses have Arrhenius behavior. The Arrhenius relation for the relaxation time is

$$\tau_\alpha = \tau_0 \exp\left(\frac{E_a}{k_B T}\right), \tag{1.5}$$

where τ_0 is a constant and E_a is the activation energy. E_a can be thought of as an energy barrier a particle must get over in order to move. Strong glasses have curves that look straight in Figure 1.4, since they obey the exponential Arrhenius relation. The curves for

more fragile glasses will be more curved, falling below the strong glass curve. Some fragile glasses are toluene, o-terphenyl, and ethanol [22]. A typical strong glass-former is SiO_2. We will be studying a model strong glass-former [16] with similar properties to SiO_2 [16] in Chapter 3. Strong liquids usually have a local structure that is tetrahedral, as is the case for SiO_2 [4]. Royall and Williams [9] have suggested that the local structure may be connected to dynamic heterogeneity, which will be discussed in the next section, Section 1.3. Fragile glasses do not obey the Arrhenius relation, instead exhibiting super-Arrhenius behavior, where the activation energy, $E_a(T)$ is a function of temperature, and $E_a(T)$ increases with decreasing T. One explanation for this difference from Arrhenius behavior is that particles must move collectively, thus increasing the energy barrier. The Vogel-Fulcher-Tamman law (VFT) is a reasonable fit to many fragile glass forming liquids, and it is given by

$$\tau_\alpha = \tau_0 \exp\left(\frac{DT_0}{T - T_0}\right), \tag{1.6}$$

suggesting that τ_α diverges at the finite temperature T_0. The inverse of the constant D, i.e. $1/D$, is an example of a fragility parameter. There are many different fragility parameters, which measure where a liquid's curve is on the Angell plot. If a fragility parameter is higher, then the system is more fragile, while a lower fragility parameter corresponds to a stronger liquid. Other fits use other fragility parameters, and we will use another one in Chapter 3. Another reasonable fit for fragile glasses is the Bässler law, which is given by

$$\tau_\alpha = \tau_0 \exp\left[K\left(\frac{T_*}{T}\right)^2\right], \tag{1.7}$$

where the relaxation time diverges at a temperature of absolute zero. Recall that Mode-Coupling theory also relates relaxation time and temperature,

$$\tau_\alpha \sim (T - T_c)^{-\gamma}, \tag{1.8}$$

This relationship suggests that the mode-coupling temperature T_c is where relaxation time diverges. Recall that relaxation time has been shown not to diverge at T_c, which is above T_g. T_c remains important, because, other theories have suggested that T_c might signify a change in dynamics. These different dependencies of the relaxation times on temperature are not only interesting, but they suggest possible temperatures for the ideal glass transition temperature.

1.2.1. The ideal glass transition temperature. Another temperature that seems to add importance to T_0 from the VFT law is the Kauzmann temperature, T_K. Consider the excess entropy that a supercooled liquid has over a crystal. We shall call it S_{exc}. We normalize S_{exc} by its value at T_m and plot it as a function of T. We can't get the entropy of the supercooled liquid below T_g, but we can extrapolate from the data above that temperature to lower temperatures. If we do so, then we see that S_{exc} appears to vanish at a finite temperature, T_K [23]. It is postulated that the entropy of the system can be broken in two. One part of the entropy corresponds to the vibrations of the system in its stuck state. The other part is the configurational entropy, S_c, which can be explained using the energy landscape. At T_g the system is stuck in an energy minimum of the energy landscape, unable to escape over the surrounding energy barriers. The configurational entropy is $S_c = \log(N_{metastable})$, where $N_{metastable}$ is the number of metastable states in the energy landscape. A metastable state is an energy minimum where the system can become trapped, but is

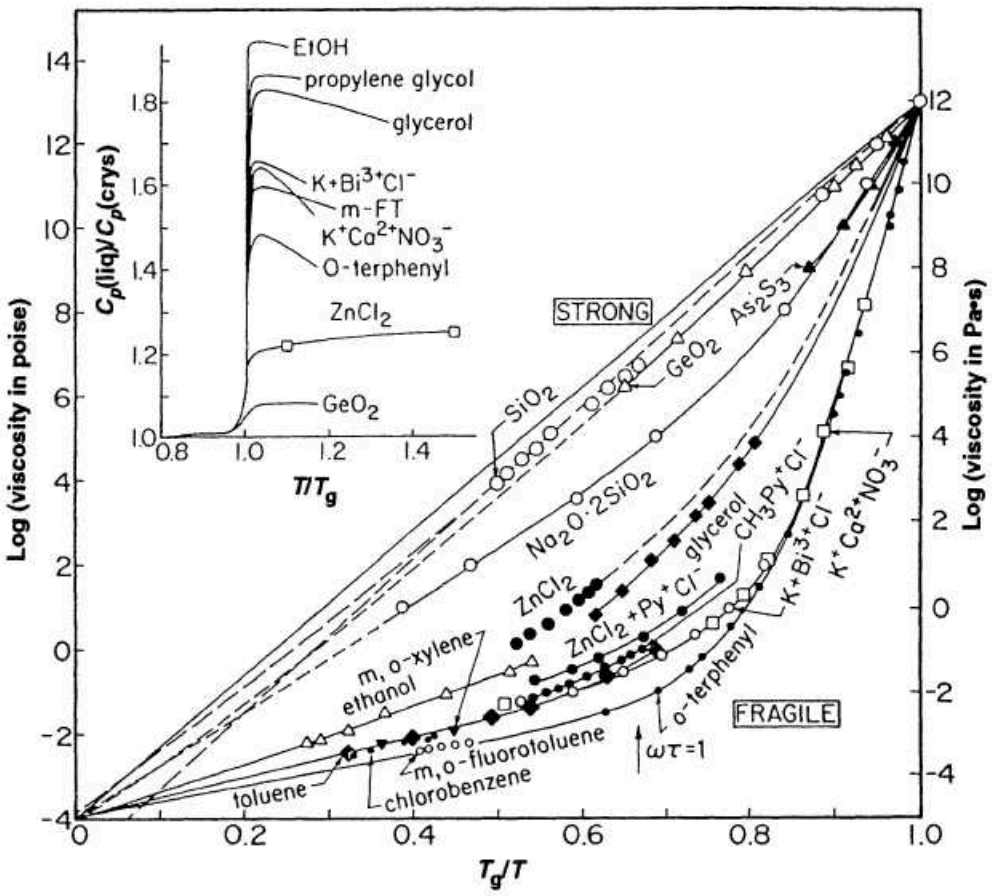

FIGURE 1.4. An Arrhenius plot of the logarithm of viscosity (in poise, P, and pascal seconds, Pa · s) versus T_g/T, taken from Figure 4 of the paper by Angell [22]. T_g is chosen to occur when the viscosity reaches 10^{13} P. It shows glasses from strong to fragile. On this figure, strong liquids will have a straight line Arrhenius behavior, obeying eq. 1.5. Fragile liquids will have a super-Arrhenius behavior, falling below the strong liquid curve. The farther below the strong liquid curve a liquid falls, the more fragile the liquid. The inset shows the change in the heat capacity at T_g. There is some correlation between fragility and the size of this change. *Republished with permission from the American Association for the Advancement of Science.*

not the lowest energy state. If we assume that the entropy of the vibrations of the glass is approximately the same as the vibrations in a crystal [4, 24], then the excess entropy is the difference between the configurational entropies of the liquid and the crystal, (a perfect crystal should have a configurational entropy of 0). Thus, if the excess entropy of a liquid over a crystal becomes negative at some temperature, then the configurational entropy of

a liquid becomes less than that of a crystal. The third law of thermodynamics is that at absolute zero temperature the entropy of a perfect crystal vanishes. Since vibrations vanish at absolute zero, (classically), the entropy is the configurational entropy. If the entropy S as a function of temperature of the liquid continued to decrease below T_K at the same rate, then S_c of the liquid would be negative at absolute zero. The configurational entropy of the liquid can't be smaller then the configurational entropy of the crystal, or else the third law of thermodynamics would be violated.

Kauzmann, who the temperature is named for, suggested that there must be an event like a phase transition at T_K to prevent the supercooled liquid entropy from being smaller than that of a crystal [23]. However Kauzmann's paradox is not really a paradox, since there is not law preventing the entropy of the liquid from being smaller than that of the glass at a finite temperature. On the other hand, a continuing decrease in excess entropy would violate the third law. To prevent the violation of the third law at absolute zero, there have been suggestions that there is a transition to a glass or a crystal at T_K. Whether there is a transition at T_K or not may not be so important, since experiments can not equilibrate a liquid at temperatures down to T_K anyway, since it is below T_g. Even though the paradox is not really the crisis Kauzmann first believed it to be, T_K turned out to be a very interesting temperature, because it is usually close to T_0 from the VFT law. Recall that the VFT law suggests that relaxation times diverge at T_0. In most liquids T_K is close to T_0 [25], though in some liquids T_K and T_0 differ by up to 20% [4].

Many theories predict a true thermodynamic phase transition to a glass at a finite temperature like T_0 or T_K, if the system could be cooled slowly enough. If the glass transition occurs at a temperature $T_0 < T_g$, as opposed to a temperature of absolute zero, then this

finite temperature transition will be hard to prove, since T_g is defined so that equilibration is out of the range of experiments. Thus, equilibrating below that temperature is, by definition, impossible, preventing the investigation of the proposed ideal glass transition temperatures.

1.2.2. Static correlation functions. Many theories expect relaxation time and length to grow as temperature is cooled. We will examine the time correlation functions that show relaxation time is growing as temperature decreases in Section 1.2.3. Static correlation functions are slightly different in liquids, supercooled liquids, and glasses, but simple ones do not show evidence of a diverging length scale. One static correlation function is the static structure factor, $S(q)$, which measures fluctuations in the density function. Note that $S(q) - 1$ is the Fourier transform of $\rho g(r)$. Similarly, $\rho g(r)$ is the Fourier transform of $S(k) - 1$, where $g(r)$ is the pair correlation function from eq. 1.1. The static structure factor is

$$S(q) = \frac{1}{N} \left\langle \sum_{n=1}^{N} \mathrm{e}^{i\mathbf{q}\cdot\mathbf{r}_n(0)} \sum_{m=1}^{N} \mathrm{e}^{-i\mathbf{q}\cdot\mathbf{r}_m(0)} \right\rangle, \tag{1.9}$$

where $r_n(t)$ is the position of particle n at time t, q is a wave vector, and N is the number of particles. If $S(q)$ showed a diverging correlation length, we would expect to see a growth in its low q values. However, $S(q)$ looks similar in a supercooled liquid as in a glass, showing no such growth. As Figure 1.1 displays, the change in $g(r)$ from the liquid curve to the curve for the glass is gradual and continuous. Another option is to look for a diverging dynamic correlation length using time correlation functions. Two-point correlation functions, in Section 1.2.3, give us a relaxation time, and four-point correlation functions, in Section 1.3.1, give us a dynamic correlation length.

1.2.3. Two-point time correlation functions. Unlike static correlation functions, time correlation functions change shape significantly as a liquid is supercooled more deeply. Time correlation functions allow you to investigate dynamics by measuring the correlation between two variables, which are measured at two different times. A useful time correlation function is the self intermediate scattering function, $F_s(q;t)$. One reason it is so useful is that neutron scattering experiments [26] can measure $F_s(q;t)$. The self intermediate scattering function is

$$F_s(q;t) = \frac{1}{N}\left\langle \sum_{n=1}^{N} \mathrm{e}^{i\mathbf{q}\cdot[\mathbf{r}_n(t)-\mathbf{r}_n(0)]} \right\rangle, \tag{1.10}$$

where $r_n(t)$ is the position of particle n at time t, N is the number of particles, and q is a wave vector. We usually use the value of the first peak of the static structure factor, $S(q)$, for q. The biggest peak of the static structure factor corresponds to the lengthscale of the short to medium range order. The self intermediate scattering function decays in time as particles becomes less correlated with their initial positions, and we like to define a representative time for its decay (otherwise known as relaxation). The alpha relaxation time is usually defined by

$$F_s(q;\tau_\alpha) = \mathrm{e}^{-1}, \tag{1.11}$$

in reference to the mean lifetime from exponential decay, and it can be seen on Figure 1.5, which shows $F_s(q;t)$ in a three dimensional binary system with a Lennard-Jones potential. We simulated an NVE system (microcanonical ensemble), meaning particle number N, volume V, and energy E are constant, with Newtonian dynamics. Kob and Andersen [27] came up with the parameters in this potential, and we will call it the KA potential. They

designed their potential to match the potential of Weber and Stillinger [28] for $Ni_{80}P_{20}$. This system will be discussed in Chapter 4. In the KA system, $q = 7.2$. Figure 1.5 shows the self intermediated scattering function for an equilibrium fluid for the liquid temperature of 1.0 in reduced Lennard-Jones units, and for the supercooled liquid temperatures of 0.44 and 0.5. The initial decay of the function is the β decay and the later decay is the α decay. The figure shows a plateau region, where particles are trapped in cages of their nearest neighbors. This plateau can be seen at intermediate times in liquids that have been supercooled enough. (This plateau can only be seen in a plot where time is on a log scale.) The β decay can be split into two parts, with the plateau being the second part, late β decay. The initial decay at early times in Figure 1.5 is the early β decay. The α relaxation is in the α decay, which is the final decay of $F_s(q;t)$. Another common time correlation function is is the average overlap function,

$$F_o(t) = \frac{1}{N}\left\langle \sum_n \Theta[a - |\mathbf{r}_n(t) - \mathbf{r}_n(0)|] \right\rangle, \tag{1.12}$$

where a is a distance and Θ is the Heaviside step function, which takes a value of 1 when its argument is positive or zero and has a value of 0 when the argument is negative. $F_o(t)$ has a value of 1 when $t = 0$, and decays to 0 if all the particles are able to move more than a distance a. As is the case for the self intermediate scattering function, the relaxation time is

$$F_o(\tau_\alpha^{ov}) = \mathrm{e}^{-1}. \tag{1.13}$$

We choose a value of a so that τ_α^{ov} for F_o has approximately the same value as τ_α for the self intermediate scattering function, F_s, where the q value in F_s corresponds to the first peak of the static structure factor, $S(q)$. This value of q probes nearest neighbor distances,

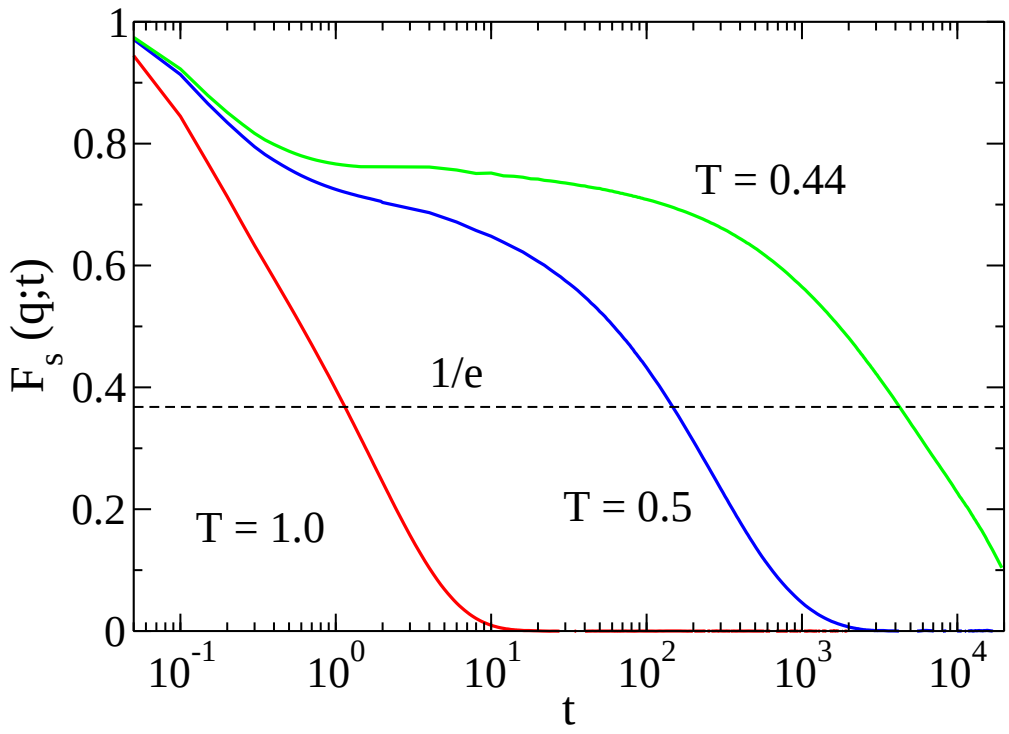

FIGURE 1.5. The self intermediate scattering function $F_s(q;t)$ in the KA system at the liquid temperature of 1.0 and at the supercooled liquid temperatures of 0.44 and 0.5. The dashed horizontal line gives the value of $1/e$, from which we find the relaxation time of eq. 1.11.

and we wish to choose a so that we are also probing nearest neighbor distances. We can say $\tau_\alpha^{ov} \approx \tau_\alpha$, since many time correlation functions that decay in time have a very similar temperature dependence of their relaxation times. From the mean square displacement, we find a decreasing diffusion coefficient as temperature decreases, and from the self intermediate scattering function, we see that the α relaxation time increases as temperature decreases. Unfortunately, we can't extract a length that is useful for seeing the glass transition from these two-point correlation functions.

To examine how much a particle moves in time, we measure the mean square displacement. The mean square displacement is given by

$$\left\langle \delta r^2(t) \right\rangle = \frac{1}{N} \left\langle \sum_{n=1}^{N} \left[\mathbf{r}_n(t) - \mathbf{r}_n(0) \right]^2 \right\rangle , \tag{1.14}$$

where $\mathbf{r}_n(t)$ is the position of particle n at time t and N is the number of particles. Figure 1.6 shows an example of the mean square displacement in the KA. It shows the mean square displacement at the liquid temperature of 1.0. At this temperature the mean square displacement has two distinct regions, an early time behavior and a late time behavior. At short times particles have ballistic motion, in this Newtonian simulation, and at long times the motion is diffusive. The self-diffusion coefficient is measured from the long time behavior of the mean square displacement. It is given by

$$D = \lim_{t\to\infty} \frac{1}{6t} \left\langle \delta r^2 \right\rangle . \tag{1.15}$$

In the early time ballistic regime the mean square displacement grows as $\langle \delta r^2 \rangle \sim t^2$, while in the late time diffusive regime it grows as $\langle \delta r^2 \rangle \sim t$. We will see that the diffusion coefficient and the α relaxation time do not always have the same temperature dependence in Chapter 2. In the KA system, shown in Figure 1.6, the diffusion coefficient shows that, for a given length of time, particles displace less when temperature is decreased in a supercooled liquid. The inverse of the diffusion coefficient hugely increases as temperature is lowered in a supercooled liquid, just like the relaxation time and the viscosity. At lower temperatures the mean square displacement still has the same short and long time behavior as it did at $T = 1.0$, i.e. ballistic and diffusive, but it also has a plateau at intermediate times, as can be seen in Figure 1.6. The two lower temperatures of 0.44 and 0.5 correspond to when the system is a supercooled liquid. The plateau represents particles being trapped in cages of their nearest neighbors and vibrating around their initial positions, before breaking free and moving diffusively. As temperature decreases the plateau gets longer and lower. A longer

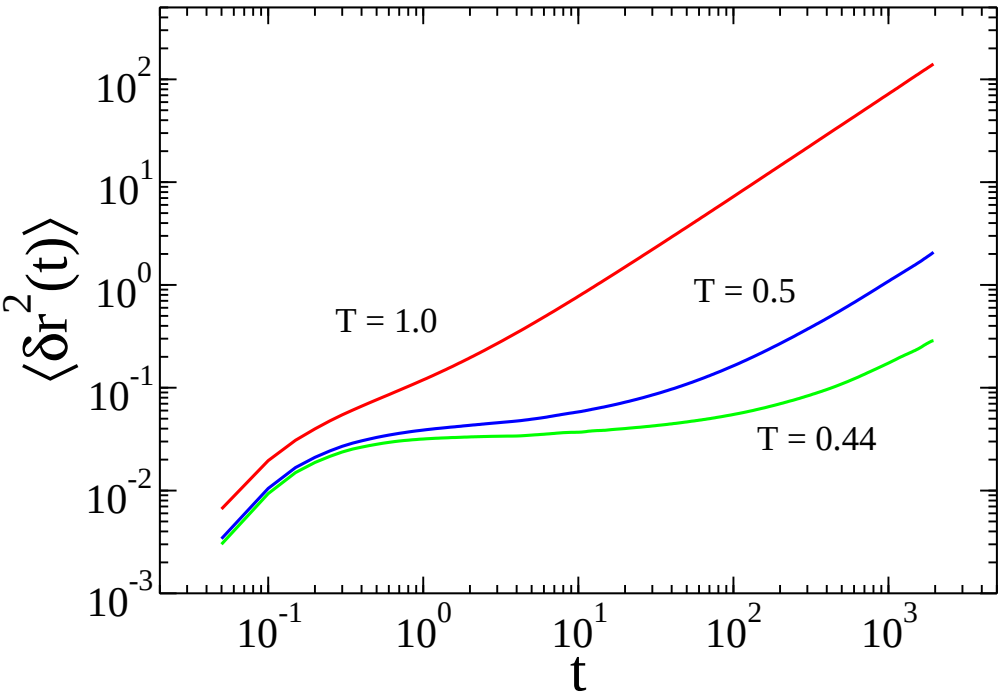

FIGURE 1.6. The mean square displacement $\langle \delta r^2(t) \rangle$ in the KA system at the liquid temperature of 1.0 and at the supercooled liquid temperatures of 0.44 and 0.5.

plateau means particles are trapped in cages for longer. A lower plateau means that the cages are smaller.

1.3. DYNAMIC HETEROGENEITY

Over a given time, in supercooled liquids, there are particles that displace very little (much less than a particle diameter), known as immobile particles and others that displace a lot (more than a particle diameter), mobile particles. At intermediate time scales, in liquids, the distribution of single particle displacements is close to Gaussian, while in supercooled liquids, the distribution has bigger tails than a Gaussian distribution [4]. At long times, (much longer than the relaxation time), even distributions in supercooled liquids approach a Gaussian distribution. Dynamic heterogeneity is a phenomenon that shows up on intermediate time scales relevant for structural relaxation. Unlike in liquids, particles in supercooled

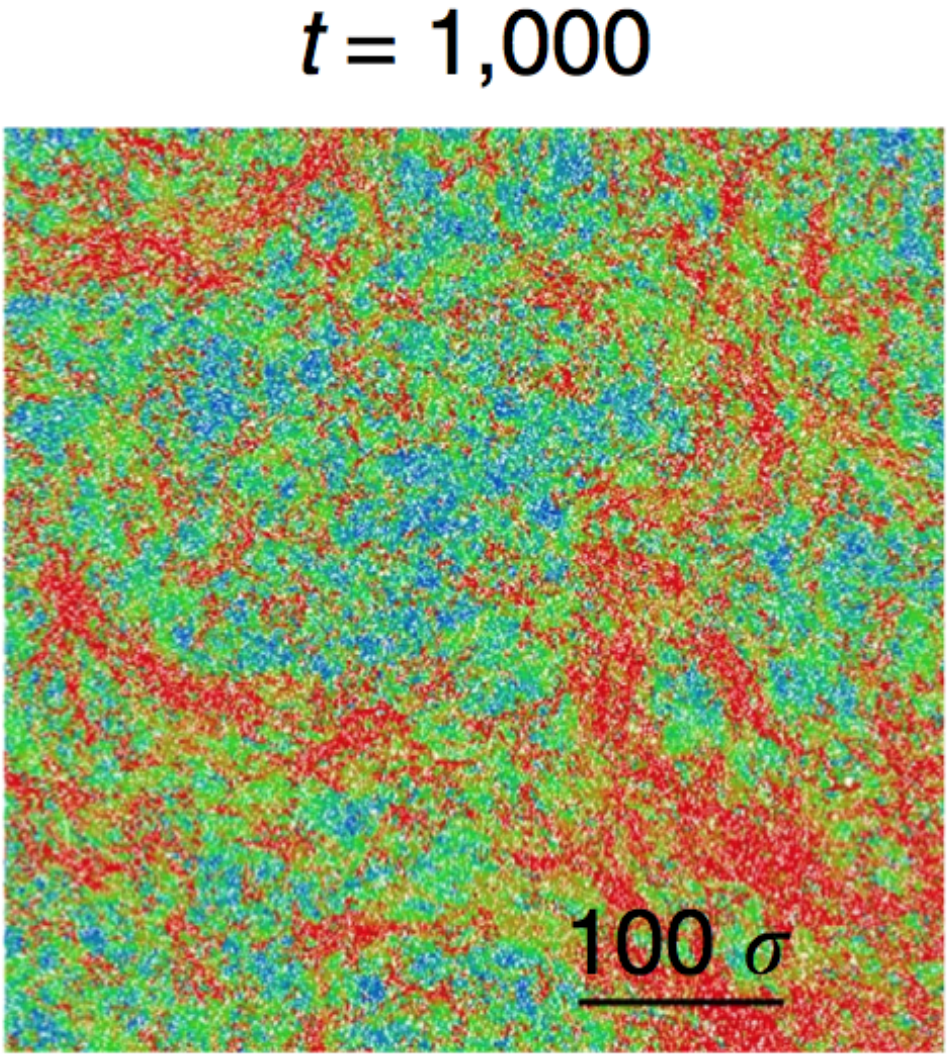

FIGURE 1.7. The displacements of around 250,000 particles in a 2D binary Lennard-Jones system. The particles are shown at their initial positions, and the color indicates how far they displaced. Blue corresponds to a displacement of 0, while red corresponds to a displacement of 1 larger particle diameter or more. This figure is from the article by E. Flenner and G. Szamel [31] which appeared in Nature Communications.

liquids can be found in regions with other particles with similar mobilities, as can be seen in Figure 1.7. In many computer simulations [29–31], researchers find clusters of particles with similar mobilities. Clusters of mobile particles can appear right next to clusters of immobile particles. Dynamic heterogeneity refers to the fact that the mobility of particles varies in different regions of a system, and particle displacements are non-Gaussian.

While two point correlation functions can't directly measure dynamic heterogeneity, they show some indirect evidence of it like stretched exponential decay of correlation functions. As liquids are supercooled, some two-point correlation functions, for example the intermediate scattering function, look more like stretched exponential functions than exponential functions. The self intermediate scattering function can be fit to a stretched exponential,

$$F_s(t) = A \exp\left[-\left(\frac{t}{\tau_\alpha}\right)^\beta\right], \tag{1.16}$$

as in eq. 1 of Ref. [14]. For liquids the final decay is usually nearly exponential and β is around 1, while for supercooled liquids $\beta < 1$. One explanation for this change upon supercooling, is that the relaxation is increasingly like a stretched exponential uniformly throughout the entire system, as the system is cooled. Another explanation, which Ediger [14] presents considerable evidence for, is that a supercooled liquid has regions with different relaxation times. Each region has essentially exponential relaxation, but when the whole system is examined, the exponential decays of each area get averaged together, leading to the stretched exponential of eq. 1.16. To choose the correct explanation we need direct evidence of having different relaxation times in different parts of the system.

Another way we can indirectly see dynamic heterogeneity in two-point correlation functions is by the violation of the Stokes-Einstein relation. One form of the Stokes-Einstein relation is

$$D = \left(\frac{6\pi\eta r}{k_B T}\right)^{-1}, \tag{1.17}$$

where η is the viscosity and r is the radius of a spherical particle. So we expect $D \sim (\eta/T)^{-1}$. In supercooled liquids, below a temperature that varies with material, the Stokes-Einstein

relation is violated, and a fractional Stokes-Einstein relation appears. The fractional Stokes-Einstein is an empirical relation between the self-diffusion coefficient and viscosity. The fractional Stokes-Einstein relation is

$$D \sim \left(\frac{\eta}{T}\right)^{-z}, \tag{1.18}$$

where $z < 1$. One explanation for why the Stokes-Einstein relation is violated is that translational diffusion is enhanced with respect to the relaxation time at lower temperatures [14]. As temperature is lowered, the distribution of relaxation times broadens, and spatially heterogeneous dynamics appear. The viscosity measures a liquid's resistance to shear stress, and it depends on the movement of all particles, but the diffusion coefficient is dominated by regions of more mobile particles. Ediger [14] explains that if the system has regions of different mobilities dispersed randomly, then the more mobile particles will naturally flow around regions of low mobility. He compares it to a circuit, where current will avoid areas of high resistance if possible. Thus the overall diffusion of particles will be dominated by the more mobile regions. In this picture spatial dynamic heterogeneity naturally leads to violation of the Stokes-Einstein relation. Note that the idea presented above is not proof of dynamic heterogeneity.

In early experiments [14] and computer simulations [29], researchers found proof of dynamic heterogeneity, and measured its time and length scales. Greater dynamic heterogeneity is characterized by seeing that the range of relaxation times in the system becomes broader and the dynamic correlation length becomes longer as temperature is decreased [14]. Schmidt-Rohr and Spiess [32] did an early experiment showing the existence of dynamic heterogeneity using solid-state NMR (nuclear magnetic resonance) to study poly(vinyl acetate),

which is commonly used in white glue. They investigated molecular orientation over two equal time intervals separated in time. They picked a set of molecules with a smaller than average change in orientation angle. When they examined these same molecules a short time later, the orientation had again changed by a smaller than average amount. They found that the length of time this correlation persisted was around the same as the relaxation time of the slow molecules. Experiments can directly probe the lifetimes of heterogeneous regions and their relaxation times. Measuring length scale in molecular liquid experiments is more indirect, but the results suggest that lengths of correlated mobility regions are around 5 to 10 molecular diameters at temperatures close to T_g [33]. Experimentalists doing colloid experiments [34], where spherical particles are suspended in a fluid, can use microscopy to get length. Early computer simulations found length by sorting particles into categories based on mobility, then testing whether a particle in a category was near other particles in the category. Some simulations probed the length scale for dynamic heterogeneity by counting the number of particles in a cluster of particles with correlated mobility [29]. Four-point correlation functions have improved the way dynamic heterogeneity is examined in computer simulations.

In computer simulations we find the strength and size of dynamic heterogeneity by examining four-point correlation functions. The four-point susceptibility, χ_4, measures the number of particles in a region of correlated mobility, and ξ_4 gives a length scale of the regions.

1.3.1. Four-point correlation functions. To examine the size of regions of correlated dynamics we could investigate a correlation between the mobilities of two particles at a distance r apart. This correlation of the mobilities of two particles results in a four-point

correlation function $G_4(r;t)$, [35], which can be given by

$$G_4(r;t) = \frac{V}{N^2}\sum_{n\neq m}\langle w_n(t)w_m(t)\delta[\mathbf{r}-(\mathbf{r}_n(0)-\mathbf{r}_m(0))]\rangle\,, \tag{1.19}$$

from Ref. [36]. In this equation, $w_n(t)$ is a weight function, which measures the mobility of particle n at a time t. We typically examine the Fourier transform of $G_4(r;t)$, which is $S_4(q;t)$, the four-point structure factor. $S_4(q;t)$ is

$$S_4(\mathbf{q};t) = \frac{1}{N}\left\langle\sum_{n,m} w_n(t)w_m(t)\mathrm{e}^{i\mathbf{q}\cdot[\mathbf{r}_n(0)-\mathbf{r}_m(0)]}\right\rangle - \frac{1}{N}\left\langle\sum_{n} w_n(t)\mathrm{e}^{i\mathbf{q}\cdot\mathbf{r}_n(0)}\right\rangle^2. \tag{1.20}$$

We typically use the real part of the self-intermediate scattering function or the overlap function as the weight functions. Different choices of the weight function usually lead to similar results, as long as they probe distances less than a particle diameter. However, Flenner and Szamel [37] found an exception to this rule when they found choices of the weight function that had very different results for S_4. Then the weight function is measuring local motion. The four-point structure factor can be used to extract information about the size of regions of correlated particle motion.

Four point functions measure fluctuations in a system, but fluctuations can vary between systems that hold different global variables constant. However, the choice of ensemble does not affect S_4. Global variables like particle number N can be held constant in a particular ensemble, but those variables fluctuate over small regions of the simulation. For finite values of the wave vector q, which is inversely proportional to length, S_4 will probe local fluctuations. Thus, S_4 is ensemble independent. The $q = 0$ value of S_4 is a special case. When $q = 0$, it probes an infinite length, and thus we only see the global fluctuations. In this case,

ensemble matters. When q is set to 0 in eq. 1.20, then you have the general equation for the susceptibility χ_4. Thus, for the susceptibility ensemble matters.

We calculate the strength of dynamic heterogeneity with the susceptibility χ_4. The susceptibility measured in a particular ensemble is

$$\chi_4(t) = \frac{1}{N}\left[\left\langle \sum_{n,m} w_n(t) w_m(t) \right\rangle - \left\langle \sum_n w_n(t) \right\rangle^2\right], \tag{1.21}$$

for any weight function $w_n(t)$. The full susceptibility, (also known as the ensemble independent susceptibility), can be defined as $\chi_4(t) = \lim_{q\to 0} S_4(q;t)$, and it is proportional to the number of particles with correlated motion in a region. Note that the full susceptibility is ensemble independent, whereas the susceptibility of eq. 1.21 depends on what ensemble it is measured in. The difference between the ensemble independent susceptibility and the full susceptibility will be discussed below. The susceptibility as a function of time usually has a peak close to the relaxation time τ_α (the relaxation time of the average of the weight function). Equation 1.21 shows that the susceptibility gives the strength of the dynamic heterogeneity by measuring fluctuations around the average dynamics. The susceptibility measures fluctuations in a particular weight function. Consider a typical weight function like the overlap function. This function is a measure of the mobility of particles in the system. The susceptibility measures fluctuations in the overlap function, i.e. deviations of the overlap function from its average value. Thus when we average over time origins, if there is a bigger range of values for the overlap function at a particular time t, then the susceptibility will be bigger. We measure the susceptibility of a particular ensemble. The ensemble has constrained variables, like having a constant energy, E. We must investigate how allowing these variables to change effects the fluctuations of the overlap (weight) function.

The fluctuations that a susceptibility, from a particular ensemble, measures will depend on the ensemble of the calculation, and the type of dynamics of the system. In an NVE/microcanonical ensemble, for example, the number of particles, the volume, and the energy are all fixed, so the susceptibility will miss any fluctuations in those variables. To get these missing fluctuations, we transform the ensemble dependent χ_4 of eq. 1.21 to an ensemble where these fluctuations are allowed by adding correction terms to the susceptibility. The dynamics of a system can affect the susceptibility too, i.e. systems with Brownian dynamics will have a different susceptibility than system with Newtonian dynamics. However, the dynamics should mostly affect the susceptibility at short times, and only small differences remain between susceptibilities by the time diffusion begins. The suppressed fluctuations must always be taken into account when interpreting the susceptibility.

The fluctuations in a system depend on what ensemble you are in. For example, a constant particle number N ensemble represses fluctuations that would occur if particle number were allowed to change. Suppose we want to convert the fluctuations of variables $\mathscr{A}$ and $\mathscr{B}$ measured in a constant-F ensemble to a constant-f ensemble. Note that F and f must be conjugate variables. The general equation for converting fluctuations in one system to fluctuations in another system is

$$\langle \delta\mathscr{A}\,\delta\mathscr{B}\rangle_F = \langle \delta\mathscr{A}\,\delta\mathscr{B}\rangle_f + \left(\frac{\partial f}{\partial F}\right)\left(\frac{\partial}{\partial f}\langle\mathscr{A}\rangle_f\right)\left(\frac{\partial}{\partial f}\langle\mathscr{B}\rangle_f\right), \tag{1.22}$$

from eq. 2.45 of Ref. [38]. In eq. 1.22, $\delta\mathscr{A} = \mathscr{A} - \langle\mathscr{A}\rangle$, F is extensive (like total energy E), and f is intensive (like temperature T). We can apply eq. 1.22 to get the correction terms for all of the suppressed fluctuations, giving the ensemble independent susceptibility. In an

NVE ensemble, for example, we add correction terms to χ_4 for the suppressed fluctuations in temperature, particle concentration, and density.

Consider doing a transformation from an NVE ensemble to an NVT (canonical) ensemble, where particle number N, volume V, and temperature T are held constant, to get the temperature correction to $\chi_4(t)|_{NVE}$, the susceptibility in the NVE ensemble. Then $\mathscr{A} = \mathscr{B} = w(t)$, where $w(t)$ is the weight function from the susceptibility, $F = E$, and $f = \beta = 1/k_BT$. If we plug these values into eq. 1.22, we find $\partial\beta/\partial E = -1/(k_BT^2c_V)$, where c_V is the specific heat per particle at constant volume, and $\partial \langle w(t) \rangle / \partial\beta = \chi_T(t)(-k_BT^2)$, where we let the multipoint response function, $\chi_T(t)$, be $\chi_T(t) = \partial \langle w(t) \rangle / \partial T$. $\chi_T(t)$ measures the response of the average of the weight function, $\langle w(t) \rangle$, to a tiny change in temperature. The final result is

$$\chi_4(t)|_{NVT} = \chi_4(t)|_{NVE} + \frac{k_BT^2[\chi_T(t)]^2}{c_V}, \tag{1.23}$$

where $\chi_4(t)|_{NVE}$ is the susceptibility measured in the NVE/microcanonical ensemble, $\chi_4(t)|_{NVT}$ is the susceptibility measured in the NVT/canonical ensemble, and c_V is the specific heat per particle at constant volume. In Chapter 2, we will examine the other terms needed to take account of the other suppressed fluctuations in an NVE ensemble .

Experiments have difficulty measuring the susceptibility, χ_4, but they can use the above conversion techniques to estimate χ_4 using a much easier measurement of a response function, like $\chi_T(t)$. Measuring induced fluctuations with three point correlation functions, like $\chi_T(t)$, is easier than measuring the natural fluctuations in a system [33]. Three point correlations

can give a lower bound on the full susceptibility χ_4, such as

$$\chi_4(t) \geq \frac{k_B T^2}{c_P}[\chi_T(t)]^2, \tag{1.24}$$

where c_P is the specific heat per particle at constant pressure, (experiments are performed at constant pressure), and $\chi_T(t)$ is again the temperature derivative of the average of the weight function used in $\chi_4(t)$. χ_T can also be thought of as a measure of the sensitivity of the two-point correlation function to changing temperature. Eq. 1.24 can be considered a lower bound since we know that its right hand side could be the temperature correction term to an NPH ensemble, where P is pressure and H is enthalpy, $H = U + PV$, where U is internal energy of a system. In such an ensemble there would be fluctuations, and thus χ_4, which measures fluctuations, would be positive in that ensemble. Note that the right hand side of eq. 1.24 is nearly identical to the temperature correction term in eq. 1.23. It turns out to be a good estimate of χ_4 at low temperatures [39]. Using eq. 1.24, experimenters find that χ_4, and therefore the number of particles with correlated mobilities, increases as temperature is lowered, but increases more slowly close to T_g [40]. Now, experiments can have reasonable estimates of the number of particles in regions of correlated mobility, but these estimates are not an exact measurement of the length of the regions.

A length scale for dynamic heterogeneity, ξ_4, can be estimated from the susceptibility, which is proportional to the number of particles, but it also can be measured, without additional assumptions, from a fit to $S_4(q;t)$. We could guess that we have compact clusters, and $\chi_4 \sim \xi_4^d$, where d is the number of spatial dimensions of a system. In Chapter 2 we found that this guess is good in a number of fragile systems at low temperatures. This guess is not so good at mildly supercooled temperatures or for the strong system of Chapter 3.

Since we do not know the actual shape of correlated particle clusters, $\chi_4 \sim \xi_4^d$ will only give us an estimate of ξ_4. Instead we fit the Ornstein-Zernicke function,

$$\frac{\chi_4(\tau_\alpha)}{1 + (q\xi_4(\tau_\alpha))^2}, \tag{1.25}$$

to the small q values of $S_4(q;\tau_\alpha)$. In eq. 2.18, $\chi_4(\tau_\alpha)$ is the full susceptibility at $t = \tau_\alpha$, and ξ_4 is a measure of the length scale of regions of with correlated particle motion. Eq. 1.25 can be fit to $q \leq 1$ and $q\xi_4 < 1.5$, according to a method developed by Flenner and Szamel [36, 41]. With this method, we find that clusters are not always compact. Indeed, $\chi_4 \sim \xi_4^x$, where x can be less than d. Thus, fitting to $S_4(q;t)$ is necessary in order to get the length scale of dynamic heterogeneity, since we do not have a lot of information on the shape of the clusters.

One big problem with four-point correlation functions is that the averaging involved in these functions hide information about the shape of the regions, although there is current work to overcome that. As we saw, we can relate χ_4 and ξ_4 to get the degree of compactness of correlated regions, but not a precise shape. If the weight function in a four-point correlation function is itself a function of a vector like $\mathbf{k}$, i.e. the microscopic self intermediate scattering function, $\hat{F}_n(\mathbf{k};t) = \cos\mathbf{k}\cdot[\mathbf{r}_n(t) - \mathbf{r}_n(0)]$, then the four-point structure factor will be a function of two vectors, $S_4(\mathbf{k},\mathbf{q};t)$. If you vary the angle between $\mathbf{k}$ and $\mathbf{q}$, then you can look for anisotropy in clusters. In Ref. [1] investigators saw higher values of ξ_4 when the vectors were parallel than when they were perpendicular. Some progress is being made to get information about shape of clusters, though perhaps larger number correlation functions, like six-point correlation functions, are needed. An example of a six-point correlation function is examining the weight function of 3 particles instead of 2 particles.

Current simulations have shown signs of a glass transition, such as increasing relaxation time and dynamic correlation length, but more clear proof remains out of reach. We would expect to see the signs of a second order phase transition if we could equilibrate liquids down to the ideal glass transition temperature. In all kinds of experiments and computer simulations, researchers can now see a growing relaxation time, a growing susceptibility, and a growing length scale for dynamic heterogeneity upon deeper supercooling. Theories of supercooled liquids and the glass transition make predictions for dynamic heterogeneity. Comparing these theories to simulations results could allow us to distinguish between different theories. However at presently accessible temperatures, predictions are very close, and therefore we need to probe lower temperatures to really distinguish between different theories. One of the challenges of this field is examining systems that are more deeply supercooled or deeper in the energy landscape. Vapor deposited glasses, described in the next section, Section 1.4 appear deep in the energy landscape, and seem to behave like glasses that were aged for thousands of years [42], or perhaps supercooled liquids that were cooled to a glass extremely slowly.

1.4. Vapor deposited glasses

Vapor deposited glasses are prepared with a technique that makes them much more stable than glasses created by cooling. One idea for how stable vapor deposited glasses are comes from the energy landscape. Figure 1.8 shows a one dimensional representation of the energy landscape, where potential energy is plotted as a function of position. The graph shows a series of hills and valleys. In the figure, glasses that were cooled slower get trapped in deeper energy minima than glasses that were created by faster cooling. The high stability of vapor deposited glasses has suggested to some that vapor deposited glasses can be thought of as

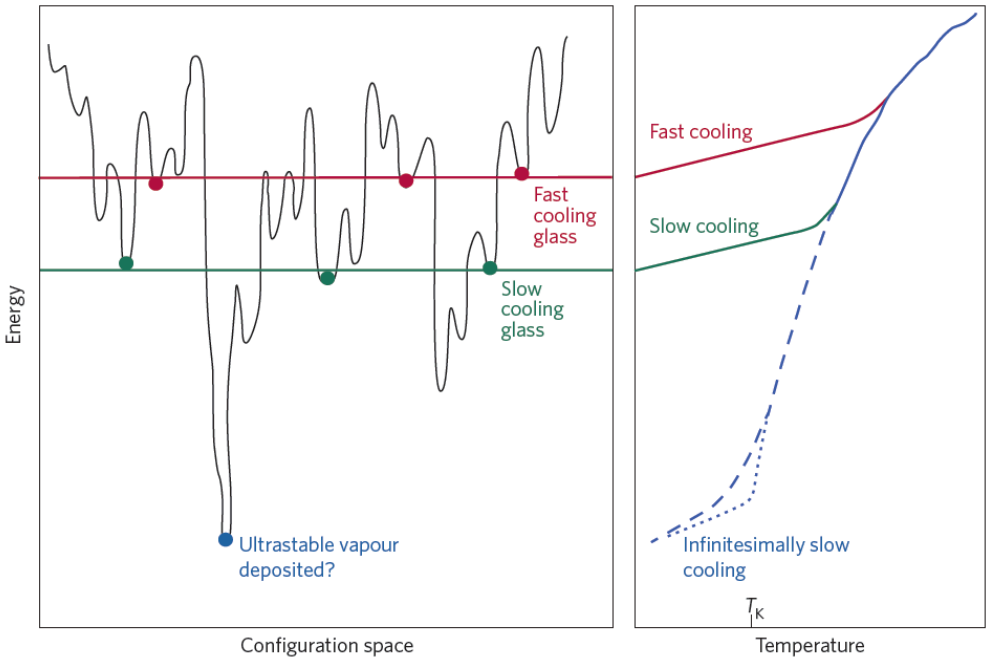

FIGURE 1.8. A one-dimensional representation of the energy landscape taken from Figure 1 of the paper by Parisi and Sciortino [44]. Glasses get stuck in various minima. The panel on the right shows the temperature dependence of the energy with a fast and a slow cooling rate. The figure suggests that ultrastable vapor deposited glasses, which will be discussed more in Chapter 4, are in a very deep energy well that might be equivalent to the liquid being cooled extremely slowly. *Republished with permission from Nature Publishing Group.*

liquids that are cooled infinitely slowly. Figure 1.8 includes an example of an infinitely slow cooling and its corresponding minimum in the energy landscape. There is no way to test this idea, since very slow cooling almost always results in a crystal instead of a glass. However, vapor deposited glasses have been compared to glasses that have been aged for hundreds of years [43]. Like glasses that are cooled more slowly, aged glasses can also explore the energy landscape and come to a lower energy minimum in the energy landscape. Due to their long apparent age, vapor deposited glasses are called ultrastable glasses.

Swallen *et al.* [45] discovered that vapor deposited glasses could be ultrastable. They create glasses by vapor depositing a material, such as indomethacin (IMC), an anti-inflammatory drug, or trisnaphthylbenzene (TNB), an organic glass former, onto a substrate that was held

at a fixed temperature that was below the glass transition temperature T_g of the material. There is a very small temperature range for the substrate that allows for the creation of highly stable glasses. The temperature that makes the most stable glasses is usually around 15% below T_g in most materials [46]. For each material, they found specific temperatures for the substrate that created highly stable glasses. They measured kinetic stability of their deposited materials by monitoring a glass as it was slowly heated at a constant rate. Kinetics is the rate of change of a system going through a physical or chemical change. Here the change we examine is melting. The kinetic stability is the stability against melting occurring. Swallen *et al.* measured the heat capacity as a function of temperature, which has a spike when the glass melts. They called the temperature where this spike occurred the onset temperature for melting. They found that this onset temperature was much higher in a vapor deposited glass than in a glass that had been produced by ordinary cooling and annealing at a constant temperature below T_g. A higher onset temperature indicates that the system needs more energy to bring it out of its glassy state. Thus, a system with a higher onset temperature has higher kinetic stability. Sepúlveda *et al.* [47] measured kinetic stability by finding a stability ratio in methyl-m-toluate, MMT. They measured how quickly a sample of MMT returned to a liquid state when it was held at a liquid temperature using the dielectric response. They called the time it took for the glass to return to a liquid the transformation time, t_{trans}, and they scaled t_{trans} by τ_α to get a stability ratio. By this measure, they found they could create a vapor deposited glass with a stability ratio that was larger than the stability ratio of a glass created by cooling and annealing by $10^{3.7}$. Kearns *et al.* [43] examined mechanical stability in vapor deposited ultrastable glasses by studying elastic moduli. Elastic moduli measure how stable a system is in the face of outside stresses.

Examples of elastic moduli are Young's modulus, the bulk modulus, and the shear modulus. For the materials IMC and TNB, they saw that each of these elastic moduli were higher in glasses prepared by vapor deposition than in those glasses prepared by ordinary cooling and annealing.

Swallen *et al.* [45] suggested a mechanism that explains the high stability of vapor deposited glasses. They suggested that the enhanced mobility on the surface allows the surface molecules to find more stable configurations than they would in the bulk of the material. This surface mobility allows a highly stable material to be created when a glass is slowly deposited one layer at a time. Zhu *et al.* [48] did an experiment on indomethacin (IMC), where they found much higher diffusion at the surface than in the bulk of a material. Shi *et al.* [49] studied the Kob Andersen binary Lennard-Jones mixture [27], and showed that surface atoms of a model thin film glass are more mobile than interior atoms. They also saw that surface atoms explored the energy landscape more efficiently than atoms in the film's interior. They determined that surface atoms were better at exploring the energy landscape by performing an energy minimization on their film, finding the inherent structure energy. They found that the surface atoms reach a deeper energy minimum relative to their initial potential energy than interior atoms. In many studies, both theoretical and computational, researchers found a relationship between surface mobility and ultrastable glasses [50–52, 46, 42].

Though our study focused on the stability of vapor deposited glasses, other interesting aspects about them have been explored. Researchers studying vapor deposition have examined anisotropy in the glasses, melting fronts, and deposition rate, among other topics. Some glasses have anisotropy. For example, in a computer simulation of trehalose, Singh and de

Pablo [52] saw that the molecules made layers parallel to the substrate. They found that the pair correlation function, $g_z(r)$ in the direction perpendicular to the substrate was very different than that of an ordinary glass (one created by cooling and/or annealing). Molecular orientation can also be anisotropic. Lyubimov *et al.* [53] did a simulation to examine the dependence of molecular orientation on substrate temperature. They found that as the substrate temperature was lowered from T_g, molecules first had no particular orientation, then went to a mildly perpendicular orientation to the substrate, to a parallel orientation to the substrate at low temperatures. The melting of vapor deposited glasses is different from that of ordinary glasses. In a computer simulation, Lyubimov, Ediger, and de Pablo [42] found that heating the stable glass created mobile particles at the top surface, and the mobility propagated into the film, melting it. Researchers have also seen these mobility fronts in experiments [54]. Holding the particles at the surface still caused the mobility to begin in the interior of the film, and the melting took longer. Ordinary glasses melt uniformly, and faster than stable films. The importance of the deposition rate has been studied by Chua *et al.* [55], who did experiments that examined the dependence of stability on the deposition rate of the glass, and how deposition rate interacts with substrate temperature. Faster deposition rates produce less kinetically stable glasses, but stability seems to level off at slow enough deposition rates.

1.5. Theories of the glass transition

The glass transition is an unsolved problem, and many theories exist to explain it. In this section, we discuss some of these theories. While some theories may not apply at all temperatures, most have useful ideas we can take away.

1.5.1. Mode coupling theory. The mode coupling theory (MCT) of the glass transition was developed by Leutheusser [56] and Bengtzelius, Götze, and Sjölander [57]. It predicts the behavior of time correlation functions like the self-intermediate scattering function and the mean square displacement, using the static structure factor as input [4].

MCT describes density fluctuations using the intermediate scattering function, $F(\mathbf{k}, t)$. Microscopic density is given by

$$\rho(\mathbf{r}, t) = \sum_i \delta(\mathbf{r} - \mathbf{r}_i(t)). \tag{1.26}$$

The Fourier transform of the microscopic density is

$$\rho_{\mathbf{q}}(t) = \sum_i \int \mathrm{d}\mathbf{r} \mathrm{e}^{i\mathbf{q}\cdot\mathbf{r}} \delta(\mathbf{r} - \mathbf{r}_i(t)) = \sum_i \mathrm{e}^{i\mathbf{q}\cdot\mathbf{r}_i(t)}. \tag{1.27}$$

The intermediate scattering function is the autocorrelation function of the Fourier transform of the microscopic density, eq. 1.27. It is given by

$$F(k, t) = \frac{1}{N} \left\langle \rho_{-\mathbf{q}}(0) \rho_{\mathbf{q}}(t) \right\rangle = \frac{1}{N} \sum_{i,j} \left\langle \mathrm{e}^{-i\mathbf{q}\cdot\mathbf{r}_i(0)} \mathrm{e}^{i\mathbf{q}\cdot\mathbf{r}_j(t)} \right\rangle. \tag{1.28}$$

In MCT the time dependence of the intermediate scattering function is derived from first principles using projection operators, resulting in the equation

$$\frac{\mathrm{d}^2 F(q,t)}{\mathrm{d}t^2} + \frac{q^2 k_B T}{m S(q)} F(q,t) + \int_0^t \mathrm{d}\tau K(q,\tau) \frac{\mathrm{d}}{\mathrm{d}t} F(q, t-\tau) = 0, \tag{1.29}$$

where m is mass, T is temperature, $K(q,t)$ is the memory function, and $S(q)$ is the static structure factor, which is equivalent to the $t = 0$ value of the intermediate scattering function, $F(q, t = 0) = (1/N) \left\langle \rho_{-\mathbf{q}}(0) \rho_{\mathbf{q}}(0) \right\rangle = S(q)$. Eq. 1.29 is a formally exact equation. It

is used as a starting point for finding other equations of MCT. The memory function cannot be calculated exactly. Therefore it must be approximated. MCT makes a particular approximation for the memory function. The memory function has a four-point function, which is an autocorrelation function of two particle density functions. In the approximation, this four-point function is factorized into two intermediate scattering functions. This approximate memory function is

$$K_{MCT}(q,t) = \frac{\rho k_B T}{16\pi^2 m} \int \mathrm{d}\mathbf{k} |V_{\mathbf{q}-\mathbf{k},\mathbf{k}}|^2 F(k,t) F(|\mathbf{k}-\mathbf{q}|,t), \tag{1.30}$$

where the vertex function is $V_{\mathbf{q}-\mathbf{k},\mathbf{k}} \equiv (\hat{\mathbf{q}} \cdot \mathbf{k}) c(k) + \hat{\mathbf{q}} \cdot (\mathbf{q}-\mathbf{k}) c(|\mathbf{q}-\mathbf{k}|)$, $\hat{\mathbf{q}}$ is a unit vector in the $\mathbf{q}$ direction, and the direct correlation function $c(k)$ is $c(k) \equiv (1/\rho)(1 - 1/S(k))$.

MCT makes a number of predictions from solutions to eq. 1.29 and eq. 1.30. MCT predicts a glass transition temperature at T_c, where relaxation time, τ, diverges. The relaxation time obeys

$$\tau(q,t) \sim A_q (T - T_c)^{-\gamma}, \tag{1.31}$$

which is eq. 57 of Ref. [15], where A_q is a function of q and γ is a constant. Eq. 1.31 can be used as a fit in real and model systems. This fit usually works from the onset temperature for glassy dynamics down to a temperature a bit above T_c. MCT has other successful predictions as well. MCT successfully predicts the time dependence of the early beta relaxation decay right before the plateau and the plateau in late beta relaxation for $F(q,t)$ [58, 59]. It also predicts stretched exponential decay in the α relaxation, which works well. Stretched exponential decay is discussed in Section 1.3. Another useful prediction of MCT [60] that many systems obey and can be seen in experiments [61] is time temperature superposition.

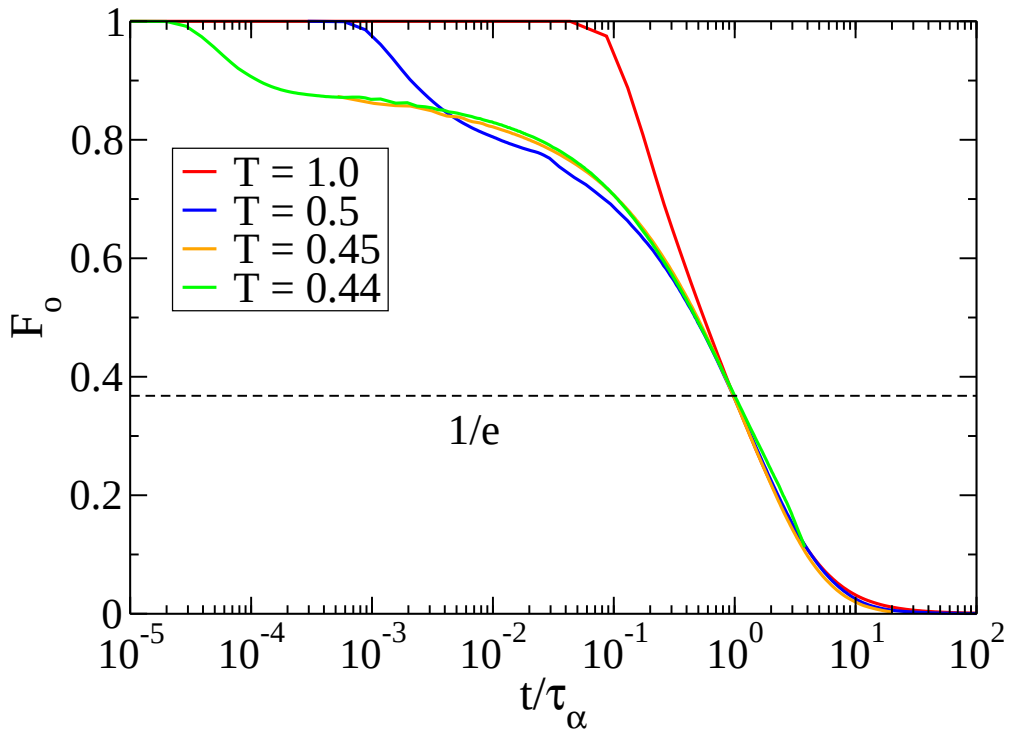

FIGURE 1.9. The average overlap function $F_o(t)$ in the KA system with $a = 0.25$ at the liquid temperature of 1.0 and at the supercooled liquid temperatures of 0.5, 0.45, and 0.44. Time has been rescaled so that all the relaxation times are equal to 1.

To understand time temperature superposition, consider a correlation function measuring mobility, such as the average overlap function, eq. 1.12. According to MCT, if time is rescaled by the α relaxation times, τ_α, then the final decays for times greater than τ_α will match up (superimpose) for all temperatures. Figure 1.9 demonstrates that the KA system obeys time temperature superposition, for the temperatures shown.

We have mentioned a number of successful prediction of MCT, but these predictions only work for a particular range of temperatures. These predictions do not apply outside of that range. MCT makes reasonable predictions over a small temperature range just below the melting temperature, T_m, equivalent to a change of relaxation time of about 2 to 3 decades. However, as we saw in Section 1.2, fits to the relaxation time versus temperature, eq. 1.31, fail below temperatures a bit above T_c, as the actual glass transition occurs at $T_g < T_c$. At

lower temperatures, systems are deeply supercooled, and have greater dynamic heterogeneity. MCT does not account for the increased fluctuations in the system that accompany dynamic heterogeneity [9]. However, extensions to MCT have tried adding fluctuations to the theory by adding corrections due to higher order correlations in the memory function [62]. Szamel [62] found an initial set of corrections, and then Janssen, Mayer, and Reichman [63] and Janssen and Reichman [64] created a way to extend corrections to infinite order. They found that their results corresponded to the results of basic mode-coupling theory above T_c, and that they could make predictions at deeply supercooled temperatures that are out of the range of current simulations.

1.5.2. Random first-order transition theory. Kirkpatrick, Thirumalai, and Wolynes were some of the many researchers that developed random first-order transition, RFOT, theory. (See their work in Refs. [65–67].) RFOT uses a mean-field approach to study the free energy landscape using an order parameter such as density [4]. We will consider the free energy landscape with a lattice model, which can be extended to continuous systems [19, 4]. The Landau potential (a thermodynamic potential) for a lattice system is

$$W(\{\mu_i\}) = -\frac{1}{\beta}\log\left(\sum_{\{n_i\}}\exp\left[-\beta H(\{n_i\}) - \beta\sum_{i=1}^{N} n_i\mu_i\right]\right), \tag{1.32}$$

where μ_i is the chemical potential at a site i, $\beta = 1/(k_B T)$, n_i is the number of particles at a site i, and H is the Hamiltonian [19, 4]. The free energy function is

$$F(\{\rho_i\}) = W(\{\mu_i^*\}) + \sum_i \mu_i^*\rho_i, \tag{1.33}$$

where the μ_i^*'s are determined by

$$\frac{\partial W}{\partial \mu_i} + \rho_i = 0 \tag{1.34}$$

[19, 4]. The above equations can be generalized to a continuous system by replacing n_i with the continuous density $\rho(\mathbf{x})$ [4]. The free energy landscape can be found by examining the free energy function, F, at all values of ρ_i [19, 4]. We can find the minima of the free energy landscape by taking the derivative of F, eq. 1.33, with respect to ρ_i. This derivative is

$$\frac{\partial F}{\partial \rho_i} = \mu_i^* \tag{1.35}$$

[4]. This equation shows that the free energy is at a stationary point, minimum or saddle point, if the chemical potential μ_i is 0. Thus, if there are no external fields or local chemical potentials, then solving eqs. 1.32 and 1.33 for F will give the stationary points of F [19, 4]. The stationary points of F include many minima. The number of free energy minima is $\mathscr{N} = \exp(\Sigma N)$, where Σ is the complexity and N is the number of particles in the system [19, 4].

RFOT has two important temperatures, where it predicts changes in the dynamics of a system. Below a temperature T_x, an equilibrium liquid breaks up into many states. At times less than the alpha relaxation time τ_α, the system is trapped in a metastable state of the free energy landscape. At times around τ_α, the system begins to explore other equilibrium states, hopping between states in the free energy landscape [19]. This hopping is known as activated dynamics. T_x is often identified with T_c [68], where RFOT envisions that there is a slow down in dynamics due to the onset of activated dynamics. Physically, when this slow down happens, the system transitions to many random aperiodic structures [69]. At

the Kauzmann temperature T_K the complexity, $\Sigma(T)$ drops to 0 [4]. Thus, at T_K, RFOT predicts a thermodynamic phase transition [4].

Mean-field theory predicts that below the temperature where the system transitions to aperiodic states, the states have infinite lifetimes [4, 69]. However, the states do not have infinite lifetimes in reality, and particle rearrangements have been seen to occur at lower temperatures. To take rearrangements into account, RFOT applies mosaic theory, which describes the rules for particle rearrangements [19]. Thermal fluctuations will allow rearrangements in the system [18], and RFOT assumes that the system has a number of rearranging regions. Consider a region of size R. The free energy cost due to rearranging is the free energy due to surface tension, YR^θ, where Y represents surface tension [67]. The free energy due to configurational entropy is $TS_c(T)R^d$, where d is the number of spatial dimensions. The configurational entropy, S_c, is like that discussed for Kauzmann's paradox. At a lengthscale $R = \xi$, there is a crossover from YR^θ dominating the free energy to $TS_c(T)R^d$ dominating the free energy. When these free energies are set equal we get the typical size of a rearranging region, ξ. In three dimensions ξ is

$$\xi \sim \left(\frac{Y(T)}{TS_c(T)}\right)^{1/(3-\theta)}, \tag{1.36}$$

as in eq. 129 of Ref. [18]. ξ is the typical size of rearranging regions. Smaller droplets are unstable, because their free energy cost from surface tension is too high. Larger droplets take a longer time to rearrange, since the time to rearrange increases with the size of the droplet [18]. They will break into small droplets that can rearrange faster.

Stevenson, Schmalian, and Wolynes [70] use RFOT to demonstrate why rearranging regions should be compact at temperatures near T_K. The free energy cost of a region

rearranging has a term that scales negatively with temperature times an entropy and the free energy cost that scales positively due to the surface tension can be thought of as a cost for the number of interactions with particles outside a rearranging region that are broken. As temperature increases you need fewer surface bonds to match the drop in the free energy due to entropy. Thus, as temperature increases, you can have more surface interactions and allow for more string like clusters. As temperature decreases, you need to minimize the number of surface interactions, and thus have more compact clusters. In Chapter 2 and Chapter 3 we investigated the compactness of clusters as temperature is decreased. Stevenson, Schmalian, and Wolynes [70] predicted that regions become compact below a crossover temperature and are compact down to T_K.

Another prediction from RFOT made by Xia and Wolynes [71] is about a relationship between the size of a rearranging region and fragility. They broke up their liquid into lattice sites. They derived a relationship between the characteristic size of rearranging regions ξ and fragility. They predicted that

$$\xi \sim D_l^{2/3}, \tag{1.37}$$

where D_l is a measure of fragility, i.e. a higher D_l means the system is more fragile. They found an expression for the free energy barrier to rearrange particles that scaled like the Vogel-Fulcher law of eq. 1.6, which has a fragility parameter D. D_l took the place of the fragility parameter in this free energy barrier equation. D_l has the value of

$$D_l = \frac{27}{16}\pi \frac{nk_B}{\Delta\tilde{c}_p} \ln^2 \frac{\alpha_L r_0^2}{\pi \mathrm{e}}, \tag{1.38}$$

where n is the density of particles. In eq. 1.38 the heat capacity per unit volume increases by $\Delta\tilde{c}_p$ when the glass is heated through the glass transition [72, 73]. In this case, the glass transition temperature is defined as the temperature where the heat capacity first shows an increase when the glass is being heated [72]. In the model used in Ref. [71], α is a spring constant at a lattice site, which determines the root mean square displacement from that site, α_L is the lowest value of α for which the free energy has a minimum, where $\alpha_L^{-1/2}$ is a root mean square displacement, and r_0 is the lattice spacing.

1.5.3. Facilitation. The theory of dynamic facilitation says that low temperature liquids near T_g are almost solid and movement inside them is rare [4]. The theory does not examine structure, but just particle movement. The rearrangement of particles is likely to quickly facilitate the rearrangement of nearby particles. The timescale of these motions is much faster than the relaxation time of the system [4]. The theory postulates that regions can only move if they are near a mobile region. This behavior begins at a temperature below the onset temperature T_o. Some researchers believe that this temperature is around the mode-coupling temperature, T_c [4, 74]. However, the theory may only be useful near T_g, where the liquid is very viscous. It is unclear if the idea that motion can only occur through motion of nearby particles is correct or not [4].

The concentration of regions of mobile particles drops as temperature is decreased. For a given particle displacement length a, the concentration of mobile particles c_a is

$$c_a \propto \exp[-J_a(1/T - 1/T_o)], T < T_o, \tag{1.39}$$

where J_a is a fitting parameter that depends on a [75]. Dynamic facilitation associates a length ξ_{fac} with the distance between regions of mobility. The theory suggests that this

length is $\xi_{fac} \sim c^{-1/d}$, where d is the number of dimensions of the system [76]. As the temperature drops, and mobile events become rarer, the distance increases. Thus, at absolute zero temperature, where there is no motion, $c = 0$, and ξ_{fac} diverges. Thus this theory considers the true glass transition to take place at $T = 0$.

For a given particle displacement length a, the concentration of defects c_a is

$$c_a \propto \exp[-J_a(1/T - 1/T_o)], T < T_o, \tag{1.40}$$

Garrahan and Chandler [76] found a relation between ξ_{fac} and fragility by examining a simple spin model. In this model they related the relaxation time, τ, which is the time scale for equilibration, the concentration of mobile sites, and temperature. They found τ as a function of T. They fit some experimental data to the $\tau(T)$ of the model, and found a value of the concentration of mobile sites, c_g, at the glass transition temperature, T_g, in five systems, with a range of fragilities. They found that c_g got smaller as they examined stronger systems. Combining this result with the relationship between ξ_{fac} and c, they found that a stronger system should have a longer dynamic correlation length, based on this spin model. We examine the relationship between dynamic correlation length and fragility in Chapter 2.

1.5.4. Geometric frustration. Kivelson *et al.* [77] assume that a liquid has a preferred local structure, which minimizes the free energy of a few particles [9]. If the preferred local structure does not fill space, then the system can become frustrated, and can't form a crystal with that structure. They postulated that at a temperature T^*, which is usually above the melting point, T_m, a liquid that is being cooled can avoid a phase transition and become supercooled if the system is geometrically frustrated. This avoided phase transition

corresponds to the system hypothetically crystallizing with the locally preferred structure. The actual crystallization would form a different structure. Frustration has been observed in the binary Lennard-Jones Wahnström model [78]. In this system the 13 particle [9] icosahedron is a locally favored structure [79]. Icosahedra can't fill space, and thus can't form a crystal [9]. Hence the system feels geometric frustration.

After the avoided transition, frustration causes the system to break up into regions of unfrustrated order that have finite length [77]. The length, R_D, of these regions is

$$R_D \sim (1 - T/T^*)^{\nu}/K_f^{1/2}, \tag{1.41}$$

where K_f is a set value for frustration in the system, ν is a constant, and T^* is the temperature where the freezing transition would have occurred if there was no frustration in the system. Kivelson *et al.* found eq. 1.41 by considering a frustrated spin system where K_f is a parameter in the Hamiltonian. The Hamiltonian had a short range term and a long range Coulombic term, which had an explicit value for frustration K_f appearing in it. Examining eq. 1.41 we see that more frustrated glasses have smaller length scales, since they have more defects, and thus it is more difficult to grow regions of local order [4]. From eq. 1.41, we see that the size of the regions where there is local order does not diverge in this theory, matching the idea that frustration never allows total order in the system.

In simulations. researchers have seen that more fragile glass-formers have less frustration than stronger glass-formers [80–82]. Grousson *et al.* [80, 81] examined a three dimensional cubic lattice spin model. It has the same Hamiltonian as was used by Kivelson *et al.* [77], where the frustration K_f explicitly appears in the Hamiltonian. They did Monte Carlo simulations on spin models with 2, 5, and 11 spin orientations. They found fragility with fits

to the relaxation time. They found that a larger frustration corresponded to less fragility, and thus a stronger system. Sausset, Tarjus, and Viot [82] investigated a monotonic Lennard-Jones two-dimensional simulation on a hyperbolic plane with negative curvature. On a flat surface the locally favored structure is hexagonal [9], and thus the preferred number of nearest neighbors is 6, a packing which leads to space being filled. If the hyperbolic plane has curvature, then hexagons can no longer fill space. The distance between two points on the plane is found with the hyperbolic metric equation. The frustration κ appears as an explicit term in this equation. They could associate the amount of curvature of the plane, (which was controlled by κ), with an amount of geometric frustration. They found that as curvature increased or equivalently as frustration increased, the fragility of the system decreased, i.e. the liquid got stronger. Note that a more definitive study on relating fragility and frustration would investigate changing frustration in a regular three-dimensional system.

Some groups have found a connection between regions of unfrustrated order in a glass and particle mobility. Dzugutov *et al.* [83] modeled a system that had icosahedra as the most common local structure. They found that icosahedral regions had slower diffusion than the average diffusion for the system. Another group, Pedersen *et al.*, also studied icosahedra, this time in the Wahnström model [78], where the icosahedron is a locally favored structure. They also saw that particles in icosahedra were less mobile than average. Sausset, Tarjus, and Viot [82], in their study of particles on a hyperbolic plane, also saw that regions with local order, (hexagonal order in this system), were correlated with regions with less particle mobility. These findings might suggest that particles in slower regions are less mobile because they are in a more energetically favorable state. However, Hocky *et al.* [79] studied the most common local structure in a number of model glass formers. They found that the correlation between

regions of the most common local structure and the particle mobility in those regions was very variable for different systems. Some systems had strong correlation between structure and dynamics, while others showed almost no correlation. Thus the length, R_D, should not too hastily be associated with the length scale of dynamic heterogeneity, which measures regions of mobile or immobile particles.

1.5.5. Review. These glass transition theories are very useful, though some have shortcomings. Many people in the field hope to find a universal theory that describes the glass transition in all glassy materials. The theory of geometric frustration, which is described in Section 1.5.4, underlines the importance of the structures that exist in glasses, but it treats every glass differently depending on its local structure. The mode-coupling theory (MCT), which is described in Section 1.5.1 does a very good job of describing dynamics over an unfortunately small range of temperatures. However, in computer simulations, it is often difficult to equilibrate below T_c, so we often operate in that range. Random first order transition (RFOT) theory, which is described in Section 1.5.2, uses MCT to describe dynamics at high supercooled temperatures. It deviates from MCT below a temperature around T_c, making it slightly challenging to confirm its predictions in computer simulations [1]. Although, some researchers have performed simulations below T_c, allowing some testing of RFOT theory's predictions. The theory of dynamic facilitation of Section 1.5.3 possibly applies to temperatures near T_g, well out of the range of computer simulations, though it can be tested at higher temperatures, where it makes predictions. Unfortunately, it does not take structure or thermodynamics [9] into account, only mobility. Many of these theories have support from computer simulations and experiments, and we often compare our simulations

to several different theories. So far, none of these theories are accepted, (by everyone), as **the** theory of the glass transition.

CHAPTER 2

Universal features of dynamic heterogeneity in fragile glass formers

This chapter is based on my first paper [1] in Professor Szamel's group, which was "Universal features of dynamic heterogeneity in supercooled liquids" by Flenner, Staley, and Szamel. I was the second author for my work on modeling and analyzing one of the systems that appeared in that paper.

2.1. Background

Supercooled liquids display universal features, like the emergence of a plateau in the mean square displacement upon cooling, and dynamic heterogeneity upon cooling. Theories about the glass transition have predictions about dynamics and dynamic heterogeneity. In order to test whether these predictions are universal, we investigated dynamic heterogeneity in not just one, but five different glass-forming systems. We found universal relationships between variables that characterize dynamic heterogeneity. A change in relationships appeared to start when the Stokes-Einstein relation was violated. The Stokes-Einstein relation states that the diffusion coefficient is related to temperature divided by viscosity, $D \sim (T/\eta)^1$. At lower temperatures, the exponent becomes less than one, and the Stokes-Einstein relation is violated.

A main motivation for this study comparing different glass-formers was to study the effect of attraction in an interparticle potential. Berthier and Tarjus [84] examined two model liquids that had the same potential except one had the attractive part of the potential cut off. They observed that the relaxation was very different in the two systems as the glass transition

was approached. Pedersen, Schrøder, and Dyre [85] found a different system that was purely repulsive, but had the same dynamics as the original attractive and repulsive potential studied by Berthier and Tarjus. Hocky, Markland, and Reichman [86] examined a particular length, known as the point-to-set length, in the systems that Berthier *et al.* and by Pedersen *et al.* studied. They saw that this length was correlated with the average dynamics, as quantified by the relaxation time, and had universal features in all the systems. Particularly, they found that data for scaled length plotted as a function of inverse temperature followed a single curve for all systems studied, as did relaxation time as a function of length and relaxation time as a function of length divided by temperature. Another group did a study on the effects of attraction in the potential and found another result regarding clusters of correlated particles. Zhang, Yunker, Habdas, and Yodh [87] studied two dimensional colloidal systems that had purely repulsive potentials and repulsive and attractive potentials. They found that the size and shape of clusters of fast particles depended on whether the attractive part of the potential was present or not. We note that Hocky *et al.* performed computer simulations, which examined slow particles in three dimensional systems.

Another motivation for this study came from a study by Flenner and Szamel [88] investigating dynamic heterogeneity in the harmonic sphere system [89]. They discovered a candidate for a temperature marking a crossover in dynamics. They examined the dynamic correlation length ξ_4 as a function of both the relaxation time τ_α and the diffusion coefficient D. They found that $\tau_\alpha \sim \exp(\xi_4)$ and $D^{-1} \sim \exp(\xi_4^{3/2})$ were good fits to all their data. However they found that a commonly used form of the Stokes-Einstein relation, $D \sim \tau_\alpha^{-1}$, was true at high temperatures. If this relation is true then τ_α and D^{-1} should have the same relationship with ξ_4. They found that they could fit $\tau_\alpha \sim \exp(\xi_4)$ and $D^{-1} \sim \exp(\xi_4)$

to high temperatures, and $\tau_\alpha \sim \exp(\xi_4^{3/2})$ and $D^{-1} \sim \exp(\xi_4^{3/2})$ to lower temperatures. The point where these fits seemed to cross occurred below the temperature range where the Stokes-Einstein relation was valid, and above the temperature range where a fractional Stokes-Einstein relation, $D \sim \tau_\alpha^{-z}$, where $z < 1$, was valid. We call the point where the fits to the Stokes-Einstein relation and the fractional Stokes-Einstein relation intersect the point of Stokes-Einstein violation, and the temperature at that point is the Stokes-Einstein violation temperature, T_s. The Stokes-Einstein violation temperature seemed like a natural point for a change in dynamics, since the need for different fits was caused by the Stokes-Einstein relation. Note that having different fits at the high temperatures would have not mattered very much if, above T_s, $\xi_4 \lesssim 1$, which is the order of a particle diameter (in reduced Lennard-Jones units,), but $\xi_4 \approx 2.5$ at T_s.

The Stokes-Einstein violation temperature, T_s, has proven to be a good marker of a crossover in the dynamics in all five glass-formers we studied. The Stokes-Einstein relation is $D \sim T/\eta$, where D is the diffusion coefficient, T is temperature, and η is the viscosity. Most of the time, researchers in this field use the relaxation time τ_α giving the relation of $D \sim 1/\tau_\alpha$, which we used in this case, in order to be consistent with previous work. We examined dynamic heterogeneity in five fragile glass-formers by measuring four point structure factor, S_4, with the overlap function and the real part of the self-intermediate scattering function as weight functions, $w_n(t)$, which measure mobility. From the four point structure factor, we found the susceptibility, χ_4, a measure of the number of particles with correlated mobility, and the dynamic correlation length, ξ_4, a measure of the length of such regions. We also examined the relaxation time. We found remarkable similarities in the different systems, with the dependence of χ_4 on ξ_4 and the dependence of ξ_4 on τ_α being the

same in different systems. We found that all systems have the same dependence of length on the relaxation time rescaled to the relaxation time where the Stokes-Einstein violation occurs. We also investigated anisotropy of dynamic correlation length in the dynamic heterogeneity, finding some anisotropy for one choice of $w_n(t)$.

2.2. Simulations

In many glassy systems that we work with we use two particle types with different sizes. This mismatch of sizes allows the system to avoid crystallization and instead form a glass. The following glass formers all have two particle sizes.

We simulated the Kob-Andersen (KA) potential [27], which is a binary Lennard-Jones potential. The potential is

$$V_{\alpha\beta}^{KA}(r) = 4\epsilon_{\alpha\beta}\left[\left(\frac{\sigma_{\alpha\beta}}{r}\right)^{12} - \left(\frac{\sigma_{\alpha\beta}}{r}\right)^{6}\right], \tag{2.1}$$

where r is the distance between two particles, ϵ is the depth of the potential energy well, σ is the diameter of the particle, and α and β are particle types 1 or 2. 80% of particles are type 1 and 20% are type 2. The parameters of eq. 2.1 are $\sigma_{11} = \epsilon_{11} = m_1 = m_2 = 1$, $\epsilon_{12} = 1.5\epsilon_{11}$, $\epsilon_{22} = 0.5\epsilon_{11}$, $\sigma_{12} = 0.8\sigma_{11}$, and $\sigma_{22} = 0.88\sigma_{11}$. The potential is cutoff at $2.5\sigma_{\alpha\beta}$. This system was studied with Newtonian dynamics. For the KA system, the units for length, energy, and time are σ_{11}, ϵ_{11}, and $\sqrt{m_1\sigma_{11}^2/\epsilon_{11}}$ respectively[1]. We set $k_B = 1$. Our simulations use 27 000 particles at a number density of $\rho = N/V = 1.20$. We simulated temperatures from 0.47 to 1.0. We ran NVE simulations. For temperatures $T < 0.5$, we instead performed NVT simulations with a Nosé-Hoover thermostat, since NVE simulations had an energy drift at

[1]Note that we can examine the Lennard-Jones units in liquid Argon. In argon these units become 3.4Å, 120Kk_B, and 3×10^{-13}s respectively [27].

these temperatures. At all temperatures, we performed at least one equilibration run at least $100\tau_\alpha$ long, and we performed four production runs which were at least $100\tau_\alpha$ long, where the relaxation time, τ_α, is defined by eq. 1.11.

We considered an inverse power law (IPL) potential [90], which just has a repulsive term. The potential is given by

$$V_{\alpha\beta}^{IPL}(r) = A_{IPL}\epsilon_{\alpha\beta}\left(\frac{\sigma_{\alpha\beta}}{r}\right)^{n_{IPL}}, \tag{2.2}$$

where $A_{IPL} = 1.945$ and $n_{IPL} = 15.48$. The values of A_{IPL} and n_{IPL} were chosen so that the potential energy fluctuations have similar magnitudes in the KA and the IPL systems [90]. The σ and ϵ parameters are the same as in the KA potential, as is the cutoff. Again the ratio of particle type 1 to particle type 2 is $N_1 : N_2 = 80 : 20$. We used Newtonian dynamics to model this system. The IPL system uses the same units for length, energy, and time as the KA system, and again $k_B = 1$ and $m_1 = m_2 = 1$. Simulations use 27 000 particles at a number density of $\rho = 1.20$. We performed the NVE and NVT production runs described for the KA system, at the same temperatures as for the KA system.

We also simulated the Weeks-Chandler-Andersen (WCA) truncation [91, 92] of the KA system. The WCA truncation cuts off the potentials at the minimum value. We used Newtonian dynamics with this system. Again, we use the same units for length, temperature, time, and mass, and set $k_B = 1$. We use a system size of 27 000 particles and a particle density of $\rho = 1.20$. We simulated temperatures from 0.4 to 1.0. In this system, we only ran NVE simulations. At all temperatures we ran at least one equilibration run for $100\tau_\alpha$ and four production runs, which were also at least $100\tau_\alpha$ long. Recall that τ_α is defined by eq. 1.11.

We simulated hard spheres (HARD) [93], which have an infinite potential below the cutoff radius and a potential of 0 above that radius. The HARD system we studied is a 50:50 binary mixture. The diameter of the larger sphere is 1.4 times that of the smaller sphere. The HARD system does not have any temperature dependence, but instead the control parameter is the volume fraction, ϕ. The volume fraction is the fraction of the total volume that the spheres occupy. In this 50:50 binary system, the volume fraction is defined as $\phi = \pi\rho(\sigma_{11}^3 + \sigma_{22}^3)/12$. We examined volume fractions from 0.5 to 0.58. The HARD system used a Monte Carlo simulation [93, 94] with local moves to change particle positions. In these simulations, a random particle can attempt a move in a cube of side length $0.1\sigma_{11}$. One unit of time consists of N attempted moves, where N is the number of particles in the simulation. We performed simulations with 10 000 and 80 000 particles.

We also simulated the harmonic sphere (HARM) system [89] with the potential

$$V_{\alpha\beta}^{HARM}(r) = \frac{\epsilon}{2}\left(1 - \frac{r}{\sigma_{\alpha\beta}}\right)^2, \tag{2.3}$$

which is cut off at $\sigma_{\alpha\beta}$. This system is a 50:50 binary mixture. The potential parameters are $\sigma_{22} = 1.4\sigma_{11}$ and $\sigma_{12} = 1.2\sigma_{11}$. The mass m is 1 for both particle types. The HARM system was studied with Newtonian dynamics and Brownian dynamics (BD)[2]. The Brownian dynamics simulations had constant particle number N and volume V. A system with Brownian dynamics obeys the equations of motion from the Supplementary Materials of Ref. [1]. The equation of motion for a particle n is

$$\dot{\mathbf{r}}_n(t) = \frac{\mathbf{F}_n}{\psi} + \vec{\eta}_n(t), \tag{2.4}$$

[2]My contribution to the paper [1] was the simulation and analysis of the HARM system with Brownian dynamics.

where the dot over $\mathbf{r}_n(t)$ indicates that we are taking a time derivative of $\mathbf{r}_n(t)$, $\mathbf{F}_n$ is the force due to the potential on particle n, ψ is a friction coefficient, and $\vec{\eta}_n(t)$ is the random noise, which satisfies the fluctuation dissipation relation, given by

$$\langle \vec{\eta}_n(t)\vec{\eta}_m(t')\rangle = \frac{2k_BT}{\psi}\delta(t-t')\delta_{nm}\mathbf{1}, \tag{2.5}$$

where $\mathbf{1}$ is the unit tensor. We include random noise to simulate collisions with nearby particles [10]. In the BD simulations, we set the friction coefficient, ψ, equal to one. Particles have equal masses and the number density is $\rho = 0.675$. In the HARM system, the unit of length is σ_{11} and the unit of temperature is $10^{-4}\epsilon/k_B$. In the Newtonian simulations, the unit of time is $\sqrt{m\sigma_{11}^2/\epsilon}$, and in the Brownian dynamics simulation, the unit of time is $\sigma_{11}^2\psi/\epsilon$. We studied systems of 10 000, 40 000, and 100 000 particles. We simulated temperatures from 5 to 20.

Along with the simulations at each temperature, we needed additional simulations to compute derivatives, which are needed to make corrections to our susceptibility. To get the corrections to the susceptibility, we needed derivatives with respect to density or volume fraction (HARD system simulations), particle concentration, and sometimes temperature (NVE simulations). Thus we performed simulations at higher and lower density or volume fraction, particle concentration, and sometimes temperature. For these simulations we did one equilibration run of at least $100\tau_\alpha$, and two production runs of at least $100\tau_\alpha$. Note that we had to examine smaller changes in each variable as we lowered temperature in order to keep the derivatives accurate. In NVT simulations, the HARD system simulations, and the Brownian dynamics simulations, we did not include a temperature correction to the susceptibility, as energy was allowed to fluctuate in those systems.

Our simulations were performed in LAMMPS (Large-scale Atomic/Molecular Massively Parallel Simulator) [95, 96] and HOOMD-blue (Highly Optimized Object-Oriented Molecular Dynamics)-blue [97, 98]. We modified LAMMPS to include the harmonic sphere potential and Brownian dynamics. The Monte-Carlo simulations were performed using a code created by Elijah Flenner.

We examined a range of systems studying the presence of attraction in potentials and the dynamics of systems. We studied the KA system, which has attractive and repulsive interparticle interactions at different particle separations. The other systems we studied have purely repulsive interparticle interactions, which allowed us to test what effect attraction or the lack of it has on dynamics. We also examined the effect of different types of dynamics. In the HARD system, we used Monte Carlo dynamics instead of Newtonian dynamics. The potential range in HARM system is the same as in the HARD system, but the potential is not infinite and we performed Newtonian dynamics simulations. We also model the HARM system with Brownian dynamics, which do not conserve momentum. Note that the Monte Carlo simulations on the HARD system also do not conserve momentum. We saw that remarkably all of our different potentials appeared to have no effect on dynamic heterogeneity, but dynamics did. When we chose the weight function, $w_n(t)$ to be the real part of the self-intermediate scattering function, we found a different length of dynamic heterogeneity in simulations where momentum was not conserved. We compared these different systems by rescaling the relaxation times in all the systems in the same way.

2.3. Stokes-Einstein relation

We used the temperature (or volume fraction) where the Stokes-Einstein relation, $D \sim 1/\tau_\alpha$, is violated to compare the different systems we described above. The diffusion coefficient D describes the long time behavior of the mean square displacement. The mean square displacement is given by

$$\left\langle \delta r^2(t) \right\rangle = 1/N \left\langle \sum_{n=1}^{N} \left[\mathbf{r}_n(t) - \mathbf{r}_n(0) \right]^2 \right\rangle, \tag{2.6}$$

where $\mathbf{r}_n(t)$ is the position of particle n at time t. The diffusion coefficient is

$$D = \lim_{t \to \infty} \frac{1}{6t} \left\langle \delta r^2(t) \right\rangle. \tag{2.7}$$

The α relaxation time comes from the self intermediate scattering function, which is

$$F_s(k;t) = 1/N \left\langle \sum_{n=1}^{N} e^{i\mathbf{k}\cdot[\mathbf{r}_n(t) - \mathbf{r}_n(0)]} \right\rangle, \tag{2.8}$$

where we chose k to be the peak of the static structure factor, eq. 2.12. The relaxation time τ_α is the time when the self intermediate scattering function decays to a given value. Here we used the typical value of $1/e$. Thus the relaxation time is given by

$$F_s(k;\tau_\alpha) = e^{-1}. \tag{2.9}$$

We also used the relaxation time from the average overlap function, $F_o(t)$. The average overlap function is

$$F_o(t) = \frac{1}{N}\left\langle \sum_n \Theta[a - |\mathbf{r}_n(t) - \mathbf{r}_n(0)|] \right\rangle, \tag{2.10}$$

where Θ is the Heaviside step function, which takes a value of 1 when its argument is positive or zero and has a value of 0 when the argument is negative. The relaxation time for the average overlap function, τ_α^{ov}, where the superscript ov refers to the overlap function, is defined as

$$F_o(\tau_\alpha^{ov}) = e^{-1}. \tag{2.11}$$

The value of a in the overlap function was chosen so that τ_α^{ov} from $F_o(t)$ was as close as possible to τ_α from $F_s(k;t)$, where k is the peak value of the static structure factor. The static structure factor is

$$S(k) = \frac{1}{N}\left\langle \sum_{n=1}^{N} \mathrm{e}^{i\mathbf{k}\cdot\mathbf{r}_n(0)} \sum_{m=1}^{N} \mathrm{e}^{-i\mathbf{k}\cdot\mathbf{r}_m(0)} \right\rangle. \tag{2.12}$$

The peak of the static structure factor occurs at $k = 7.2$ in the KA, IPL, and WCA systems, and occurs at $k = 6.1$ in the HARM and HARD systems. Given the k values from the peak of static structure factors, we choose the a value of 0.25 in the overlap function for the KA, IPL, and WCA systems and 0.3 in the HARM and HARD systems. Note that we used both the relaxation time, τ_α, from the self intermediate scattering function, and the relaxation time τ_α^{ov} from the average overlap function. For the information of the reader, τ_α is used in Figure 2.1 and Figure 2.4, while τ_α^{ov} is used in Figure 2.3.

One form of the Stokes-Einstein relation is

$$D \sim \frac{1}{\tau_\alpha}. \tag{2.13}$$

We often see that in supercooled liquids the Stokes-Einstein relation is violated, and in some studies [99] a fractional Stokes-Einstein relation is found, given by

$$D \sim \tau_\alpha^{-z}, \tag{2.14}$$

where $z < 1$. The violation of the Stokes-Einstein relation means that at temperatures below the temperature where Stokes-Einstein violation first appears, diffusion is enhanced with respect to relaxation time, as we saw in Section 1.3. For $T < T_s$, an increase in relaxation time by an order of magnitude, for example, no longer leads to an order of magnitude decrease in diffusion as it did at higher temperatures.

We used the relaxation time where the Stokes-Einstein relation, eq. 2.13, is violated to rescale relaxation time. The relaxation time where the high temperature fit of the Stokes-Einstein relation intersects with the low temperature fit of the fractional Stokes-Einstein relation is called the Stokes-Einstein violation relaxation time, τ_α^s. The temperature that corresponds to that relaxation time is the Stokes-Einstein violation temperature, T_s. We rescaled the Stokes-Einstein violation relaxation time, τ_α^s, in all the systems to the τ_α^s for the HARM system, where $\tau_\alpha^s = 303$. In Figure 2.1, we plot a rescaled diffusion coefficient as a function of the rescaled relaxation time, scaling the relaxation time so that all the systems have Stokes-Einstein violation at the same rescaled relaxation time. For the HARM system, the power in the fractional Stokes-Einstein relation is $z = 0.65$, for rescaled relaxation times above τ_α^s. We saw that the temperature, T_s, where the Stokes-Einstein relation was violated

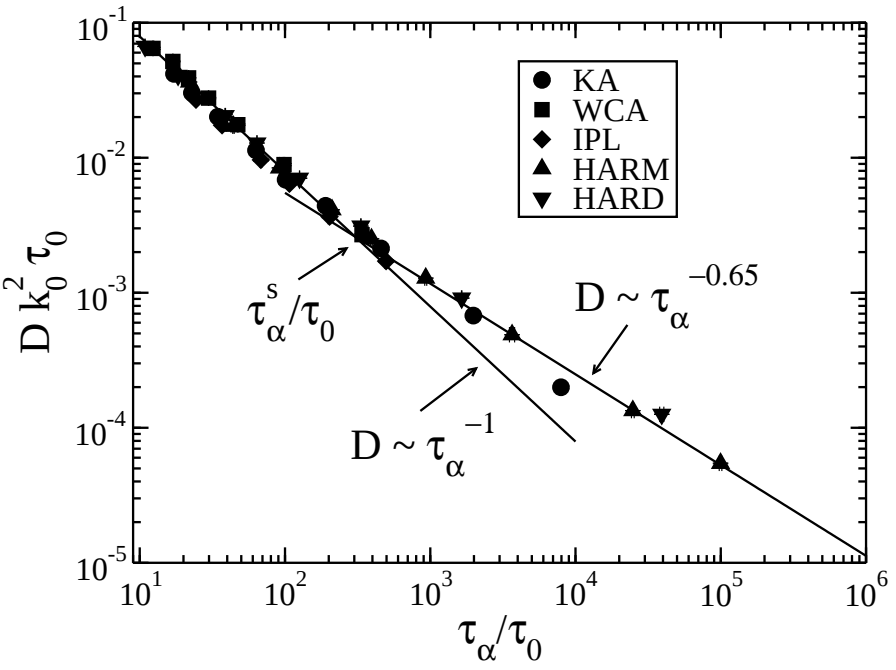

FIGURE 2.1. Rescaled self-diffusion coefficient, D, as a function of rescaled α relaxation time, τ_α. The fits are to the HARM system data using a fit of $D \sim \tau_\alpha^{-1}$ for $T \geq 12$ and a fit of $D \sim \tau_\alpha^{-z}$ for $T \leq 7$. The fits intersect at τ_α^s/τ_0. This figure originally appeared in Ref. [1].

was below the onset temperature of glassy dynamics, T_o, and above the mode-coupling temperature, T_c. For the onset temperature, we considered two definitions described in Section 1.2. We used the onset temperature defined by where the inherent structure energy energy began to quickly decrease [11], and we also used the onset temperature from a fit of relaxation time as a function of temperature to $\log(\tau/\tau_o) = J(1/T - 1/T_o)$, where J and τ_o are fitting constants [13]. T_c is defined to be the temperature where the relaxation time appears to diverge when relaxation time is plotted as a function of temperature. The ranges for ϕ_o, ϕ_c, and ϕ_s for the HARD system and T_o, T_c, and T_s for the other systems are given in Table 2.1, which is reproduced from the Supplementary Material of Ref. [1].

TABLE 2.1. Onset, mode-coupling, and Stokes-Einstein violation temperatures/volume fractions in five systems.

System	T_o/ϕ_o	T_c/ϕ_c	T_s/ϕ_s
KA	0.95-0.7	0.44-0.43	0.6-0.55
WCA	0.95-0.6	0.3-0.28	0.45-0.4
IPL	0.95-0.7	0.44-0.43	0.6-0.55
HARM	14-11	5.6-5.1	10-9
HARD	0.52-0.54	0.59	0.56-0.57

2.4. RESULTS

We studied the relationships between the susceptibility, χ_4, dynamic correlation length, ξ_4, and relaxation time, τ_α. Recall that the equation for dynamic susceptibility in a particular ensemble is

$$\chi_4(t) = \frac{1}{N}\left[\left\langle \sum_{n,m} w_n(t) w_m(t) \right\rangle - \left\langle \sum_n w_n(t) \right\rangle^2\right], \tag{2.15}$$

where $w_n(t)$ is a weight function measuring mobility. We would need to add correction terms to eq. 2.15 to get the full susceptibility. Another way to get the full susceptibility is to take the $q \to 0$ limit of $S_4(q;t)$. The full χ_4 is a measure of the number of particles in a region with correlated mobility, and ξ_4 is a measure of the length of such a region. The relationship between these variables tells us about the compactness of regions. We measured the full χ_4 and ξ_4 from a fit to the four point structure factor,

$$S_4(\mathbf{q};t) = \frac{1}{N}\left\langle \sum_{n,m} w_n(t) w_m(t) \mathrm{e}^{i\mathbf{q}\cdot[\mathbf{r}_n(0)-\mathbf{r}_m(0)]} \right\rangle - \frac{1}{N}\left\langle \sum_n w_n(t) \mathrm{e}^{i\mathbf{q}\cdot\mathbf{r}_n(0)} \right\rangle^2, \tag{2.16}$$

where $w_n(t)$ is a weight function measuring mobility of particles. We also examined the relationship between ξ_4 and τ_α. Different theories have different predictions about how ξ_4 and τ_α are related. We found where various fits hold, looking for a crossover in dynamics

from high temperatures to low temperatures. This crossover occurred at the temperature (or volume fraction) where Stokes-Einstein violation first appears. We found that rescaling the relaxation time by the Stokes-Einstein violation relaxation time lead to ξ_4 as a function of τ_α to have the same relationship in all systems above the Stokes-Einstein violation relaxation time. We related χ_4 to length, ξ_4, and found that $\chi_4 \sim (\xi_4)^3$, meaning that cluster of particles with correlated mobility become compact. This onset of compact regions occurred at a length that corresponds to Stokes-Einstein violation in all systems. We also investigated anisotropy in dynamic heterogeneity, finding that below T_s (or ϕ_s), there is some anisotropy in another dynamic correlation length, and it is the same in all systems.

2.4.1. Compact regions. We examined the relationship between the full susceptibility, χ_4, which determines the strength of the dynamic heterogeneity, and is related to the number of particles in regions with correlated particle motion, and the dynamic correlation length, ξ_4, the length scale of the regions. We found susceptibility and length by doing a fit to S_4^{ov}, which is the four point structure factor with the overlap function as its weight function, $w_n(t) = \Theta(a - |\mathbf{r}_n(t) - \mathbf{r}_n(0)|)$, where Θ is the Heaviside step function. S_4^{ov} is

$$\begin{aligned} S_4^{ov}(q;t) &= \frac{1}{N}\left\langle \sum_{n,m} \Theta(a - |\mathbf{r}_n(t) - \mathbf{r}_n(0)|)\Theta(a - |\mathbf{r}_m(t) - \mathbf{r}_m(0)|)e^{i\mathbf{q}\cdot[\mathbf{r}_n(0) - \mathbf{r}_m(0)]} \right\rangle - \\ &\quad \frac{1}{N}\left\langle \sum_{n} \Theta(a - |\mathbf{r}_n(t) - \mathbf{r}_n(0)|)e^{i\mathbf{q}\cdot\mathbf{r}_n(0)} \right\rangle^2 . \end{aligned} \tag{2.17}$$

The dynamic correlation length, ξ_4^{ov}, and the full susceptibility, χ_4^{ov} can be found by fitting $S_4^{ov}(q;\tau_\alpha)$ to the Ornstein-Zernicke function,

$$\frac{\chi_4^{ov}}{1 + (q\xi_4^{ov})^2}, \tag{2.18}$$

for small q values, where the superscript ov refers to the weight function of the four point structure factor being the overlap function. In eq. 2.18, χ_4^{ov} is the full dynamic susceptibility, and ξ_4^{ov} is the dynamic correlation length. We fitted to $q \leq 1$ and $q\xi_4 < 1.5$, according to a method developed by Flenner and Szamel [36, 41]. Note that for the choice of the overlap function as the weighting function, we are examining the behavior of the less mobile particles. Thus, the dynamic correlation length that we measured is probing the length scale of the less mobile regions. To get more precise measurements of χ_4^{ov} and ξ_4^{ov}, we often add the $q = 0$ value to the S_4^{ov} data. The full ensemble independent susceptibility, $\chi_4^{ov}(t)$, is the q going to 0 limit of the four point structure factor, $S_4(q;t)$, since

$$\chi_4^{ov}(t) = \lim_{\mathbf{q}\to 0} S_4^{ov}(\mathbf{q};t). \tag{2.19}$$

We can get the full susceptibility by first measuring the susceptibility in a particular ensemble, *ens*. We examined the susceptibility, $\chi_4^{ov}|_{ens}$, with the overlap function as its weight function, $w_n(t) = \Theta(a - |\mathbf{r}_n(t) - \mathbf{r}_n(0)|)$, as was the case for S_4^{ov}. The susceptibility in a particular ensemble is given by

$$\chi_4^{ov}(t)|_{ens} = \frac{1}{N}\left[\left\langle\left(\sum_n \Theta(a - |\mathbf{r}_n(t) - \mathbf{r}_n(0)|)\right)^2\right\rangle|_{ens} - \left\langle\sum_n \Theta(a - |\mathbf{r}_n(t) - \mathbf{r}_n(0)|)\right\rangle^2\right]. \tag{2.20}$$

The full susceptibility $\chi_4^{ov}(t)$ is a measure of all fluctuations in a system. $\chi_4^{ov}(t)|_{ens}$ of eq. 2.20, on the other hand, misses certain fluctuations that need to be taken into account for the full susceptibility, since it is measured in a particular ensemble, which suppresses some fluctuations. To get these missing fluctuations, we find correction terms to eq. 2.20, for each suppressed fluctuation, using eq. 1.22. In the NVE ensemble, for example, we must

add correction terms for the fluctuations due to temperature, density, and concentration of particle type.

Starting from the NVE ensemble with the NVE susceptibility, $\chi_4(t)|_{NVE}$, the ensemble independent susceptibility is

$$\begin{aligned}\chi_4^{ov}(t) &= \chi_4^{ov}(t)|_{NVE} + \frac{k_B T^2 \chi_T^2(t)}{c_V} + [F_o(t) + \rho\chi_\rho(t)]^2[x_1 S_{11} + 2\sqrt{x_1 x_2} S_{12} + x_2 S_{22}] + \\ & 2[F_o(t)\chi_c(t) + \rho\chi_\rho(t)\chi_c(t)][x_1 x_2 (S_{11} - S_{22}) + (x_2 - x_1)\sqrt{x_1 x_2} S_{12}] + \\ & \chi_c^2[x_1 x_2^2 S_{11} - 2x_1 x_2 \sqrt{x_1 x_2} S_{12} + x_2 x_1^2 S_{22}], \end{aligned} \tag{2.21}$$

where c_V is the specific heat per particle, $\chi_T(t) = \partial F_o(t)/\partial T$, $\chi_\rho(t) = \partial F_o(t)/\partial \rho$, $\chi_c(t) = \partial F_o(t)/\partial c$, $F_o(t)$ is the average overlap function, $c = N_i/N$ is concentration, $x_2 = N_2/N$, $\rho = N/V$ is number density, c_V is constant volume specific heat per particle, and $S_{\alpha\beta} = \lim_{q\to 0} S_{\alpha\beta}(q)$, where $S_{\alpha\beta}(q)$ is the partial structure factor. The partial structure factor is given by

$$S_{\alpha\beta}(q) = \frac{1}{\sqrt{N_\alpha N_\beta}} \left\langle \sum_{m=1}^{N_\alpha} \sum_{n=1}^{N_\beta} e^{i\mathbf{q}\cdot(\mathbf{r}_n(0) - \mathbf{r}_m(0))} \right\rangle, \tag{2.22}$$

where α and β are particle types either 1 or 2. To get $S_{\alpha\beta}$, we average $S_{\alpha\beta}(q)$ over small wave vectors, q. In NVT or Brownian dynamics simulations or the HARD system, we do not use the temperature correction term, $(k_B T^2 \chi_T^2(t))/c_V$. The temperature correction term includes the specific heat.

The specific heat at constant volume is

$$C_V = \left(\frac{\partial E}{\partial T}\right)_V, \tag{2.23}$$

from eq. 2.3.10 of Ref. [10], where $c_V = C_V/N$, E is the internal energy, and the subscript V indicates that we hold volume constant. In our calculations, we calculated the specific heat by examining the fluctuations in the energy. In our closed equilibrium systems with no external fields, the total internal energy of a system is

$$E = \langle H \rangle = \langle K \rangle + \langle U \rangle \,, \tag{2.24}$$

from eq. 2.46 of Ref. [38] where H is the Hamiltonian, U is the potential energy, and

$$\langle K \rangle = \frac{1}{2} m \left\langle v^2 \right\rangle = \frac{3}{2} N k_B T, \tag{2.25}$$

from eq. 2.48 of Ref. [38], is the kinetic energy. The specific heat appears in the temperature correction term to the susceptibility, which is only needed for the NVE ensemble. However, the specific heat in the NVE ensemble is related to the specific heat in the NVT ensemble by transforming between ensembles, using eq. 1.22. In an NVT ensemble the fluctuations in the kinetic energy are

$$\left\langle \delta K^2 \right\rangle_{NVT} = \frac{3N}{2} (k_B T)^2, \tag{2.26}$$

from eq. 2.72 of Ref. [38]. In eq. 2.26,

$$\left\langle \delta K^2 \right\rangle_{NVT} = \left\langle K^2 \right\rangle_{NVT} - \langle K \rangle_{NVT}^2 \tag{2.27}$$

from eq. 2.43 of Ref. [38], and

$$\delta K = K - \langle K \rangle_{NVT} \tag{2.28}$$

from eq. 2.44 of Ref. [38]. If we transform eq. 2.26 to an NVE ensemble, we find

$$\left\langle \delta K^2 \right\rangle_{NVE} = \frac{3}{2} N k_B^2 T^2 \left(1 - \frac{3 N k_B}{2 C_V} \right). \tag{2.29}$$

This equation allows us to measure kinetic energy fluctuations, and relate them to the specific heat.

We can also get an equation for the full susceptibility in a hard sphere system, where the parameter that controls the dynamics is volume fraction ϕ, instead of temperature, T. We choose to replace ρ with ϕ, since calculations prove to be easier using ϕ. In a binary mixture, the volume fraction is

$$\phi = \pi(N_1 \sigma_{11}^3 + N_2 \sigma_{22}^3)/(6V), \tag{2.30}$$

where σ_{11} and σ_{22} can be thought of as particle diameters of particles 1 and 2. The full susceptibility in a hard sphere system is

$$\begin{aligned}
\chi_4^{ov}(t) &= \chi_4^{ov}(t)|_{NV} + \chi_\phi^2(t) \left(\frac{\pi\rho}{6} \right)^2 [d_1^6 x_1 S_{11} + 2 d_1^3 d_2^3 \sqrt{x_1 x_2} S_{12} + d_2^6 x_2 S_{22}] + \\
&\quad \chi_\phi(t) \chi_c(t) \left(\frac{\pi\rho}{3} \right) [d_1^3 x_1 x_2 S_{11} - d_1^3 x_1 \sqrt{x_1 x_2} S_{12} + d_2^3 x_2 \sqrt{x_1 x_2} S_{12} - d_2^3 x_1 x_2 S_{22}] + \\
&\quad \chi_c^2(t) [x_2^2 x_1 S_{11} - 2 x_1 x_2 \sqrt{x_1 x_2} S_{12} + x_1^2 x_2 S_{22}] + F_o(t)^2 [x_1 S_{11} + 2\sqrt{x_1 x_2} S_{12} + x_2 S_{22}] + \\
&\quad F_o(t) \chi_\phi(t) \left(\frac{\pi\rho}{3} \right) [d_1^3 x_1 S_{11} + (d_1^3 + d_2^3) \sqrt{x_1 x_2} S_{12} + d_2^3 x_2 S_{22}] + \\
&\quad 2 F_o(t) \chi_c(t) [x_1 x_2 S_{11} + (x_2 - x_1) \sqrt{x_1 x_2} S_{12} - x_1 x_2 S_{22}],
\end{aligned} \tag{2.31}$$

from Refs. [88, 93], where $\chi_4^{ov}(t)|_{NV}$ refers to the fact that we are measuring at a constant particle number N and volume V, and $\chi_\phi(t) = \partial F_o(t)/\partial\phi$. The additional point at $S_4^{ov}(q =$

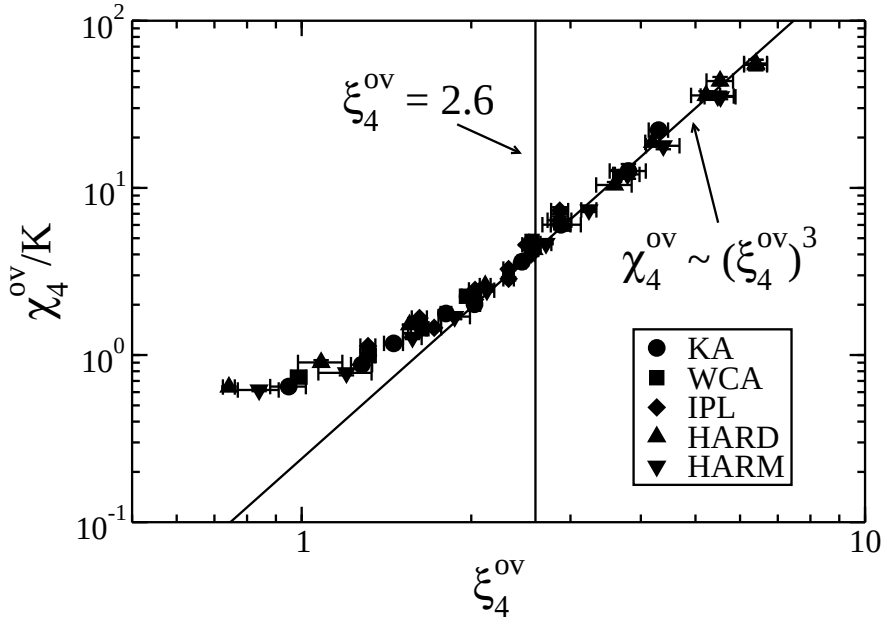

FIGURE 2.2. Rescaled susceptibility, χ_4^{ov}, as a function of the dynamic correlation length, ξ_4^{ov}. This figure originally appeared in Ref. [1].

$0;t)$ from the full susceptibility improves our fit to $S_4^{ov}(q;t)$. From $S_4^{ov}(q;t)$ we can solve for ξ_4^{ov} and the full χ_4^{ov}. We use the full χ_4^{ov} from the fit to $S_4^{ov}(q;t)$ in the rest of this work when we talk about susceptibility.

In Figure 2.2 we examined the rescaled full susceptibility χ_4^{ov} versus the dynamic correlation length ξ_4^{ov}. By just rescaling χ_4^{ov}, we found that all 5 systems studied obey the power law $\chi_4^{ov} \sim (\xi_4^{ov})^3$, for lengths above $\xi_4^{ov} = 2.6$. This relation implies that the regions of less mobile particles are compact. We note that the length of 2.6 corresponds to the relaxation time, τ_α^s, where Stokes-Einstein violation occurs in all the systems. Thus Stokes-Einstein violation appears to mark a beginning of compact regions. Surprisingly, length did not have to be rescaled to get this result, although we suspect that this lack of a need for rescaling is probably a coincidence.

2.4.2. Size of dynamic heterogeneity. We also investigated the dynamic correlation length as a function of rescaled relaxation time, which appears in Figure 2.3. Again, the data collapsed onto a single curve. Again, we did not have to rescale length to get this result. Recall that we found a particular scaling constant for τ_α when we plotted D as a function of τ_α. We used this same scaling constant again in our plot of dynamic correlation length as a function of the relaxation time τ_α^{ov}. Note that τ_α and τ_α^{ov} have a similar temperature dependence. We investigated four different fits to the data. We found that a mode-coupling power law fit of $\xi_4^{ov} \sim (\tau_\alpha)^{1/z}$, where $z = 4.8$, was a poor fit to the data, only matching the data over a change of around one order of magnitude in the relaxation time. Flenner and Szamel [41] originally saw this behavior in Ref. [100] for the HARD system. We also did a fit from Adam-Gibbs theory or RFOT theory. The fit of $\xi_4^{ov} \sim [\ln(\tau_\alpha)]^{1/\zeta}$, with $\zeta = 1$ worked well at higher temperatures, but not for the final low temperature data points. When $\zeta = 3/2$, the fit worked well at all relaxation times above the Stokes-Einstein violation relaxation time τ_α^s. From Section 2.1, recall that in the harmonic sphere system, Flenner and Szamel [88] found that $\tau_\alpha \sim \exp(\xi_4)$ fit the data from the onset of supercooling to a temperature slightly above the mode coupling temperature, T_c. At lower temperatures they found the fit of $\tau_\alpha \sim \exp((\xi_4)^{3/2})$ worked well. The other fit that worked well for the data, including at the largest relaxation times, was $\ln(\xi_4^{ov}) = A\sqrt{\ln(\tau_\alpha)} + B$, which is from facilitation theory. The last two fits of $\xi_4^{ov} \sim [\ln(\tau_\alpha)]^{2/3}$ and $\ln(\xi_4^{ov}) = A\sqrt{\ln(\tau_\alpha)} + B$ both fit all the data for relaxation times greater than τ_α^s well. We would need even lower temperature liquids to distinguish between these fits. We suggest that we would need to simulate systems that have relaxation times that are two orders of magnitude larger than our current largest relaxation times in order to distinguish between these fits. The longest runs for the HARM

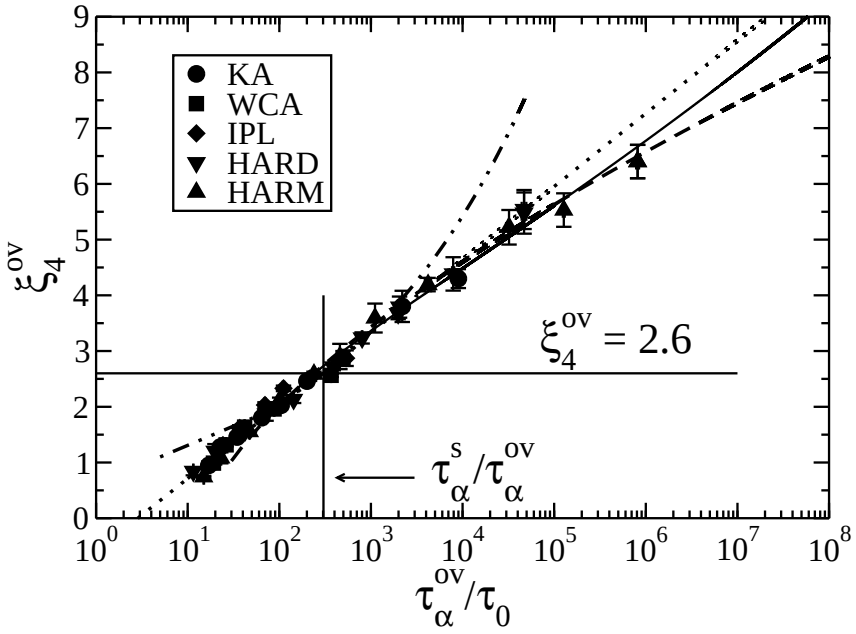

FIGURE 2.3. Dynamic correlation length ξ_4^{ov} as a function of rescaled relaxation time τ_α^{ov}. The fits are: a mode-coupling type fit of $\xi_4^{ov} \sim (\tau_\alpha^{ov})^{1/z}$ (dash-dotted line), $\xi_4^{ov} \sim \ln(\tau_\alpha^{ov})$ (dotted line), a dynamic facilitation fit of $\ln(\xi_4^{ov}) = A\sqrt{\ln(\tau_\alpha^{ov})} + C$ (solid line), $\xi_4^{ov} \sim \ln(\tau_\alpha^{ov})^{2/3}$ (dashed line). The solid vertical line shows the Stokes-Einstein violation relaxation time, where the two fits intersected in Figure 2.1. The solid horizontal line marks the value of ξ_4^{ov} where clusters of correlated particles become compact. After this point, $\chi_4^{ov} \sim (\xi_4^{ov})^3$, as is seen in Figure 2.2. This figure originally appeared in Ref. [1].

system took 18 weeks on the CSU Cray, meaning that we would need to perform simulations at a temperature where a single run would take over 3 years.

2.4.3. SHAPE OF DYNAMIC HETEROGENEITY. We can probe anisotropy of regions of correlated particles by using the four-point structure factor, $S_4^{\cos}(\mathbf{k}, \mathbf{q}; t)$, which uses the real part of the self intermediate scattering function as the weight function, $w_n(t) = \cos[\mathbf{k} \cdot \delta\mathbf{r}_n(t)]$,

where $\delta\mathbf{r}_n(t) = \mathbf{r}_n(t) - \mathbf{r}_n(0)$. This four point structure factor is

$$S_4^{\cos}(\mathbf{k},\mathbf{q};t) = \frac{1}{N}\left\langle \sum_{n,m} \cos[\mathbf{k}\cdot\delta\mathbf{r}_n(t)]\cos[\mathbf{k}\cdot\delta\mathbf{r}_m(t)]e^{i\mathbf{q}\cdot[\mathbf{r}_n(0)-\mathbf{r}_m(0)]}\right\rangle - \frac{1}{N}\left\langle \sum_{n} \cos[\mathbf{k}\cdot\delta\mathbf{r}_n(t)]e^{i\mathbf{q}\cdot\mathbf{r}_n(0)}\right\rangle^2 . \tag{2.32}$$

Note that the $S_4^{cos}(\mathbf{k},\mathbf{q};t)$ has two vectors, $\mathbf{k}$ and $\mathbf{q}$. The wave vector $\mathbf{k}$ probes dynamics along $\mathbf{k}$, while $\mathbf{q}$ is associated with the initial particle separation $\delta\mathbf{r}_{nm}(0) = \mathbf{r}_n(0) - \mathbf{r}_m(0)$. By varying the angle, θ, between $\mathbf{k}$ and $\mathbf{q}$ in $S_4^{\cos}(\mathbf{k},\mathbf{q};t)$, we can probe the correlations of dynamics in different directions relative to an initial particle separation $\delta\mathbf{r}_{nm}(0)$. We chose to examine angles θ of 0 and of $\pi/2$ in $S_4^{\cos}$ to compare parallel and perpendicular dynamics. We again examined a length, ξ_4, found from the Ornstein-Zernicke fit versus relaxation time. We used the same fitting procedure described in Section 2.4.1, where we found the additional point at $q = 0$, to calculate length. For this point we needed the dynamic susceptibility with the real part of the self intermediate scattering function as its weight function. This susceptibility is given by

$$\chi_4^{\cos}(\mathbf{k};t) = \frac{1}{N}\left[\left\langle\left(\sum_n \cos[\mathbf{k}\cdot\delta\mathbf{r}_n(t)]\right)^2\right\rangle - \left\langle\sum_n \cos[\mathbf{k}\cdot\delta\mathbf{r}_n(t)]\right\rangle^2\right]. \tag{2.33}$$

The length we calculated from the fit to $S_4^{\cos}(\mathbf{k},\mathbf{q};t)$ is a function of the angle between the wave vectors $\mathbf{k}$ and $\mathbf{q}$ that appeared in $S_4^{\cos}(\mathbf{k},\mathbf{q};t)$. Thus we write the lengths in terms of the angle, θ, giving ξ_4^θ for the dynamic correlation length. The results of length ξ_4^θ plotted as a function of rescaled relaxation time appear in Figure 2.4.

For $\tau_\alpha > \tau_\alpha^s$ (the Stokes-Einstein relaxation time) the data collapse onto an upper curve for ξ_4^0 and a lower curve for $\xi_4^{\pi/2}$. For $\tau_\alpha < \tau_\alpha^s$, within each curve for the different angles

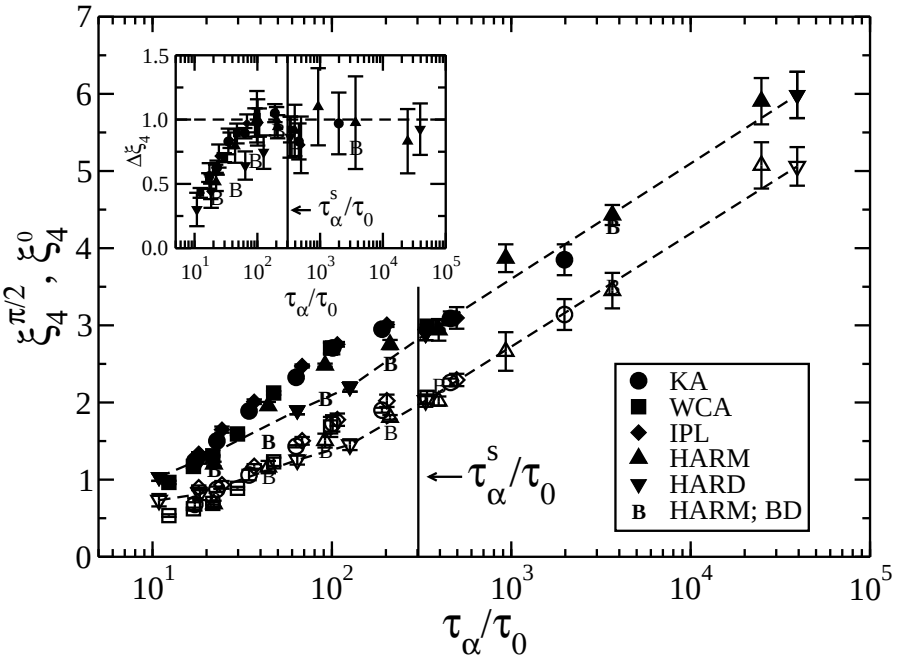

FIGURE 2.4. Dynamic correlation length ξ_4^θ as a function of rescaled relaxation time τ_α. We examined $\theta = 0$ and $\pi/2$. The dashed lines follow the data for the HARD system. Note that there are two HARM data sets. The downward pointing triangles show the Newtonian dynamics data that we have examined up till now, and the B symbol shows the Brownian dynamics (BD) data. The inset figure shows the difference between ξ_4^0 and $\xi_4^{\pi/2}$, $\Delta\xi_4 = \xi_4^0 - \xi_4^{\pi/2}$, as a function of τ_α. In the inset the dashed line marks $\Delta\xi_4 = 1$. This figure originally appeared in Ref. [1].

θ, the data shows some dependence on the system. Interestingly this secondary split in the curves, (within each angle curve), for relaxation times below τ_α^s, has nothing to do with the potential of the system, but only with the dynamics of the system. The systems with Newtonian dynamics are the KA, IPL, WCA, and HARM systems. We also simulated the HARM system with Brownian dynamics, and this data matches the HARD system, which used Monte Carlo steps to simulate dynamics. All the systems where Newtonian dynamics was used collapse onto an upper curve, for each θ, and the data for systems that did not have Newtonian dynamics collapse onto a slightly lower curve. We suggest that the reason

for this difference could have to do with momentum, which is conserved in the KA, IPL, WCA, and HARM systems and is not conserved in the HARD system and the HARM system with Brownian dynamics. We suggest a possible reason why the Newtonian systems seem to have more particle correlation then the HARD or Brownian HARM systems do. Recall from eq. 2.32 that the $\mathbf{q}$ wave vector is related to the distance between two particles at $t = 0$, and the $\mathbf{k}$ wave vector can probe particle motion in a different direction than $\mathbf{q}$. Consider two nearby particles moving in the same direction, as in the $\theta = 0$ case. If one bumps into another and momentum is conserved, then some momentum will be transferred. Then the particles will possibly move off together in the same direction, thus adding an additional correlation to their motion. When particles moving at a right angle collide, there is transfer of momentum, and thus these particles may still have some correlation of motion after the collision. The HARD and HARM (Brownian) systems don't have the additional help of momentum transfer, possibly explaining why there is a little less correlation in length of dynamic heterogeneity than in the Newtonian systems.

The inset of Figure 2.4 shows that the difference between lengths calculated from parallel and perpendicular wave vectors is the same in all systems below a certain temperature. It shows $\Delta\xi_4$, the difference between the lengths at our two angles, where $\Delta\xi_4 = \xi_4^0 - \xi_4^{\pi/2}$. The difference between ξ_4^0 and $\xi_4^{\pi/2}$ is always positive, and is 1 for all systems for relaxation times greater than the Stokes-Einstein violation relaxation time, τ_α^s. We note that having $\xi_4^0 > \xi_4^{\pi/2}$ could indicate string-like motion. String-like motion is when one less mobile particle moves and another less mobile particle moves in to replace it. String-like motion has been seen for the more mobile particles [29, 101], but our lengths come from the less mobile particles. In Figure 2.2, we saw that the less mobile particles formed compact regions, which seems

to contradict having string-like motion. More work would be needed to examine whether motion of the less mobile particles is string-like. The constant difference, $\Delta\xi_4$, shows that the anisotropy in ξ_4^θ is uniform for relaxation times above the Stokes-Einstein relaxation time, τ_α^s.

CHAPTER 3

Strong glass

This chapter is based on a paper [2] by Staley, Flenner, and Szamel entitled "Reduced strength and extent of dynamic heterogeneity in a strong glass former as compared to fragile glass formers".

3.1. Introduction

We examined a model strong glass-former, which are defined by the Angell classification. In the Angell classification strong glasses exhibit Arrhenius behavior, $\tau_\alpha = \tau_0 \exp\left[E_a/(k_B T)\right]$, where τ_α is the relaxation time, τ_0 is a constant, E_a is the activation energy, k_B is the Boltzmann constant, and T is temperature, while fragile glasses deviate from Arrhenius behavior. Another way to describe strong and fragile glasses is to let the activation energy be a function of temperature, $E_a(T)$, as in $\tau_\alpha = \tau_0 \exp\left[E_a(T)/(k_B T)\right]$. A strong glass has a constant activation energy as temperature changes, so we say $E_a(T) = E_0$, and a fragile glass has an activation energy that increases as temperature decreases. The activation energy is sometimes thought of as the energy barrier a particle must overcome in order to move. One idea for why some systems might have a growing $E_a(T)$ is given by Adam-Gibbs theory. In this approach $E_a(T)$ should equal the energy barrier of each molecule multiplied by the number of molecules needed to form the smallest region that has cooperative rearrangements [102]. Thus a growing $E_a(T)$ would be related to a growing length scale of cooperative rearrangements. Strong glass-formers, which have a constant $E_a(T)$, should not have a growing length scale of cooperative rearrangements, while fragile glasses should. One candidate for

the length scale of cooperative rearrangements is the length scale of dynamic heterogeneity [14, 4].

In this chapter, we examined dynamic heterogeneity with four-point correlation functions. We used the four point structure factor, S_4, with a weight function, $w_n(t)$, to get a length of regions with correlated mobility. From a fit to the structure factor we got the length scale of dynamic heterogeneity, which gives the length of regions of correlated mobility. We also calculated the susceptibility, χ_4, with a weight function, $w_n(t)$. The full susceptibility is $\chi_4(t) = \lim_{q\to 0} S_4(q;t)$. It measures fluctuations in dynamics, and it is related to the number of particles with correlated mobility. Calculating these four-point correlation functions is possible in computer simulation, which track the motion of each individual particle at all desired times, but is very difficult in experiments. However, Berthier *et al.* [39] used the mathematics associated with transforming variables between different types of ensembles (recall eq. 2.21) to demonstrate that there is a quantity that can be more easily tracked in experiments. This quantity can well approximate the full susceptibility, $\chi_4(t)$, as was discussed in Section 1.3.1.

Berthier *et al.* [39] made use of transforming the dynamic susceptibility between ensembles to get a lower limit on the full susceptibility. The full susceptibility, which allows for all the fluctuations in the system, can be obtained by making a measurement in a given system, such as the NVE ensemble, and then adding correction terms corresponding to all the fluctuations that were suppressed in the NVE ensemble (see eq. 2.21). In a system where certain variables like particle number are not allowed to fluctuate, the susceptibility cannot measure the fluctuations in dynamics due to those suppressed fluctuations. The full susceptibility must measure fluctuations from all possible sources. The full susceptibility

is $\chi_4(t) = \chi_4(t)|_{NVE} + \mathcal{X}(t)$, where $\chi_4(t)|_{NVE}$ is the susceptibility measured in the NVE ensemble and $\mathcal{X}(t)$ is all the correction terms. One correction term to a constant E ensemble comes from the missing energy fluctuations. We got this term by transforming from the NVE ensemble to the NVT ensemble, in eq. 1.23. This term is $\chi_{4,T}(t) = k_B T^2 \chi_T(t)^2 / c_V$, where c_V is the specific heat at constant volume, $\chi_T(t)$ is a temperature derivative of the average of the weight function, $w_n(t)$ from $S_4(q;t)$. $\chi_T(t)$ is given by $\chi_T(t) = \partial \langle w(t) \rangle / \partial T$, where $\langle w(t) \rangle$ is the average of that weight function $w_n(t)$. Berthier *et al.* [39] noted that this correction term becomes increasingly important to the full susceptibility as temperature decreases. If we use the real part of the self-intermediate scattering function as the weight function and assume that time-temperature superposition holds reasonably well, then the correction term that adds energy fluctuations becomes $\chi_{4,T}(t) = k_B E_0^2 / (T^2 c_V)$ for a strong glass-former. Note that this correction term has a different form in a fragile glass-former. Berthier *et al.* found that the sum of all of the other terms besides the energy fluctuation term that contribute to the full susceptibility are greater than 0. Thus the full susceptibility diverges, since $\chi_{4,T}(t)$ diverges as temperature is decreased. Since susceptibility is related to the number of correlated particles in a region, its divergence would imply a diverging correlation length. So, despite having a constant activation energy, strong glasses can be expected to have a growing length scale as temperature is decreased.

In Chapter 2 [1], we examined dynamic heterogeneity in five different fragile liquids, finding some universal features of dynamic heterogeneity in all of the systems. Recall that we found that all the systems had matching behavior when time was rescaled by the relaxation time, which corresponded to the temperature T_s or volume fraction ϕ_s where Stokes-Einstein

violation occurred. Remarkably, in all the models we studied Stokes-Einstein violation corresponded to the onset of clusters of correlated particles becoming compact.

Nagamanasa *et al.* [103] did an experiment on a 2D colloid mixture. They saw that clusters of the most mobile particles changed shape from string-like to compact at a particular number density, just as we saw. Mishra and Ganapathy [99] did experiments on a quasi-two-dimensional colloidal ellipsoid system, for systems with particles with attractive potentials and systems with repulsive potentials. For these systems the Stokes-Einstein relation, $D = (k_B T)/(6\pi\eta r)$, where η is the viscosity and r is the radius of a spherical particle, was violated at a particular volume fraction, ϕ. The Stokes-Einstein-Debye relation, $D_r = (k_B T)/(8\pi\eta r^3)$, where D_r is the rotational diffusion constant, was also violated at the same volume fraction, ϕ. This volume fraction corresponded to the onset of compact clusters of the most mobile particles. Along with our previous work [1] described in Chapter 2, this evidence suggests that the Stokes-Einstein violation temperature (or volume fraction) marks a change in compactness of clusters of correlated particles.

We wished to extend the work of Chapter 2 to a strong glass-former. All of the systems in that chapter were fragile glass-formers. Coslovich and Pastore [16] created a strong glass-former that forms a network-like structure. They compared their model to the van Beest, Kramer, and van Santen [104], BKS, model, a popular model of SiO_2, which is considered a typical strong network glass-former. The BKS model uses the more accurate long range Coulomb potential, which takes charges on atoms in account. Coslovich and Pastore found good agreement between their pair correlation functions and those pair correlation functions from the BKS model, reasonable agreement with the BKS model for the activation energies they got by fitting the diffusion coefficient to an Arrhenius law, and reasonable agreement

with experiments for the vibrational density of states. Their new network-forming liquid model can be simulated much more quickly than the BKS model, which used computationally expensive long range electrostatic potentials.

Several other groups [105, 17, 106] have studied the strong glass model created by Coslovich and Pastore [16]. Kawasaki, Kim, and Onuki [105] simulated Coslovich and Pastores model examining dynamics and fluctuations around the average dynamics, which are known as dynamic heterogeneity. They found that a couple particles at a time made large jumps at low temperatures. Then surrounding particles rearranged themselves. This correlated motion of the nearby particles resulted in a measurable dynamic heterogeneity. They also examined the Stokes-Einstein equation, finding that it is weakly violated in this system. Kim and Saito [17] simulated the model created by Coslovich and Pastore and compared it to three fragile liquids. They examined dynamics heterogeneity in the system, and found that this strong liquid had weaker dynamic heterogeneity than the fragile liquids they examined. They also saw shorter dynamic heterogeneity lengths in the strong liquid than in the fragile liquids.

This chapter examines dynamic heterogeneity in a model strong glass-former, focusing on the difference between a strong glass-former and the universal features seen in several fragile glass-formers [1]. Section 3.2 describes our model and simulations. Section 3.3 examines structure, average dynamics, and Stokes-Einstein violation. Section 3.4 considers dynamic heterogeneity in the system. We found many differences between the dynamic heterogeneity in the model strong glass-former and in the fragile glass-formers.

3.2. Simulations

We modeled the network forming system created by Coslovich and Pastore [16], which we call the CP model. The interaction potential of the CP model is

$$V_{\alpha\beta}(r) = \epsilon_{\alpha\beta}\left[\left(\frac{\sigma_{\alpha\beta}}{r}\right)^{12} - (1-\delta_{\alpha\beta})\left(\frac{\sigma_{\alpha\beta}}{r}\right)^{6}\right], \tag{3.1}$$

where α β represent particles of species 1 or 2, and $\delta_{\alpha\beta}$ is the Kronecker delta. The potential has the parameters of $\epsilon_{11} = 1$, $\epsilon_{12} = 24$, $\epsilon_{22} = 1$, $\sigma_{11} = 1$, $\sigma_{12} = 0.49$, and $\sigma_{22} = 0.85$. Its masses are $m_1 = 1$ and $m_2 = 0.57$. We appended a smoothing function [107] to the potential at $r = 2.2\sigma_{\alpha\beta}$, just as Coslovich and Pastore [16] did. This function allows the potential to be continuous at $r = 2.2\sigma_{\alpha\beta}$ up to the second derivative. We used a system of $N = 27\,000$ particles with one third being of type 1 (as would be the case in SiO_2). We used a number density of $\rho = N/V = 1.655$. In our simulation, we progressed time forward using a time step of size $\delta t = 0.001$ for temperatures greater than 0.5 and of size $\delta t = 0.004$ for temperatures less than 0.5. We used the reduced units of σ_{11} for length, ϵ_{11} for energy, and $\sqrt{m_1\sigma_{11}^2/\epsilon_{11}}$ for time.

We ran NVE simulations in LAMMPS [95, 96], using a potential programmed by H. Staley. All temperatures were equilibrated for at least 100 relaxation times. (This particular relaxation time is defined later, in Section 3.3). We ran 4 independent equilibrium NVE runs for each temperature for at least $100\tau_\alpha^{a=0.35}$, to get enough statistics. The longer runs were run on the ISTeC Cray Model XE6 at Colorado State University. We compared our results to the harmonic sphere (HARM) system described in Chapter 2, which is a fragile glass-former.

3.3. Structure and dynamics

We examined the structure and dynamics of the strong CP system, comparing it with the HARM system, one of our previously studied fragile glass-formers, of Chapter 2. In the CP system, we saw two peaks in the structure factor, the lower q value one corresponding to intermediate range tetrahedral order, while the higher q value one corresponded to the nearest neighbor distance. Having a small peak in addition to the usual main peak is expected in network forming systems, and since we have two peaks, we examined dynamics at both q values. We show that the CP model is a strong glass-former using an Arrhenius fit. We also found that the Stokes-Einstein relation is violated in the CP system, just as we saw for fragile liquids we studied in Chapter 2.

We compared the structure factors and the partial structure factor in the CP system and the harmonic sphere (HARM) system [89]. Recall that the partial structure factors are given by

$$S_{\alpha\beta}(q) = \frac{1}{\sqrt{N_\alpha N_\beta}} \left\langle \sum_{m=1}^{N_\alpha} \sum_{n=1}^{N_\beta} e^{i\mathbf{q}\cdot(\mathbf{r}_n(0)-\mathbf{r}_m(0))} \right\rangle . \tag{3.2}$$

The total structure factor can be recovered from the partial structure factors using $S(q) = N^{-1}(N_1 S_{11} + N_2 S_{22} + 2\sqrt{N_1 N_2} S_{12})$. Figure 3.1 shows the partial structure factors in the strong CP system and in the fragile HARM system. The total structure factor in the HARM system has a single main peak, which has contributions from all the partial structure factors. In the strong CP system, the total structure factor has two main peaks at $q = 5.0$ and 8.2. The first peak has contributions from all the partial structure factors, and the second peak has contributions from S_{11} and S_{22}, while S_{12} reduces that peak. The peak at $q = 8.2$ corresponds

to nearest neighbor particles, while the peak at $q = 5.0$ corresponds to the tetrahedral order in the system.

We examined the average overlap function as an explicit function of the distance a, since we used two a values. Thus, the average overlap function is

$$F_o(a;t) = \frac{1}{N}\left\langle \sum_n w_n(a;t) \right\rangle, \tag{3.3}$$

where $w_n(a;t) = \Theta[a - |\mathbf{r}_n(t) - \mathbf{r}_n(0)|]$ is the overlap function, Θ is the Heaviside step function, and $\mathbf{r}_n(t)$ is the position of particle n at time t. We chose two a values for eq. 3.3 so that the relaxation time of $F_o(a;t)$ matches that of the self-intermediate scattering function $F_s(q;t)$ at $q = 5.0$ and 8.2. Recall that the self intermediate scattering function is

$$F_s(q;t) = \frac{1}{N}\left\langle \sum_{n=1}^{N} \mathrm{e}^{i\mathbf{q}\cdot[\mathbf{r}_n(t) - \mathbf{r}_n(0)]} \right\rangle. \tag{3.4}$$

The a value that corresponds to $q = 5.0$ is $a = 0.35$, and the a value of 0.2 corresponds to $q = 8.2$. We note that in this system the plateau values of $F_o(a;t)$ are very low, particularly for higher temperatures and smaller a values. Thus we used a new definition for the relaxation times, τ_α^a, where $F_o(a = 0.35; \tau_\alpha^{0.35}) = 0.2$ and $F_o(a = 0.2; \tau_\alpha^{0.2}) = 0.1$.

Figure 3.2 shows the average overlap function from the liquid temperature of $T = 0.69$, to the supercooled liquid temperature of $T = 0.3$, which is below the mode-coupling temperature of the system, $T_c = 0.31$ (see Figure 1.3). For temperatures below 0.51 a plateau developed at intermediate times. This plateau corresponds to particles being trapped in a cage of their nearest neighbors. In the plateau region, for times between 1 and 100, the average overlap function displays oscillations. The magnitude of these oscillations decreases

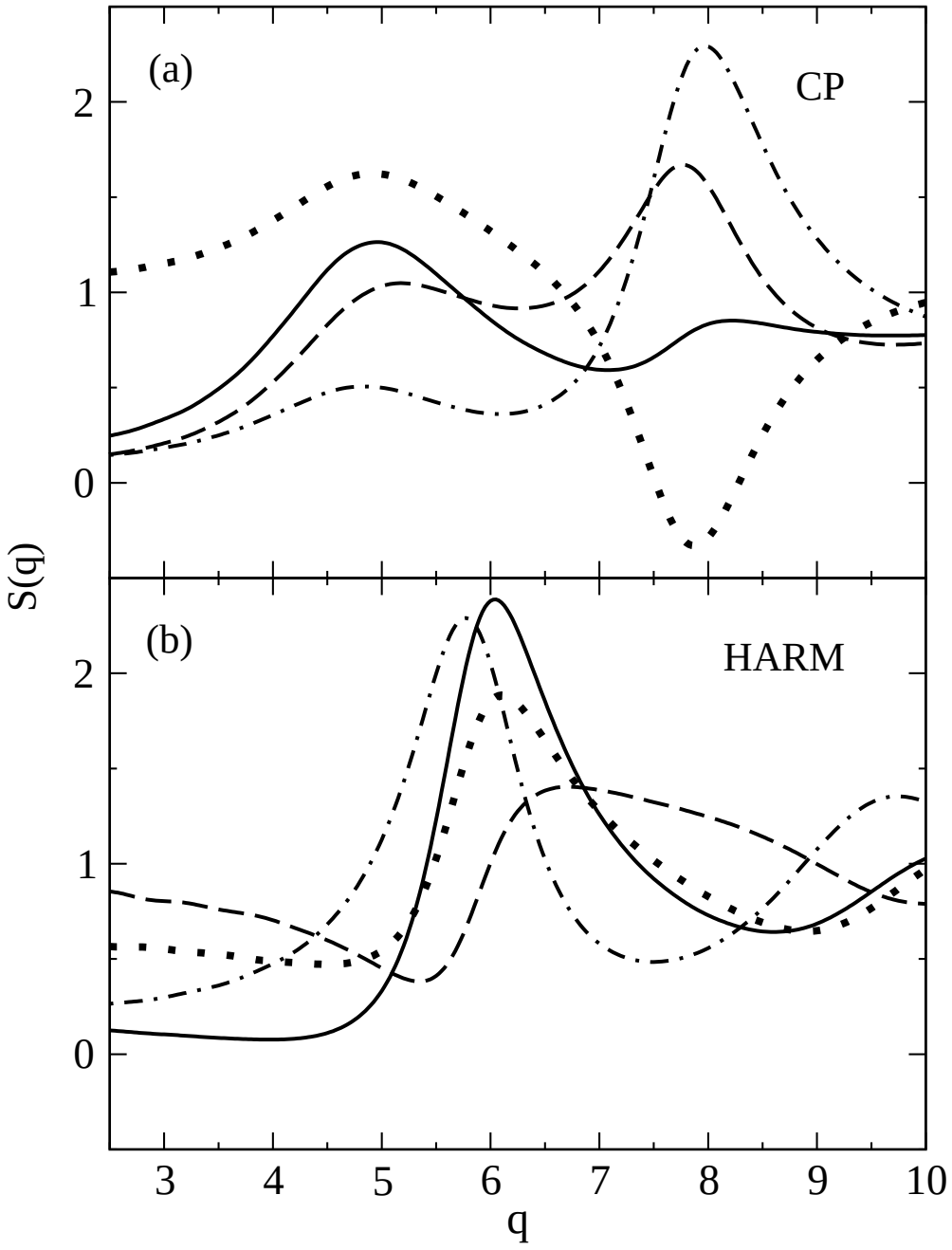

FIGURE 3.1. The total structure factors (solid lines), the partial structure factors $S_{11}(q)$ (dashed lines), the partial structure factors $S_{12}(q)$ (dotted lines), and the partial structure factors $S_{22}(q)$ (dash-dotted lines), for the CP model at $T = 0.42$ (top panel) and for the HARM system at $T = 10$ (bottom panel). The CP system has a main peak at $q = 8.2$ in the total structure factor. The peak at the lower q value of 5.0 in the total structure factor of the CP system corresponds to intermediate range tetrahedral order. For the HARM system there is one peak, which occurs at $q = 6.1$.

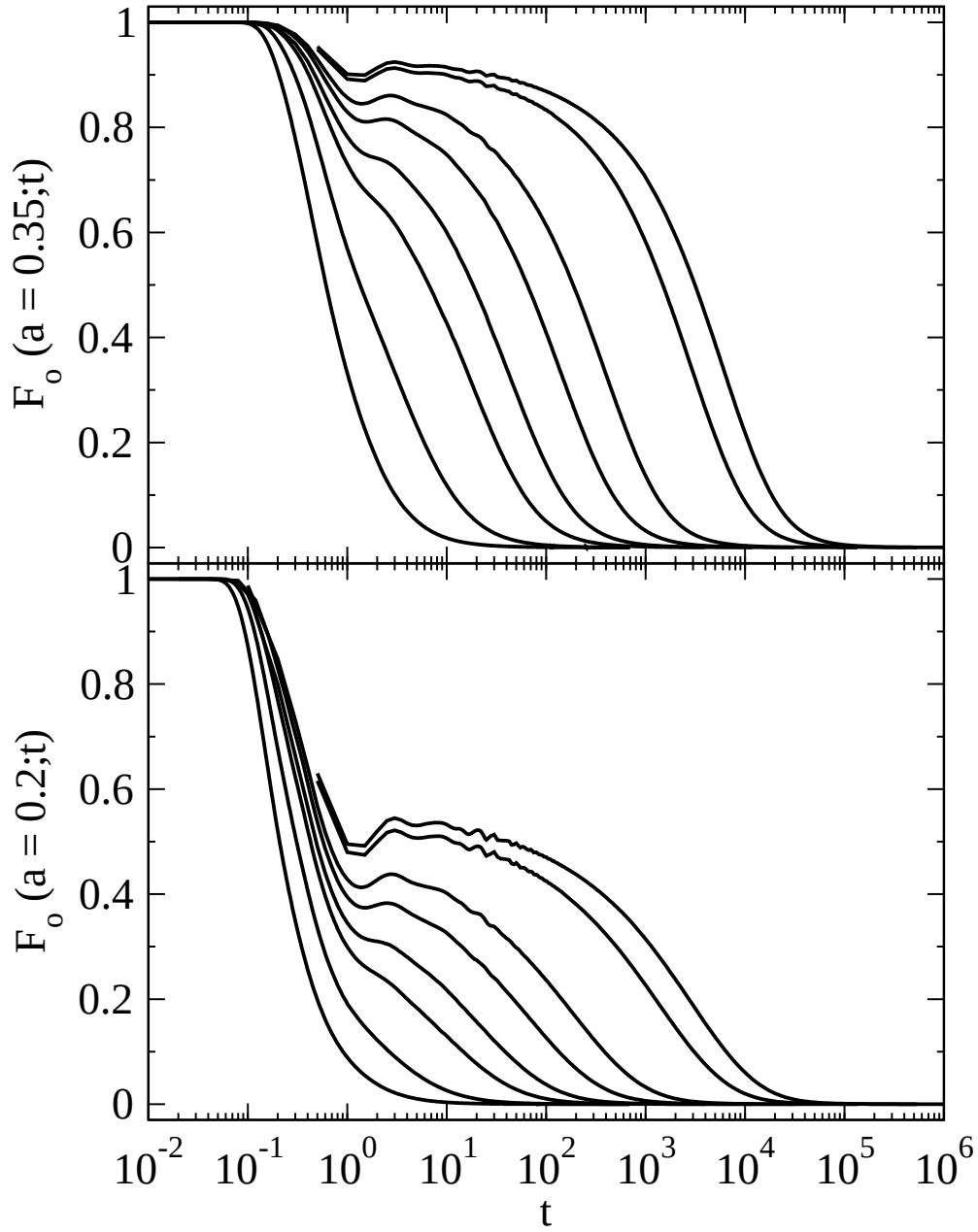

FIGURE 3.2. The average overlap function with overlap distance a of 0.35 (top panel) and 0.2 (bottom panel). The temperatures are $T = 0.69$, 0.51, 0.42, 0.39, 0.36, 0.34, 0.31, and 0.3 listed from left to right.

as the system size increases, but they do not disappear or change location. We suspect they are due to vibrations in the system.

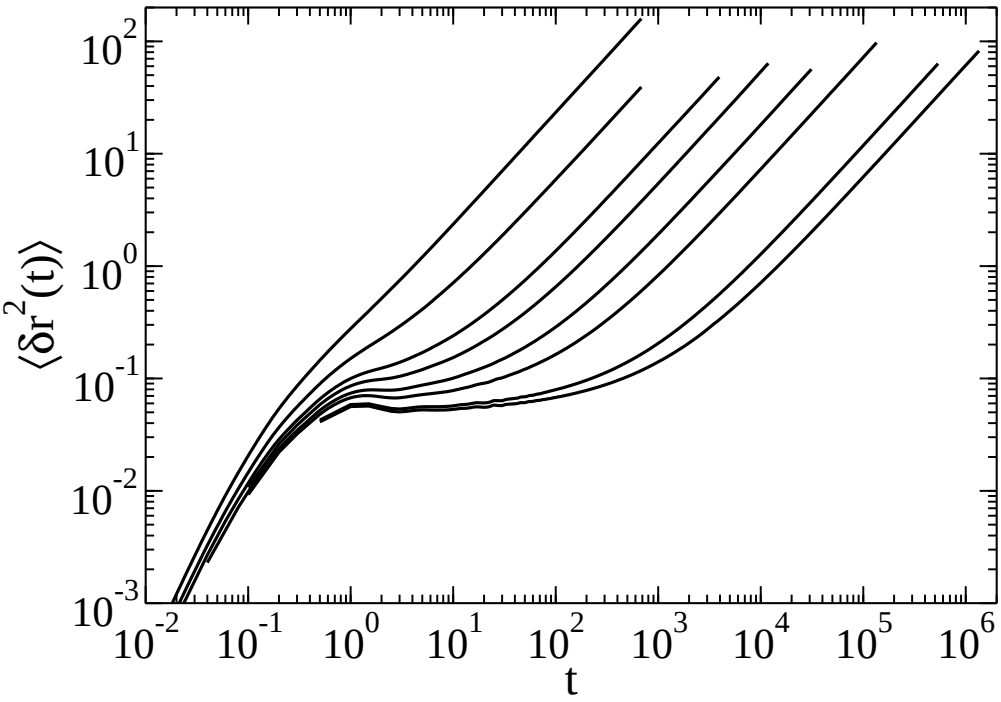

FIGURE 3.3. The mean square displacement $\langle \delta r^2(t) \rangle$ at the temperatures of $T = 0.69$, 0.51, 0.42, 0.39, 0.36, 0.34, 0.31, and 0.3 listed from left to right.

The mean square displacement $\langle \delta r^2(t) \rangle$ is given by

$$\left\langle \delta r^2(t) \right\rangle = \frac{1}{N} \left\langle \sum_{n=1}^{N} \left[\mathbf{r}_n(t) - \mathbf{r}_n(0) \right]^2 \right\rangle . \tag{3.5}$$

Figure 3.3 shows the mean square displacement in the CP system. At short times particles had ballistic motion, obeying $\langle \delta r^2 \rangle = 3 k_B T t^2$. At long times particles had diffusive motion, obeying $\langle \delta r^2 \rangle = 6Dt$. From a fit of the mean square displacement at long times we can extract the diffusion coefficient. At intermediate times there was a plateau for supercooled temperatures. This plateau again corresponds to particles being trapped in cages of their nearest neighbors. The mean square displacement encodes similar information as the average overlap function, which also had a plateau at intermediate times. We feel that we can reasonably compare the CP system to the HARM system, because the plateau heights of the mean square displacements in the two systems are comparable.

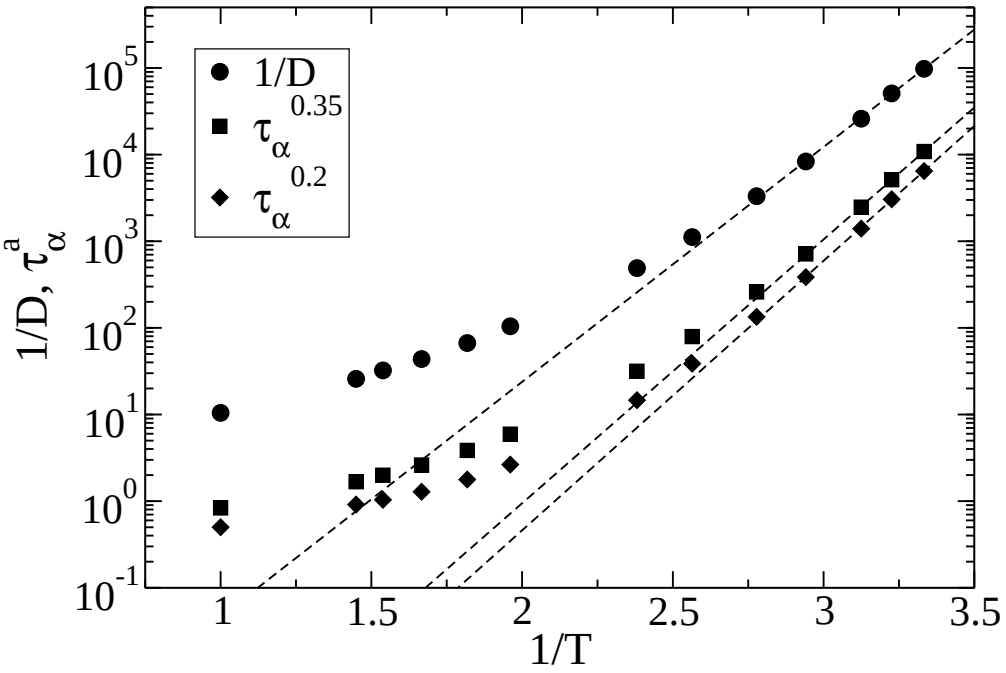

FIGURE 3.4. The inverse diffusion coefficient versus inverse temperature and the relaxation times versus inverse temperature. The black dashed lines show fits to the Arrhenius equations, which are $1/D = A_1 \exp(E_1/T)$ and $\tau_\alpha^a = A_2^a \exp(E_2^a/T)$.

We have stated that the CP system is strong according to the Angell classification. An Angell plot is normally of viscosity η versus temperature T. However, it was difficult to measure η at low temperatures, so we show the diffusion coefficient D and the relaxation time τ_α instead. Figure 3.4 shows Arrhenius fits to the inverse diffusion coefficient as well as the two relaxation times τ_α^a at our two a values. Recall that a strong liquid obeys an Arrhenius fit where the energy does not depend on temperature. We performed the Arrhenius fits of $1/D = A_1 \exp(E_1/T)$ and $\tau_\alpha^a = A_2^a \exp(E_2^a/T)$ for $T < 0.4$. These fits held for temperatures of $T \leq 0.39$. We found the fit parameters of $A_1 = 9 \times 10^{-5}$ and $E_1 = 6.24$, for the inverse diffusion fit. For $\tau_\alpha^{0.35}$, the fit parameters are $A_2^{0.35} = 7.7 \times 10^{-7}$ and $E_2^{0.35} = 7.01$. The fit parameters for $\tau_\alpha^{0.2}$ are $A_2^{0.2} = 2.7 \times 10^{-7}$ and $E_2^{0.2} = 7.17$.

Similarly, Kawasaki, Kim, and Onuki [105], who also simulated the CP system, found that viscosity can be fitted to an Arrhenius equation for $T \lesssim 0.4$. Coslovich and Pastore

[16] also found that the system is strong. They measured strength with a fragility index K_i using fits to

$$\tau(T) = \begin{cases} \tau_i \exp[E_i/T] & T > T_i \\ \tau_i' \exp\left[\frac{1}{K_i(T/T_j)-1}\right] & T < T_i \end{cases}, \tag{3.6}$$

where

$$\tau_i' = \tau_i \exp\left[E_i/T_i - \frac{1}{K_i(T_i/T_j) - 1}\right]. \tag{3.7}$$

T_i is the temperature below which the fit of the relaxation time is super-Arrhenius, and T_j and E_i are fitting parameters. Coslovich and Pastore found a low value for the fragility index, K_i, meaning the system is strong. At a number density of 1.655, (which we use in this chapter), $K_i = 0.09$. They found a K_i of around 0.4 in the Kob Andersen [27] system and a K_i value in the range of 0.8 to 0.9 for the Wahnström [78] system. They noticed that the CP system was stronger than any previously studied Lennard-Jones mixture. The strongest Lennard-Jones system they found was an additive mixture described in [108] which had a K_i value of 0.24.

As in our fragile systems we wished to examine Stokes-Einstein violation. In the CP system we had the complication of having two length scales, and thus two sets of relaxation times. To eliminate the dependence on length scale, we instead calculated the viscosity, which is a measure of the resistance of a liquid to a shear force. Following eq. 8.4.10 from Ref. [10], viscosity can be calculated using

$$\eta = \frac{\beta}{V} \int_0^\infty \left\langle \sigma^{\alpha\beta}(t) \sigma^{\alpha\beta} \right\rangle \mathrm{d}t, \tag{3.8}$$

where $\sigma^{\alpha\beta}$ is an element of the stress tensor, $\alpha, \beta \in$ x, y, z, $\alpha \neq \beta$, and $\left\langle \sigma^{\alpha\beta}(t)\sigma^{\alpha\beta} \right\rangle$ is called the shear stress autocorrelation function. $\sigma^{\alpha\beta}$ is given by eq. 8.4.28 of Ref. [10], which gives

$$\sigma^{\alpha\beta}(t) = \sum_n m_n v_n^\alpha v_n^\beta - \frac{1}{2}\sum_n \sum_{m \neq n} \frac{r_{nm}^\alpha r_{nm}^\beta}{r_{nm}} \frac{dV_{nm}(r_{nm})}{dr_{nm}}, \tag{3.9}$$

where V_{nm} is the potential between particles n and m, r_{nm}^α is the component of $\mathbf{r}_n - \mathbf{r}_m$ in the α direction, $\mathbf{r}_n$ is the position of particle n, v_n^α is the alpha component of the velocity of particle n, $\mathbf{v}_n$. With viscosity, we were able to use the true Stokes-Einstein relation, $D \sim (\eta/T)^{-1}$. Figure 3.5 shows the shear stress autocorrelation function $\left\langle \sigma^{\alpha\beta}(t)\sigma^{\alpha\beta}(0) \right\rangle$ in the CP system. To get the viscosity we integrate this function. As temperature decreases the viscosity gets bigger. Kawasaki, Kim, and Onuki [105] also examined the shear stress autocorrelation function for this system, and their results look quantitatively similar to ours. They suggested that the oscillations in the shear-stress autocorrelation function were sound modes.

We used the viscosity of eq. 3.8 to examine the Stokes-Einstein relation of $D = c(\eta/T)^{-z}$ in Figure 3.6. At high temperatures, $T \geq 0.51$, we found $z = 1.02 \pm 0.02$. Therefore the Stokes-Einstein relation holds for $T \geq 0.51$. At low temperatures, $T \leq 0.42$, we found the fitting parameter of $z = 0.83 \pm 0.02$, meaning that the Stokes-Einstein relation is violated at low temperatures. The point where the two lines intersect indicates the onset of Stokes-Einstein violation. The lines intersect at $\eta_s/T_s = 18.8$, which corresponds to a temperature $T_s = 0.5$, which we call the Stokes-Einstein violation temperature. We note that the temperature for the onset of slow dynamics is $T_o = 0.5$, which we define as the temperature where a plateau emerges in $F_s(q;t)$ and $F_o(a,t)$. Coslovich and Pastore [16] and Kim and Saito [17] saw a plateau emerge at this temperature.

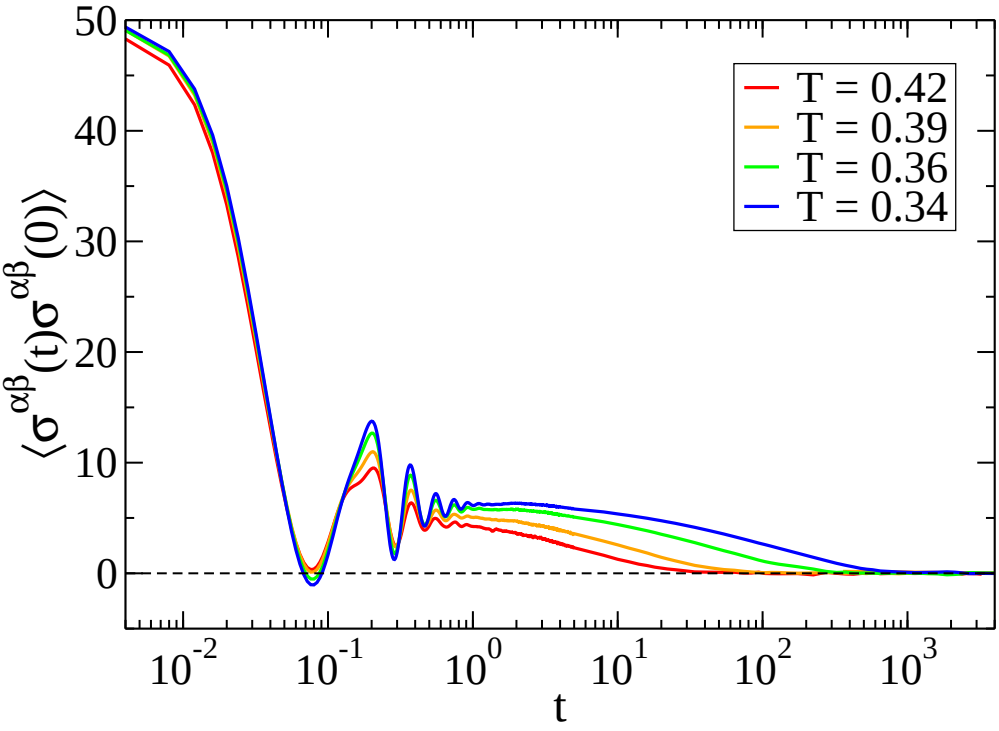

FIGURE 3.5. The shear stress autocorrelation function at four supercooled liquid temperatures.

Kawasaki, Kim, and Onuki [105] also examined the Stokes-Einstein equation in the CP system for D as a function of η/T, finding that it is weakly violated in this system. We also found a weak violation. In the CP system we found that when the Stokes-Einstein relation breaks down diffusion is related to viscosity by $D \sim (\eta/T)^{-0.83}$. In Chapter 2 we examined another Stokes-Einstein relation of $D \sim \tau_\alpha^{-1}$ [1]. The fragile HARM system had a much stronger Stokes-Einstein violation of $D \sim \tau_\alpha^{-0.65}$ [1] for the harmonic sphere system [89]. Of course, these Stokes-Einstein relations are different, thus the power may not be the same as it would be in a different Stokes-Einstein relation.

3.4. DYNAMIC HETEROGENEITY

In Chapter 2, we saw a connection between Stokes-Einstein violation and dynamic heterogeneity in five fragile glass-formers [1]. For temperatures below the Stokes-Einstein violation

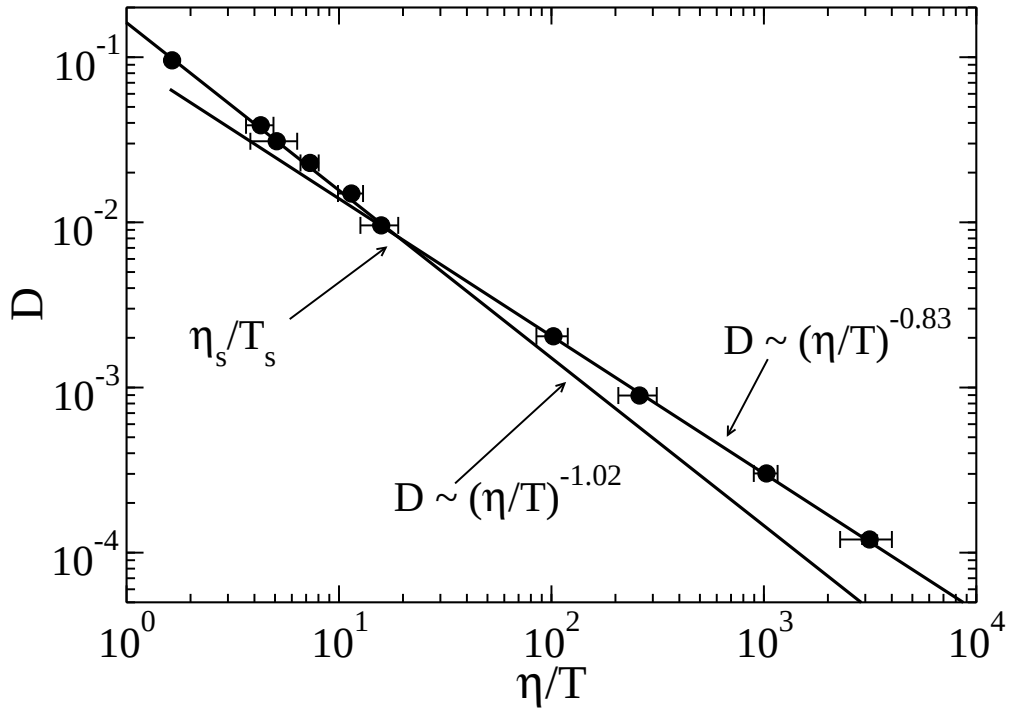

FIGURE 3.6. The diffusion coefficient as a function of viscosity η over temperature T. The temperatures shown are 1.0, 0.69, 0.65, 0.6, 0.55, 0.51, 0.42, 0.39, 0.36, and 0.34, listed from left to right. The lines are fits to the power law $D = c(\eta/T)^{-z}$ for the fitting ranges of $T \geq 0.51$ and $T \leq 0.42$. The lines intersect at $\eta_s/T_s = 18.8$, which corresponds to a Stokes-Einstein relation violation temperature of $T_s = 0.5$.

temperature, T_s, regions with correlated particle dynamics became compact. This behavior was also seen in a two-dimensional colloid experiment [99]. In the strong glass-former studied here, regions with correlated particle motion are not compact below T_s. Also, the length scale of dynamic heterogeneity is much smaller in the strong glass-former than it was in any of the fragile glass-formers, and it grows much more slowly as temperature is decreased.

We calculate dynamic susceptibility in the NVE ensemble using

$$\chi_4^a(t)|_{NVE} = \frac{1}{N}\left(\left\langle\left[\sum_n w_n(a;t)\right]^2\right\rangle - \left\langle\sum_n w_n(a;t)\right\rangle^2\right). \tag{3.10}$$

Recall that we expect the full susceptibility to grow as temperature is decreased. Figure 3.7 shows that we also observe this trend in the ensemble dependent susceptibility $\chi_4^a(t)|_{NVE}$. A

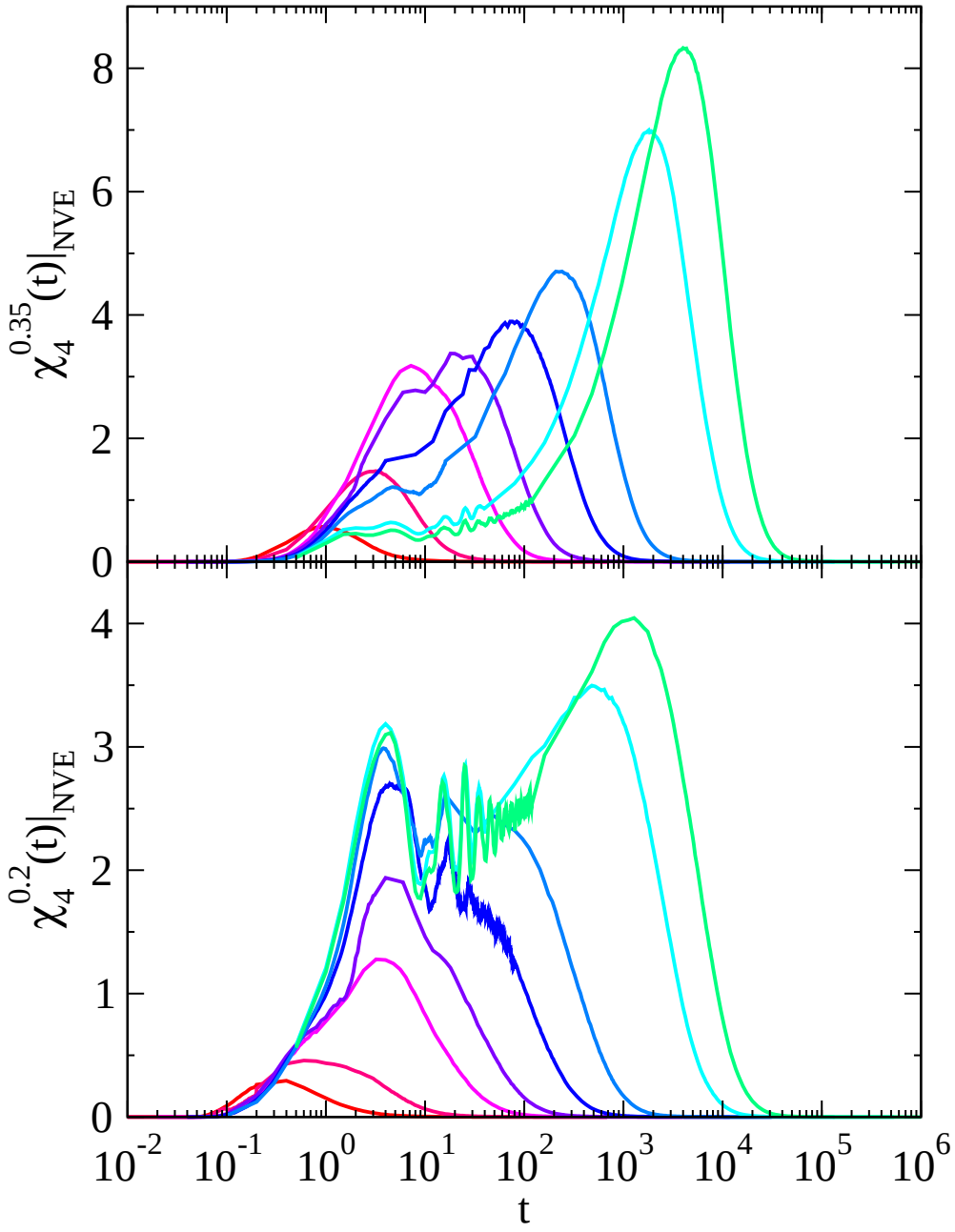

FIGURE 3.7. The dynamic susceptibility $\chi_4^a(t)|_{NVE}$ from constant energy simulations with $a = 0.35$ (top panel) and $a = 0.2$ (bottom panel) in the overlap functions. From left to right, the peaks correspond to temperatures of 0.69, 0.51, 0.42, 0.39, 0.36, 0.34, 0.31, and 0.3.

side peak emerges as temperature is decreased, which we did not see for the fragile formers [1]. As we saw in the average overlap function, the susceptibility displays oscillations for times between 1 and 100.

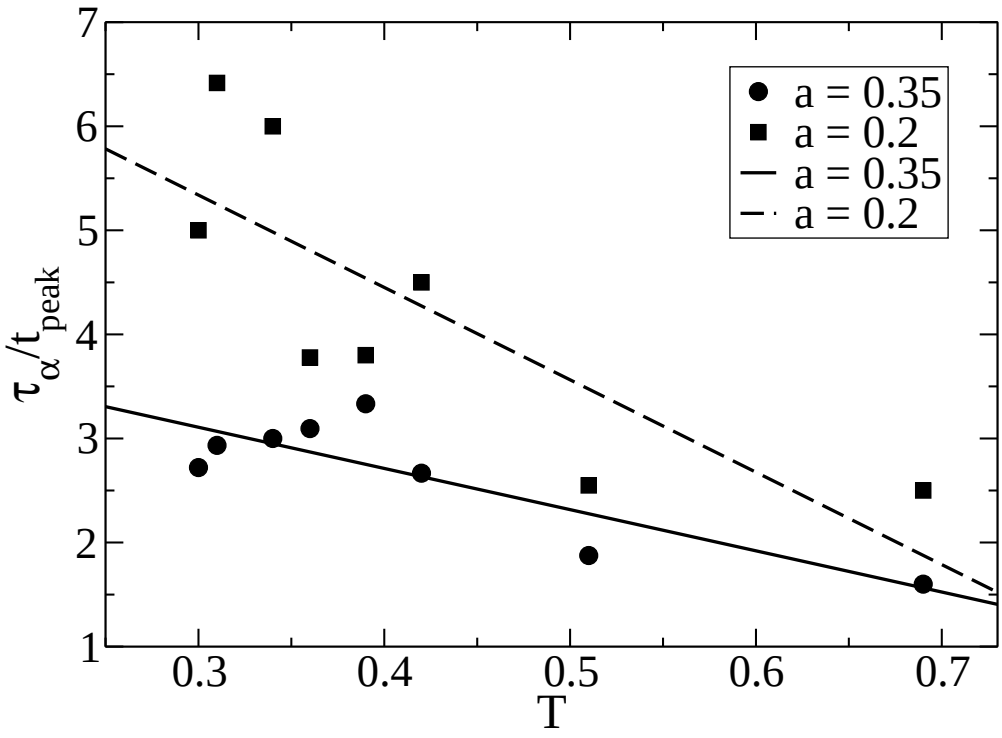

FIGURE 3.8. The ratio of the relaxation time, τ_α^a, to the time of the peak of the susceptibility, τ_p^a, versus temperature. The lines are linear fits to the data.

In many systems [109, 110] we find that the relaxation time tracks the time of the peak of the susceptibility. In Figure 3.8 we examine the ratio of the relaxation time τ_α^a to the time of the peak of the susceptibility τ_p^a as a function of temperature for both a values. Unlike in other systems, where τ_α^a and τ_p^a have the same temperature dependence, in the CP system, the ratio of τ_α^a to τ_p^a is not constant as temperature changes. In fact, the ratio had a weak temperature dependence, growing slightly as temperature decreases. Normally we would track the length scale of dynamic heterogeneity at the time where the susceptibility is strongest, the peak time τ_p. But length is often in fact measured at the relaxation time τ_α, as this time is usually equivalent to τ_p. Since these two times are not equivalent in our system, we measured the strength, χ_4, and length scale of dynamic heterogeneity, ξ_4, at both times.

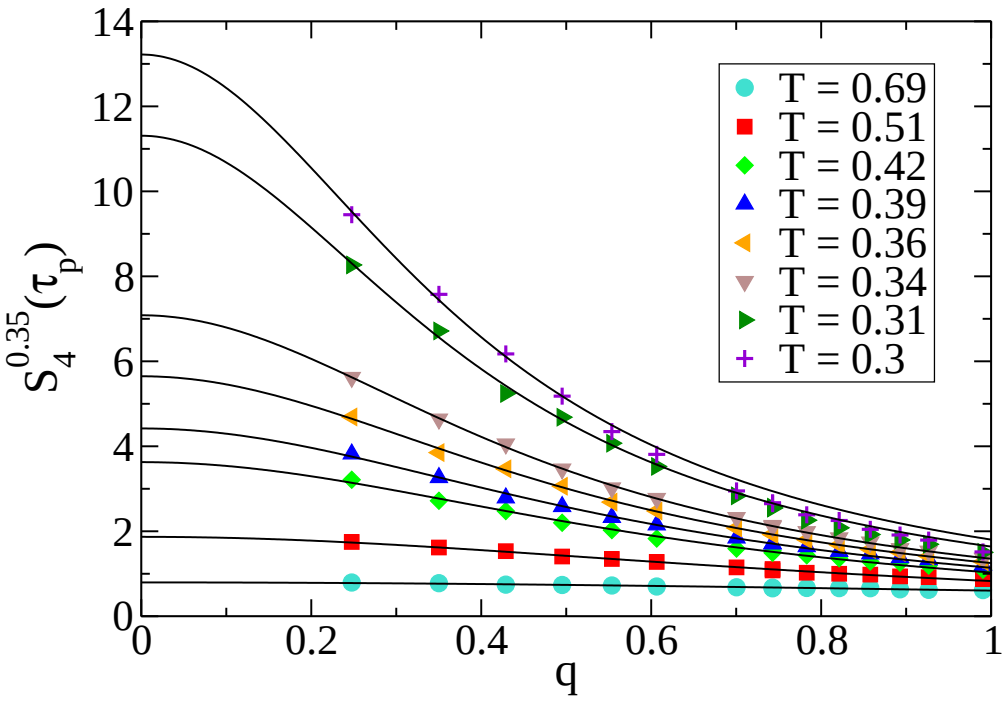

FIGURE 3.9. The four-point structure factor, $S_4^{0.35}(\tau_p)$, with the $a = 0.35$ in the overlap function, at the time of the peak, τ_p, of the susceptibility. The solid lines show the Ornstein-Zernicke fits to the data.

We measured the four point structure factor with the overlap function as the weighting function, giving

$$S_4^a(q;t) = \frac{1}{N}\left\langle \sum_{n,m} w_n(a;t) w_m(a;t) e^{i\mathbf{q}\cdot(\mathbf{r}_n(0)-\mathbf{r}_m(0))} \right\rangle, \tag{3.11}$$

where $w_n(a;t) = \Theta(a - |\mathbf{r}_n(t) - \mathbf{r}_n(0)|)$. As usual we fit $S_4^a(q;t)$ to the Ornstein-Zernicke equation $\chi_4^a(t)/[1 + (\xi_4^a(t)q)^2]$, for $q \leq 1$ and $q < 1.5/\xi_4^a(t)$, to get the full susceptibility $\chi_4^a(t)$, and the dynamic correlation length $\xi_4^a(t)$. We examined dynamic heterogeneity at our two a values of 0.35 and 0.2, and at our two times of τ_α and τ_p. Figure 3.9 shows the Ornstein-Zernicke fits for $S_4^a(q;t)$, where $a = 0.35$ and $t = \tau_p$. The fits worked well for the specified ranges, as they did for the other values of a and t.

Figure 3.10 shows the full susceptibility, χ_4, plotted against the dynamic correlation length, ξ_4, at our two a distances and two times. We applied a fit of $\chi_4^a = A(\xi_4^a)^z$ to each data set for temperatures below the Stokes-Einstein violation temperature, T_s, and temperatures above T_s. For all the data, the power z increased when going from temperature above T_s to temperatures below T_s. We note that the power law fits of the data intersect near the point of Stokes-Einstein violation, which is marked by a dashed vertical line. This increase in z was also seen in the fragile glasses [1]. However, for all the fragile glasses we examined z was approximately 3 for temperatures below T_s. This power of z gives an expression of $\chi_4 \sim (\xi_4)^3$. Recall that χ_4 is related to the number of particles with correlated motion, and ξ_4 gives a length scale of correlated motion. Thus a z value of 3 would imply that regions with particles that have correlated motion are compact. In the strong CP system, z did not reach 3 for temperatures below T_s. However, the Stokes-Einstein violation temperature did mark a change in the power of our fitting equation.

Figure 3.11 shows the dynamic correlation length as a function of rescaled time again at our two a values and two times. Just as in Figure 2.3, we rescaled the relaxation time or peak time to the value at the Stokes-Einstein violation temperature. Figure 3.11 has a rescaled time to match the relaxation time of 303, which corresponds to the relaxation time at the Stokes-Einstein violation temperature in the HARM system. Recall that in the fragile systems we only needed to rescale relaxation time to its Stokes-Einstein violation value to collapse the data of length plotted as a function of time for all the systems studied. For the strong CP system, we felt it was valid to directly compare lengths without rescaling since the plateau heights of the mean square displacement were similar in the HARM and CP systems, as we discussed in Section 3.3. In the strong CP system, rescaling time resulted in

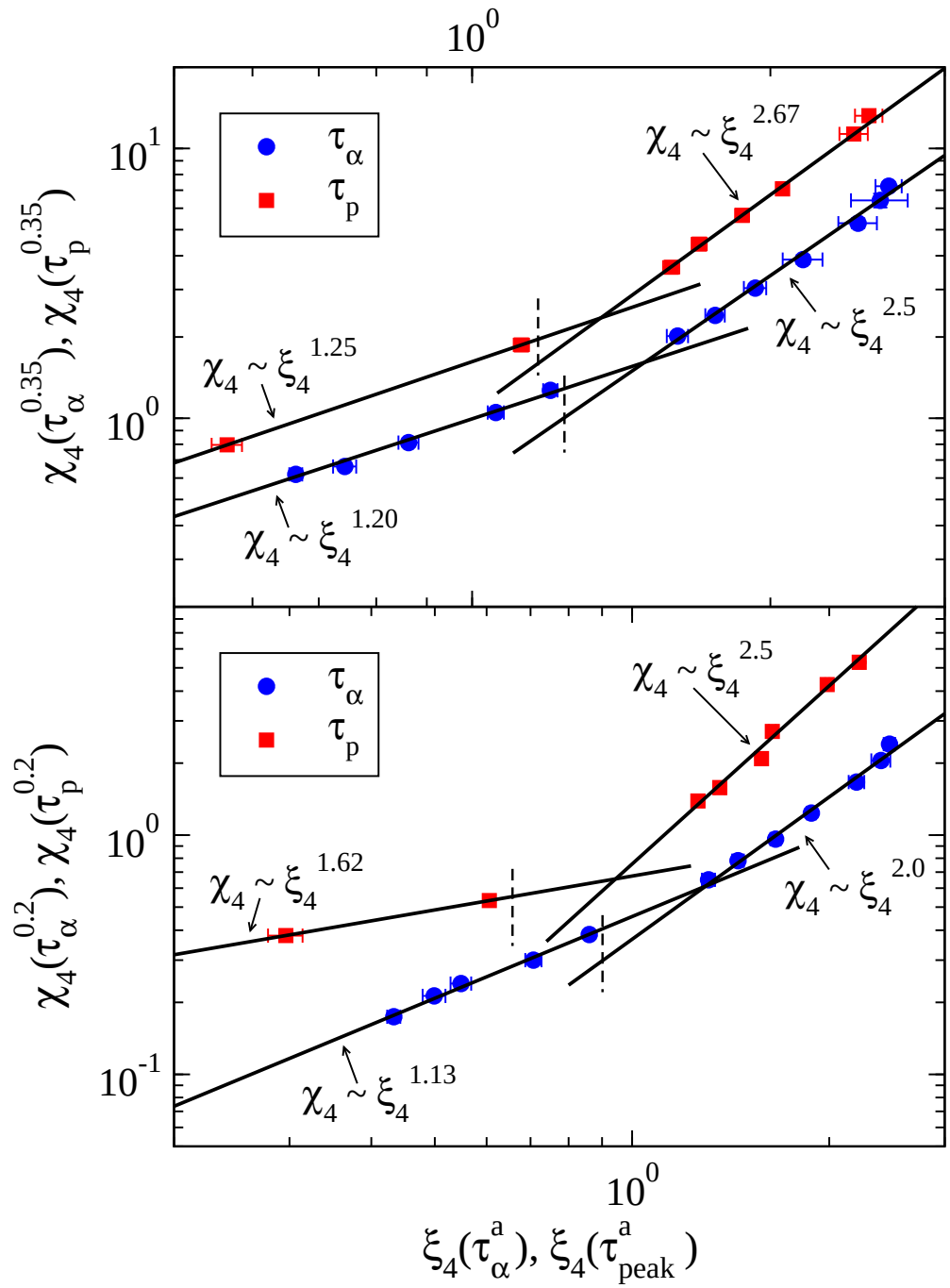

FIGURE 3.10. The full susceptibility χ_4 calculated from a fit to the four-point structure factor versus dynamic correlation length ξ_4 at the a values of 0.35 (top panel) and 0.2 (bottom panel) in the overlap function and at two times. The blue circles show results at the relaxation times τ_α^a, and the red squares show results at the time of the peak of the dynamic susceptibility τ_p^a. The black lines are fits to $\chi_4^a = A(\xi_4^a)^z$ for temperatures above and below the Stokes-Einstein violation temperature, T_s. The dashed black vertical lines show the length ξ_4^s that corresponds to T_s.

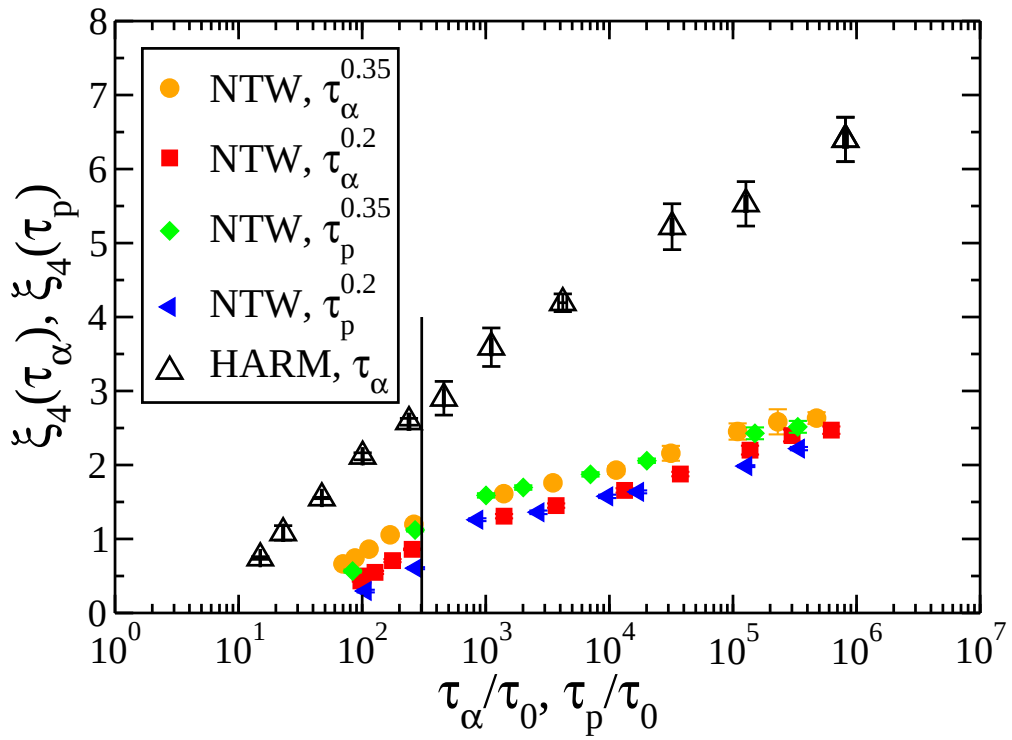

FIGURE 3.11. The dynamic correlation length ξ_4 as a function of the rescaled times, τ_α/τ_0 and τ_p/τ_0. Closed symbols correspond to the strong glass-former of the CP model and the open symbols correspond to the fragile glass-former of the HARM model. The black vertical line marks the rescaled Stokes-Einstein violation time, τ_α^s/τ_0 or τ_p^s/τ_0. The scaling factors τ_0 were chosen so that all the data sets cross this line at the relaxation time or peak time corresponding to Stokes-Einstein violation.

much smaller lengths ξ_4 than were seen in the fragile systems. Recall that Kim and Saito [17] also reported that the strong CP system had smaller length scales for dynamic heterogeneity than they saw in fragile liquids. The dynamic correlation length grows more slowly with decreasing temperature than it did for fragile glass-formers.

Interestingly, the Stokes-Einstein violation temperature, T_s, looks important in Figure 3.11. T_s seems to mark a change in behavior of dynamic correlation length as a function of relaxation or peak time. We can not precisely define the relationship between ξ_4 and time, since we do not have enough data. Specifically, for temperatures above the Stokes-Einstein violation temperature, T_s, the dynamic correlation length is very small, falling below 1.

Length needs to be at least 1 to include more than one particle in the correlated region. The tiny lengths we see for temperatures above T_s make it hard to interpret that data. Indeed, since T_s corresponds to the onset temperature, T_o, for slow particles, there probably is not any correlated particle mobility above that temperature. Thus getting more data at higher temperatures is probably not useful. For temperatures below T_s we see that dynamic correlation lengths do not increase nearly as much as the dynamic correlation length scale in the fragile glass formers [1], and does not even reach 3 at our lowest temperature. Fitting this small change in length is very difficult to do accurately. On the other hand, we can see that there appears to be a change in the slope of ξ_4 as a function of time on the linear log scale.

CHAPTER 4

Cooling a Kob Andersen system

This chapter describes work that was published in the paper by Staley, Flenner, and Szamel [3] entitled "Cooling-rate dependence of kinetic and mechanical stabilities of simulated glasses".

4.1. Introduction

Vapor deposited glasses created at a particular substrate temperature have been found to have higher stability than glasses created by cooling or annealing for a number of materials [45, 47, 111–113]. Recall that Swallen *et al.* [45] found that some vapor deposited glasses were ultrastable, having stabilities equivalent to glasses that had been aged tens to thousands of years [42]. They deposited a material onto a substrate, and chose the substrate temperature that created the most stable glasses. They discovered that this temperature was around 85% of the glass transition temperature T_g. One way they measured stability was to heat a glass at constant pressure untill it was a liquid while measuring the heat capacity, which shows a peak when a glass melts. They defined the beginning of the peak to be the onset temperature for melting. They used this temperature to compare the stability of glasses, since a more stable glass will melt at a higher temperature.

Computer simulations have tried to reproduce the high stability seen in vapor deposited glasses. Jack *et al.* [114] examined inactive states. Inactive states are in contact with a heat bath meaning that their vibrational degrees of freedom are in thermal equilibrium, while their structural degrees of freedom are deep in in the energy landscape. They used the s-ensemble to make inactive states. Inactive states were created by applying the s field,

which made large net displacements less likely at each time step. Thus trajectories with more particle motion were suppressed. They studied the s-ensemble in the Kob-Andersen (KA) system [27], the model system we examine in this chapter. They applied the s field starting from equilibrium configurations at a temperature T. They found that the inactive states created by the s ensemble had larger kinetic stability and lower inherent structure energy than the equilibrium supercooled liquid at a temperature lower than T. Thus, the s ensemble successfully created stable glasses in simulations. Of course, the s field is a computer construction, and can not be used in real experiments.

Another group that created stable glasses in simulations was Hocky *et al.* [115]. They examined a two dimensional KA system with pinned particles, carefully creating systems that were isotropic and uniform. They found that pinning increased kinetic stability. Systems with random pinning have fewer possible configurations, and so the glass transition temperature is higher than in a system without pinning. Also, when a system with random pinning is created from an equilibrium system, then the new system will also be in equilibrium. Thus a system with random pinning can be more deeply supercooled than an ordinary system it was created from, since the system with random pinning will be closer to its glass transition temperature. This greater supercooling in a system with random pinning accounts for its higher stability. We used their particular measure of kinetic stability, and it appears in Section 4.3.

Léonard and Harrowell [51] created a stable glass by attempting to mimic vapor deposition in a simplified system. They investigated a three-spin facilitated Ising model in three dimensions. A spin model has uniform square cells. In each cell there is a spin that points in a certain direction (in this system up or down). A spin cannot flip unless a set number of

its neighbors are spin up. They modeled the cold substrate with down spins, and made the incoming deposited layer of hot particles all up spins. They found a higher kinetic stability in their "deposited" films than in a bulk simulation created by cooling and annealing.

Some researchers tried to directly model vapor deposition of molecules and particles. Singh and de Pablo [52] first tried a procedure where they modeled the vapor deposition of the molecule trehalose, which is two bonded glucose molecules. They prepared the system by first creating a fixed position substrate with an empty vacuum region above it. To simulate vapor deposition, they first introduced 1 to 5 hot molecules, then minimized the energy of the system. Then an equilibration run was performed, where the temperature of the molecules and the substrate was held constant. By this time, the molecules had neared the substrate. The molecules were then cooled to the substrate temperature at a constant density, during which time, the molecules adhered to the substrate. Then another equilibration was performed at the substrate temperature. Finally, there was another energy minimization, and then the steps were repeated. They succeeded in creating glasses with higher kinetic stability than the stability in glasses created by cooling at a constant rate. They saw anisotropy in density in the direction perpendicular to the surface, since molecules were creating layers.

Singh, Ediger, and de Pablo [46] and Lyubimov, Ediger, and de Pablo [42] modeled vapor deposition in the binary Lennard-Jones system created by Kob and Andersen [27], KA. They prepared their systems in similar ways as Singh and de Pablo [52]. Singh, Ediger, and de Pablo [46] and Lyubimov, Ediger, and de Pablo [42] also created glasses by cooling to compare them with their vapor deposited glasses. Singh, Ediger, and de Pablo cooled their particles at a constant density, while Lyubimov, Ediger, and de Pablo [42] cooled their

particles at a constant pressure. The study of Lyubimov *et al.* came after the study by Singh *et al.*, and they examined thicker deposited glasses and considered results from the center of the film, getting rid of any anisotropy in particle concentration or density due to the substrate or the surface of the film. These effects caused Singh *et al.* to report stability that was too high in their glasses. Lyubimov *et al.* found that their results for energy were different from the energy results of Singh *et al.*, concluding that the anisotropy of the glass affected potential energy. Both groups measured higher kinetic stability than for a glass created by cooling at a constant rate. Both groups examined an onset temperature for melting as Swallen *et al.* [45] did. Recall that a higher onset temperature for melting means the glass is more stable. They found that their onset temperature for melting was larger for their vapor deposited glasses than for their reference glasses created by cooling. Lyubimov *et al.* saw anisotropy of the system in the surface normal direction, with particle concentration of small particles varying as a function of distance from the surface. This anisotropy affected the density, which varied with particle concentration. The glasses created in both papers had higher densities than the ones they created by cooling at a constant rate. Singh *et al.* believed that this difference is not very important [46], and Lyubimov *et al.* pointed out that their vapor deposited glasses were created at the same pressure as their glasses created by cooling at a constant rate.

Vapor deposition experiments and computer simulations alike must compare the stability of their glasses with that of glasses created by cooling in order to understand the significance of their values of stability. We wanted to do a thorough simulational study of the stability of glasses created by cooling at a constant rate, examining different measures of stability. We hope that our study will establish measures of stability that are useful in different systems.

To this end we studied kinetic and mechanical stability in the very commonly modeled Kob Andersen [27] (KA) system. Lyubimov *et al.* [42] found that the energy, a measure of stability, was affected by anisotropy and density in a system. We saw how great the effect of varying densities could be. The systems we created were isotropic and uniform. We created glasses by constant cooling from a supercooled liquid. We examined kinetic stability by heating the glasses. We also studied dynamic heterogeneity during the heating process. We examined mechanical stability by investigating the potential energy and the shear modulus of the glass.

4.2. Simulations

We used the Kob-Andersen potential,

$$V_{\alpha\beta}^{KA}(r) = 4\epsilon_{\alpha\beta}\left[\left(\frac{\sigma_{\alpha\beta}}{r}\right)^{12} - \left(\frac{\sigma_{\alpha\beta}}{r}\right)^{6}\right], \tag{4.1}$$

in three dimensions. In eq. 4.1, r is the distance between a pair of particles, and the subscripts α and β refer to particle types 1 or 2. We present our results in the reduced Lennard-Jones units of σ_{11} for length, ϵ_{11}/k_B for temperature, and $\sqrt{m_1\sigma_{11}^2/\epsilon_{11}}$ for time. We simulated 8000 particles at the commonly used number density of $\rho = 1.20$. We performed NVT simulations using the Nosé-Hoover thermostat. We ran simulations in LAMMPS [95, 96, 116, 117] and HOOMD-blue [97, 98]. We ran simulations on a GPU (graphics processing unit), mostly using an NVIDIA Tesla K20c GPU. We used a time step size of 0.002 and, as is suggested by the LAMMPS website, a time constant of 100 times the times step size for the time parameter in the thermostat. In this system the onset temperature for slow dynamics is $T_o \approx 1.0$ [27] and the mode-coupling temperature is $T_c = 0.435$ [27], as we saw in Section 1.5.1.

4.2.1. Cooling. When a system is cooled below the glass transition temperature, as is the case in this chapter, it cannot reach equilibrium, and it will age. When a system is aging, the time averages change with how long we average. In order to get an average for correlation functions, we performed many cooling trajectories, and averaged over trajectories instead of time. We began with 80 equilibrium configurations of a $T = 0.5$ fluid. We cooled each configuration down to a temperature of $T = 0.3$ at the rates of 3.33×10^{-n}, where $n = 3$, 4, 5, 6, and 7. We also cooled at our slowest rate 3.33×10^{-8} from four initial configurations.

We calculated the average potential energy $\langle U \rangle$, the order parameter Q_6, given by eq. 4.6, and the pair correlation function $g(r)$, given by eq. 4.2, at $T = 0.3$ for each cooling rate by averaging over configurations from $T = 0.31$ to $T = 0.29$. We also calculated the inherent structure energy E_{IS}. Stillinger [118] describes the potential energy landscape as having a height at each point in configuration space, which has $3N$ coordinates. The space is made up of maxima, minima, and saddle points. The inherent structures refer to the local minima in the landscape. Vibrations move the system in a between potential energy basins. The inherent structure energy is the energy of the system at the bottom of the nearest local minimum. In simulations, we find this energy by doing an energy minimization, which moves the system downward in the potential energy landscape, until the system can't go down any more and is trapped in a well. We calculated E_{IS} by performing an energy minimization on each final configuration at $T = 0.3$. We used the fast inertial relaxation engine (FIRE) algorithm [119], which is described in Section 4.5.1, to do energy minimizations. We then averaged the minimized energies over final configurations of all the trajectories to get the average inherent structure energy, $\langle E_{IS} \rangle$.

4.2.2. Heating. We studied the dynamics on melting, as has been done in computer simulations [115] and experiments [45]. We found that a sudden change of temperature from $T = 0.3$ to the liquid temperature of 0.5 produced large unphysical oscillations in both the kinetic and potential energies, as seen in Figure 4.1. These oscillations were due to using a Nosé-Hoover thermostat. (The Nosé-Hoover thermostat is used to get a canonical ensemble. The simulator fixes the desired temperature, and the simulation is meant to proceed allowing for typical fluctuations seen in the canonical distribution.) So instead we heated from $T = 0.3$ to $T = 0.5$ at a constant rate over a time of 10. We then ran at $T = 0.5$ until the mean square displacement grew linearly with time. We call this ramping up of temperature and subsequent run at a constant temperature a heating trajectory. We note that the time of 10 over which temperature was ramped up is only a small fraction of a total heating trajectory, which were at least a time of 5000.

For cooling rates of $\dot{T} > 3.33 \times 10^{-8}$ we ran one heating trajectory from each of the 80 initial conditions produced by the cooling runs, for each cooling rate. For the glass produced by cooling at the slowest rate of 3.33×10^{-8}, we heated to $T = 0.5$ and the additional temperatures of 0.47 and 0.55. We used these additional temperatures to investigate the temperature dependence of kinetic stability. For each of the four final configurations created from cooling at the slowest cooling rate, we ran 15 different heating trajectories started with different random initial velocities, to each of the three temperatures mentioned. All heating trajectory results are averaged over all heating trajectories for each initial cooling rate.

4.2.3. Annealing. We wanted to examine the glass's shear modulus. We used the method of eq. 4.18, which will be described in more detail in Section 4.5.2. This equation for the shear modulus requires using the long time behavior of a four-point structure factor,

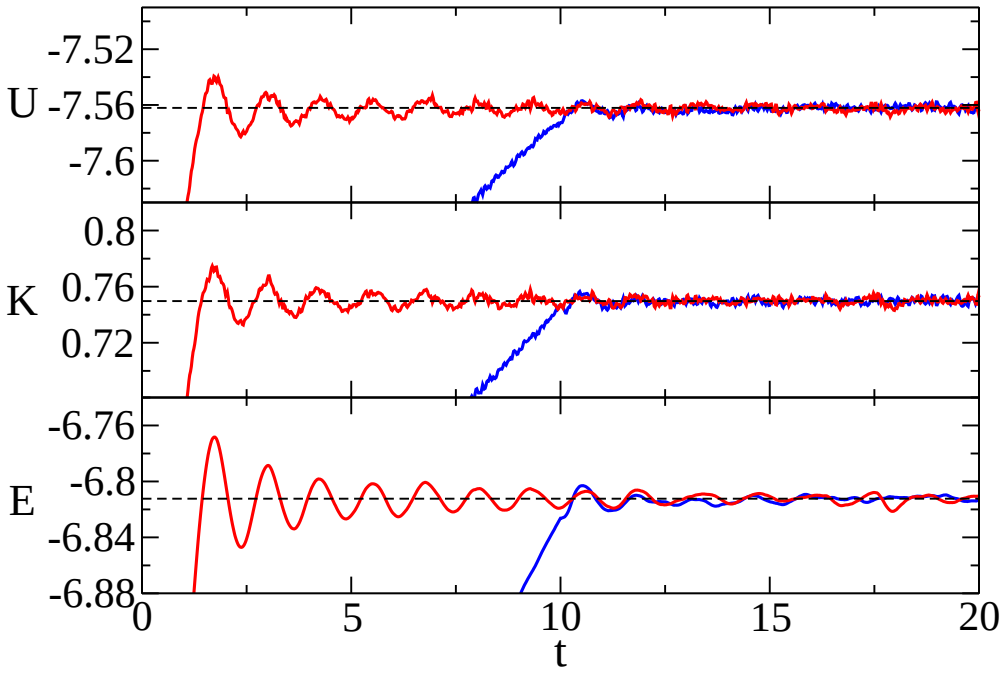

FIGURE 4.1. Energy over a time of 20. Glasses started at a temperature of 0.3, after being cooled at the rate of 3.33×10^{-7}. The blue curves show the energy of the system as it was reheated to $T = 0.5$ over a time of 10. The system was then held at $T = 0.5$. This procedure was our normal heating method. The red curve shows an alternative procedure, which we chose not to use. In this procedure, the temperature of the glasses was instantaneously set to 0.5, and then held there. Each of the energy curves is an average over 10 trajectories. The top panel is potential energy, U, the middle panel is kinetic energy, K, and the bottom panel is total energy, $E = U + K$. The black dashed line shows the average energy for the final time of 6, in each panel.

eq. 4.19, as described in Section 4.5.2. We ran annealing trajectories, (constant temperature runs), at $T = 0.3$ after cooling at different rates. The temperature of 0.3 was the substrate temperature that created the the most stable vapor deposited glasses in the KA system. Thus, we could compare our glasses to vapor deposited glasses, which stay at the substrate temperature once they are deposited. For the cooling rates $\dot{T} > 3.33 \times 10^{-8}$ we did 80 annealing runs at each cooling rate from each of the independent initial conditions. We found that the glass was aging too quickly at the fastest two cooling rates to get the shear modulus. We had to be careful that our system wasn't aging, since aging changes the result of the shear modulus. For the cooling rates of 3.33×10^{-n} where $n = 5$, 6, and 7 we averaged

over time origins for $t \leq 100$ for each annealing trajectory. We note that our averaging occurred at times before aging began. For the slowest cooling rate of 3.33×10^{-8}, we ran 5 annealing trajectories from each of the 4 initial configurations, with different random initial velocities. At this cooling rate we averaged over time origins for $t \leq 400$ for each annealing trajectory. As at the faster cooling rates, the time average was done before the aging began.

4.2.4. Checks for crystallization. We checked that we were examining the properties of a glass and not a crystal after cooling the system to $T = 0.3$ by doing two checks for crystallization. We examined the pair correlation function,

$$g_{\alpha\beta}(r) = \frac{1}{\rho} \left\langle \frac{1}{N} \sum_{n}^{N_\alpha} \sum_{m \neq n}^{N_\beta} \delta(\mathbf{r} - [\mathbf{r}_m(0) - \mathbf{r}_n(0)]) \right\rangle, \tag{4.2}$$

where α and β refer to particle types 1 or 2, and $\mathbf{r}_n(t)$ is the position of particle n at time t. Figure 4.2 shows the pair correlation function between pairs of different types of particles. We note that the peaks in the pair correlation functions appear in the same locations in the $T = 0.3$ glass and in the supercooled liquid of $T = 0.5$. The peaks are slightly more pronounced at $T = 0.3$. In a crystal the pair correlation function develops many more peaks. We would see taller peaks and more of them if the system had crystallized. (Recall Figure 1.1.) Thus crystalline order has not developed.

We also examined the order parameter, Q_6, to check for crystallization in the system. Q_6 is a bond orientational order parameter, which uses spherical harmonics, in three-dimensions. This type of order parameter was developed by Steinhardt, Nelson, and Ronchetti [120]. This order parameter probes the correlation in the orientations of vectors that point from one particle to its neighboring particles. If there is any orientational correlation in the vectors, the order parameter will be bigger. Here we examined the particular Q_6 parameter used in

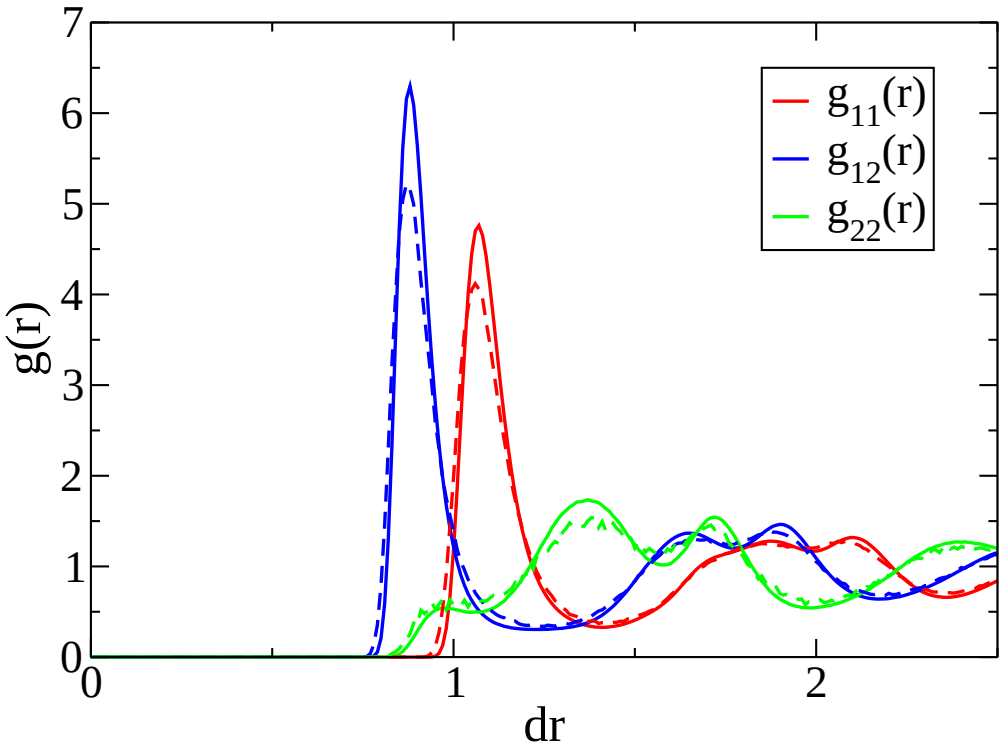

FIGURE 4.2. The pair correlation function, $g_{\alpha\beta}(r)$, at a temperature of 0.3 after cooling at the rate of $\dot{T} = 3.33 \times 10^{-7}$ (solid lines). At all other cooling rates $g_{\alpha\beta}(r)$ looks nearly identical. We also show $g_{\alpha\beta}(r)$ in equilibrium at $T = 0.5$ for reference (dashed lines).

the Supplementary materials of Singh *et al.* [46]. To calculate the order parameter, Q_6, first we define q_{lm} of particle i as

$$q_{lm}(i) = \frac{1}{N_b(i)} \sum_{j=1}^{N_b(i)} Y_{lm}(\mathbf{r}_{ij}), \tag{4.3}$$

where l is a positive integer, and m is an integer that runs from $-l$ to $+l$. $N_b(i)$ is the number of nearest neighbors of particle i. The nearest neighbors are within a sphere of radius r_c around particle i. Here, in the KA system, we used $r_c = 1.8$, which corresponds to the second peak of the pair correlation function $g(r)$. $Y_{lm}(\mathbf{r}_{ij})$ is a spherical harmonic function, where $\mathbf{r}_{ij}$ is a vector that points from particle i to particle j. Then we find the

TABLE 4.1. Q_6 parameter.

Cooling Rate	Q_6	Standard Deviation
3.33×10^{-3}	0.0257	0.00019
3.33×10^{-4}	0.0257	0.00021
3.33×10^{-5}	0.0258	0.00020
3.33×10^{-6}	0.0259	0.00021
3.33×10^{-7}	0.0261	0.00030
3.33×10^{-8}	0.0263	0.00009

locally averaged parameter,

$$\bar{q}_l(i) = \sqrt{\frac{4\pi}{2l+1} \sum_{m=-l}^{l} |\bar{q}_{lm}(i)|^2}, \tag{4.4}$$

where

$$\bar{q}_{lm}(i) = \frac{1}{N_b(i)+1} \sum_{j=1}^{N_b(i)+1} q_{lm}(j). \tag{4.5}$$

Finally, Q_6 is

$$Q_6 = \frac{1}{N} \sum_{i}^{N} \bar{q}_6(i). \tag{4.6}$$

Table 4.1 shows Q_6 at $T = 0.3$ for the different cooling rates. The values are comparable to the values given in the Supplementary Material of Ref. [46], where they also examined a KA glass at $T = 0.3$. The small values support the fact that there is no crystalline order, as was found in Ref. [46].

4.3. KINETIC STABILITY

During the heating trajectories, we monitored the system as it melted to examine how quickly it returned to equilibrium. The longer a system takes to return to equilibrium, the

more kinetically stable it is. We examined a quantitative measure of kinetic stability of the system prepared at our different cooling rates.

We monitored the average overlap function of eq. 4.7 over time. During the heating trajectories, the system was not in equilibrium, and thus the average overlap function depended not only on time, t, but at what time in the heating trajectory we started measuring the overlap function from. We define a waiting time, t_w, which is the time we waited after the beginning of the heating trajectory to measure the overlap function. Thus the average overlap with waiting time included is given by

$$q_s(t, t_w) = \frac{1}{N} \left\langle \sum_m q_m(t, t_w) \right\rangle, \tag{4.7}$$

where $q_m(t, t_w) = \Theta\left(a - |\mathbf{r}_m(t + t_w) - \mathbf{r}_m(t_w)|\right)$, Θ is Heaviside's step function, and $\mathbf{r}_m(t)$ is the position of a particle m at a time t. The alpha relaxation time, τ_α, of the average overlap function is defined by $F_o(\tau_\alpha) = 1/e$. We chose $a = 0.25$, so that the alpha relaxation time of the average overlap function would match that of the self intermediate scattering function. The self intermediate scattering function is

$$F_s(q; t) = \frac{1}{N} \left\langle \sum_{n=1}^{N} \mathrm{e}^{i\mathbf{q}\cdot[\mathbf{r}_n(t) - \mathbf{r}_n(0)]} \right\rangle, \tag{4.8}$$

where we used $q = 7.25$ in this system, which corresponds to the first peak of the static structure factor,

$$S(q) = \frac{1}{N} \left\langle \sum_{n=1}^{N} \mathrm{e}^{i\mathbf{q}\cdot\mathbf{r}_n(0)} \sum_{m=1}^{N} \mathrm{e}^{-i\mathbf{q}\cdot\mathbf{r}_m(0)} \right\rangle. \tag{4.9}$$

We determined this a value previously [1]. Unlike in equilibrium, the time when the average overlap function decays to $1/e$ depends on the waiting time. Thus we define $q_s(\tau_s, t_w) = e^{-1}$, as the out of equilibrium relaxation time, where τ_s is a function of t_w.

Figure 4.3 shows the average overlap function for the heating trajectories for the various cooling rates at a waiting time of 0 and the average overlap function for the equilibrium supercooled liquid at $T = 0.5$. The kink in the heating trajectory curves at $t = 10$ is due to our procedure of ramping up the temperature for a time of 10 and then running at a constant temperature. The plateaus at intermediate times in the average overlap function indicate that particles are trapped in cages of their nearest neighbors. For the glasses prepared at slower cooling rates, the plateau height increases and the plateau lengthens. This behavior indicates first that the cage diameter decreases, indicating particle can't vibrate as much, and second that the particles are trapped for longer. Note that this decrease of the cage diameter is a trend that is observed in equilibrium supercooled liquids as they become increasingly supercooled [88]. The cage diameter decreasing means that the amplitude of particle vibrations is smaller. It would be interesting to investigate this phenomenon and examine the frequency of vibrations. We see that the out of equilibrium relaxation time, τ_s, increases as cooling rate is decreased.

Figure 4.4 shows the mean square displacement,

$$\left\langle \delta r^2(t) \right\rangle = \frac{1}{N} \left\langle \sum_{n=1}^{N} \left[\mathbf{r}_n(t) - \mathbf{r}_n(0) \right]^2 \right\rangle, \tag{4.10}$$

for the heating trajectories from the different cooling rates and for the equilibrium run at $T = 0.5$. At long times each heating trajectory goes to the equilibrium curve. Like the average overlap function, the mean square displacement develops a plateau at intermediate times.

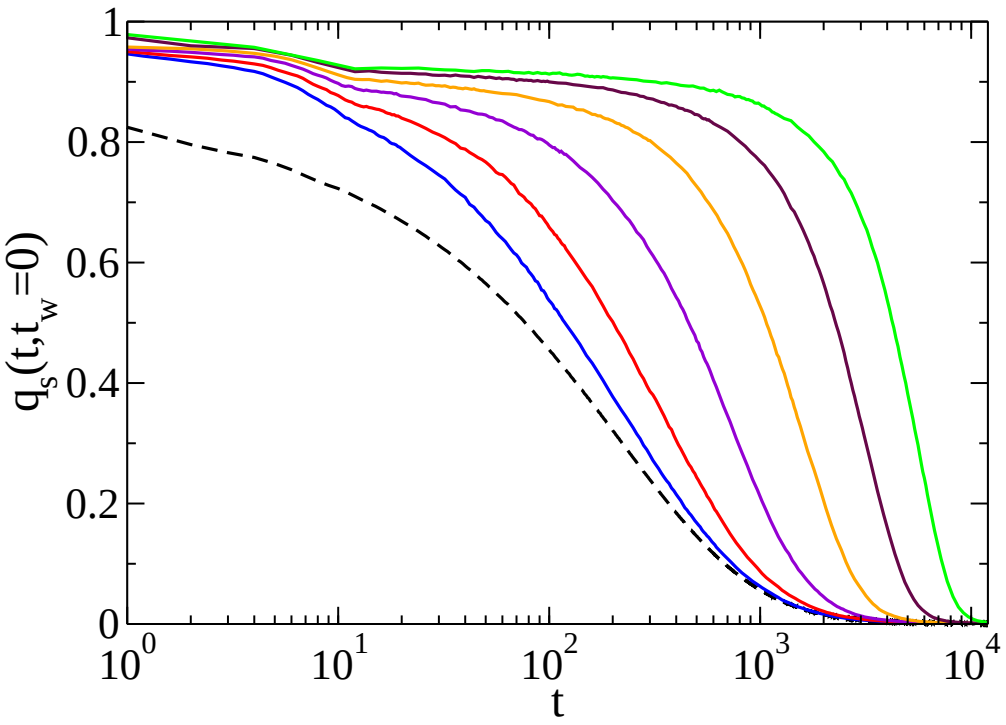

FIGURE 4.3. The average overlap function for the heating trajectories with a waiting time of 0 (solid lines) and the average overlap function in equilibrium at $T = 0.5$ (dashed lines). The initial cooling rates were $\dot{T} = 3.33 \times 10^{-n}$, where $n = 3$, 4, 5, 6, 7, and 8 listed from left to right.

For slower initial cooling rates this plateau lengthens and decreases in height, again indicating that particles are trapped in cages of their nearest neighbors for longer and the cages are smaller. As cooling rate decreases, the time it takes for the mean square displacement curves to return to the equilibrium curve increases, as was the case for the average overlap function. Thus we feel that the mean square displacement encodes similar information as the average overlap function. We chose to focus on the average overlap function to measure kinetic stability, as Hocky *et al.* [115] did.

We investigate how the average overlap function, $q_s(t, t_w)$, depends on waiting time in Figure 4.5. As waiting time increases, $q_s(t, t_w)$ approaches the equilibrium average overlap function curve. We define the transformation time t_{trans} as the time it takes for the system to return to equilibrium. We measured t_{trans} by finding the waiting time, t_w, when τ_s first

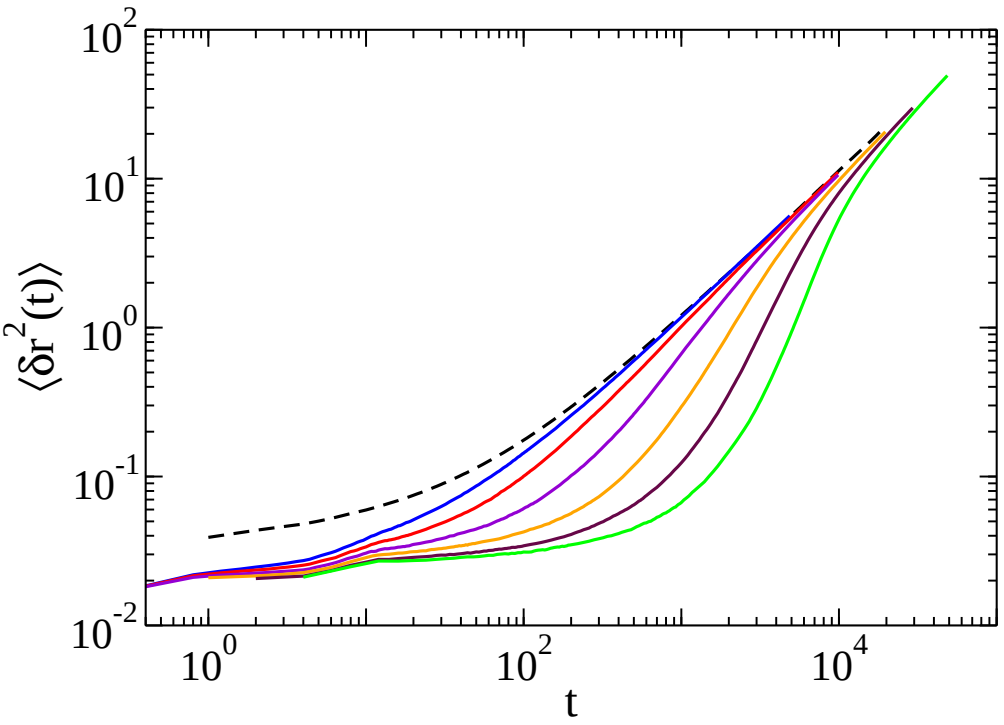

FIGURE 4.4. The mean square displacement for the heating trajectories (solid lines) and the mean square displacement for the equilibrium run at $T = 0.5$ (dashed line). The initial cooling rates were $\dot{T} = 3.33 \times 10^{-n}$, where $n = 3$, 4, 5, 6, 7, and 8 listed from left to right.

equals τ_α, and called that waiting time t_{trans}. We report a stability ratio $S = t_{trans}/\tau_\alpha$, for each initial cooling rate. The stability ratio is t_{trans} scaled by the equilibrium relaxation time at the heating temperature, which here is $T = 0.5$.

We show the waiting time dependent relaxation time, τ_s, as function of waiting time, t_w, in Figure 4.6. The arrows point to the transformation times, t_{trans}. The stability ratio, $S = t_{trans}/\tau_\alpha$ is plotted as a function of cooling rate in Figure 4.7. S grows more quickly at slower cooling rates than at faster cooling rates. We fit $\log(S) = A\log(\dot{T}) + B$ to the slowest three cooling rates, obtaining the fitting parameters $A = -0.20$ and $B = 0.31$. Using this fit, we can compare our stability ratio to the most stable simulated glasses, where $S \approx 400$ [115], and experimental ultrastable glasses, where $S \approx 10^{3.5}$ [47]. To match the largest S of simulations we would need to decrease the cooling rate by around 4 orders of

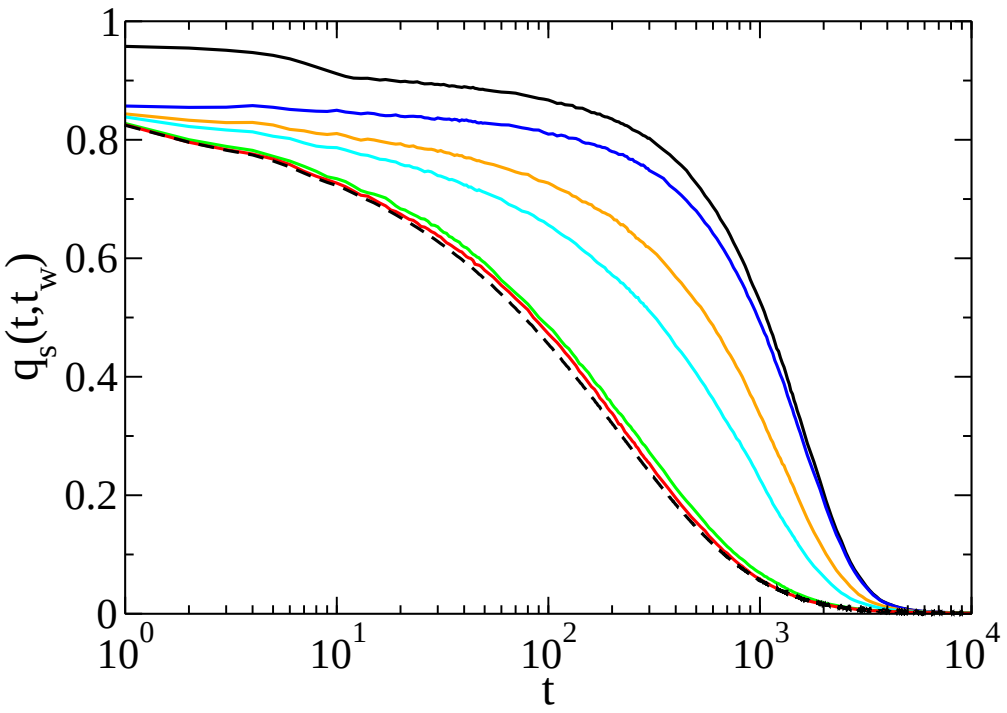

FIGURE 4.5. The average overlap function at different waiting times for the cooling rate of $\dot{T} = 3.33 \times 10^{-6}$ (solid lines) and the average overlap function for the equilibrium fluid at $T = 0.5$ (dashed line). Note that there is no waiting time dependence in equilibrium. The waiting times are 0, 10, 500, 1000, 3000, 4000 listed from top to bottom.

magnitude. To match the experimental S, we would need to decrease cooling rate by around 8 orders of magnitude. Thus even obtaining highly stable simulational glasses, as stable as those systems produced by random pinning, using ordinary cooling, is not possible given our current computational resources.

We note that we could heat our cooled system to any liquid temperature and examine dynamics upon melting. In experiments, S depends on the temperature to which you heat the glass [47]. In experiments, researchers have found that heating to a lower temperature leads to a smaller stability ratio. To investigate if this trend held for our simulations, we heated the glasses cooled at the slowest cooling rate of 3.33×10^{-8} to the two additional temperatures of 0.47 and 0.55. We found that $S = 50.1 \pm 4.8$ for $T = 0.47$, $S = 65.6 \pm 3.1$ for $T = 0.5$, and $S = 69.1 \pm 2.0$ for $T = 0.55$. Thus, we found that the stability ratio increases

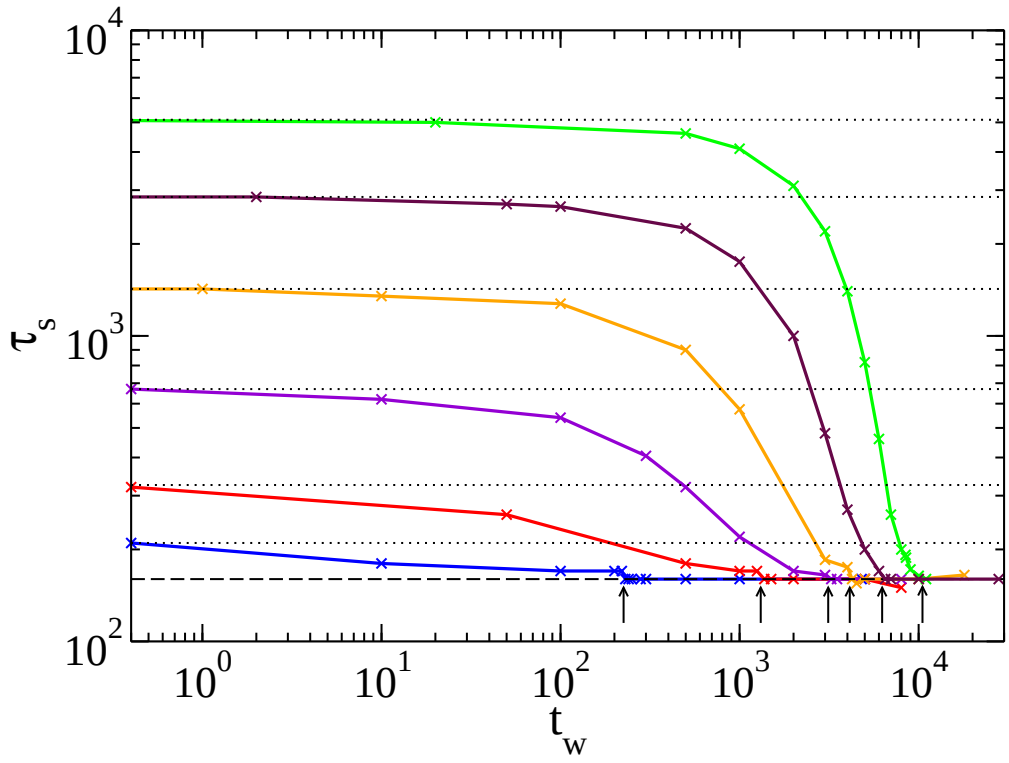

FIGURE 4.6. The out of equilibrium relaxation time, τ_s, versus waiting time, t_w. The solid lines are for heating trajectories from systems cooled at the initial rates of 3.33×10^{-n}, where $n = 3, 4, 5, 6, 7, 8$, listed from bottom to top. The dashed horizontal line shows the equilibrium relaxation time $\tau_\alpha = 158.7$ at $T = 0.5$. The dotted horizontal lines show the out of equilibrium relaxation times, τ_s, at $t_w = 0$. The arrows indicate the transformation times, t_{trans}, we found for each cooling rate.

as the heating temperature increases, just as in experiments [47]. In our case, this trend is due to the fact that both the transformation time, t_{trans}, and the equilibrium relaxation time, τ_α, increase as the heating temperature decreases, but τ_α increases faster than t_{trans}.

4.4. Dynamic heterogeneity

We have seen dynamic heterogeneity in supercooled liquids. We studied whether the melting process of a glass is also dynamically heterogeneous. Melting was heterogeneous, with certain regions melting faster than others. Interestingly we saw that the initial cooling rate used to create the glass affected the dynamic heterogeneity of the melting glass. Systems

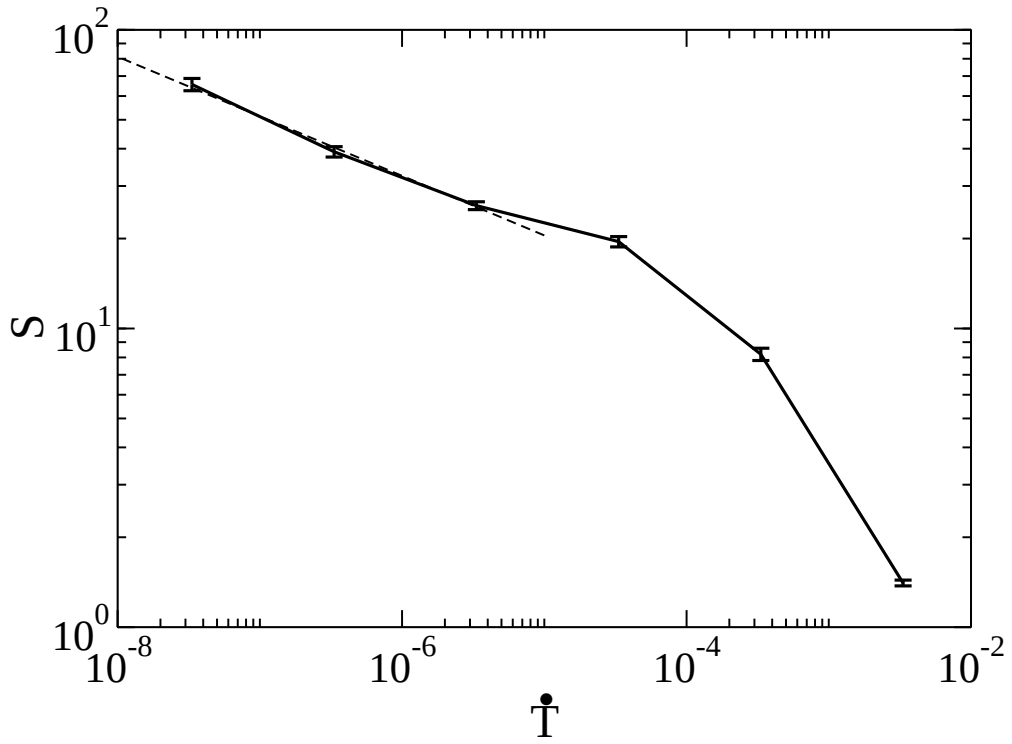

FIGURE 4.7. The stability ratio, $S = t_{trans}/\tau_\alpha$, versus cooling rate, $\dot{T}$. The solid line is to guide the eye. The dashed line shows the fit of $\log(S) = A\log(\dot{T}) + B$ to the lowest three cooling rates.

created at slower cooling rates had more heterogeneous melting than systems created with faster cooling rates.

We used the self van Hove function to measure the distribution of particle displacements at a particular time, t. The self van Hove function is

$$G_s(\mathbf{r}, t) = \frac{1}{N}\left\langle \sum_{n=1}^{N} \delta[\mathbf{r} + \mathbf{r}_n(0) - \mathbf{r}_n(t)] \right\rangle. \tag{4.11}$$

In liquids, the self van Hove function should be a Gaussian at long times [10].

We often calculate the probability distribution of the logarithm of single particle displacements [121] from

$$P(\log_{10}(\delta r); t) = \ln(10) 4\pi \delta r^3 G_s(\delta r, t), \tag{4.12}$$

where δr is a displacement. This probability more clearly shows subpopulations of particles that have different displacements. If the distribution of displacements seen in $G_s(\delta r; t)$ is Gaussian, then $P[\log_{10}(\delta r); t]$ should have a single peak with a height of 2.13 [121]. It will also have the same shape at all times and its peak position will move to larger displacements as time grows.

Figure 4.8 shows $P[\log_{10}(\delta r); x_t \cdot \tau_s]$, where x_t is a constant, for both particle types at 0.5, 1, 2, 4, and 8 times the relaxation time, $\tau_s(t_w = 0)$ (or τ_α for the $T = 0.5$ equilibrium run). It shows equilibrium curves for $T = 0.5$, and heating trajectory curves for three different initial cooling rates.

We note that most of the curves have peaks below 2.13, and thus the distribution of $G_s(\delta r; t)$ is non-Gaussian. Only at the very longest times, corresponding to 8 times τ_s for the systems created from the very slowest cooling rate, do we see the peak height approach 2.13. For faster cooling rates or equilibrium runs, even the $P[\log_{10}(\delta r); x_t \cdot \tau_s]$ peaks at $x_t = 8$ do not reach a height of 2.13. Thus, the length of time of returning to equilibrium divided by the out of equilibrium relaxation time τ_s is decreasing as cooling rate decreases. We note that the length of time the system takes to return to equilibrium is actually growing as cooling rate decreases, but its duration relative to τ_s is decreasing as cooling rate decreases. Another feature of Figure 4.8 is the emergence of a side peak or even a double peak in $P[\log_{10}(\delta r); x_t \cdot \tau_s]$.

We see a side peak emerging for type 1 particles at intermediate times at the slower cooling rates, and for type 2 particles even in equilibrium at $t = 2\tau_\alpha$. We note that equilibrium supercooled liquids can have multiple peaks, due to heterogeneous dynamics developing [121]. As cooling rate slows, $P[\log_{10}(\delta r); x_t \cdot \tau_s]$ has a double-peak structure at intermediate

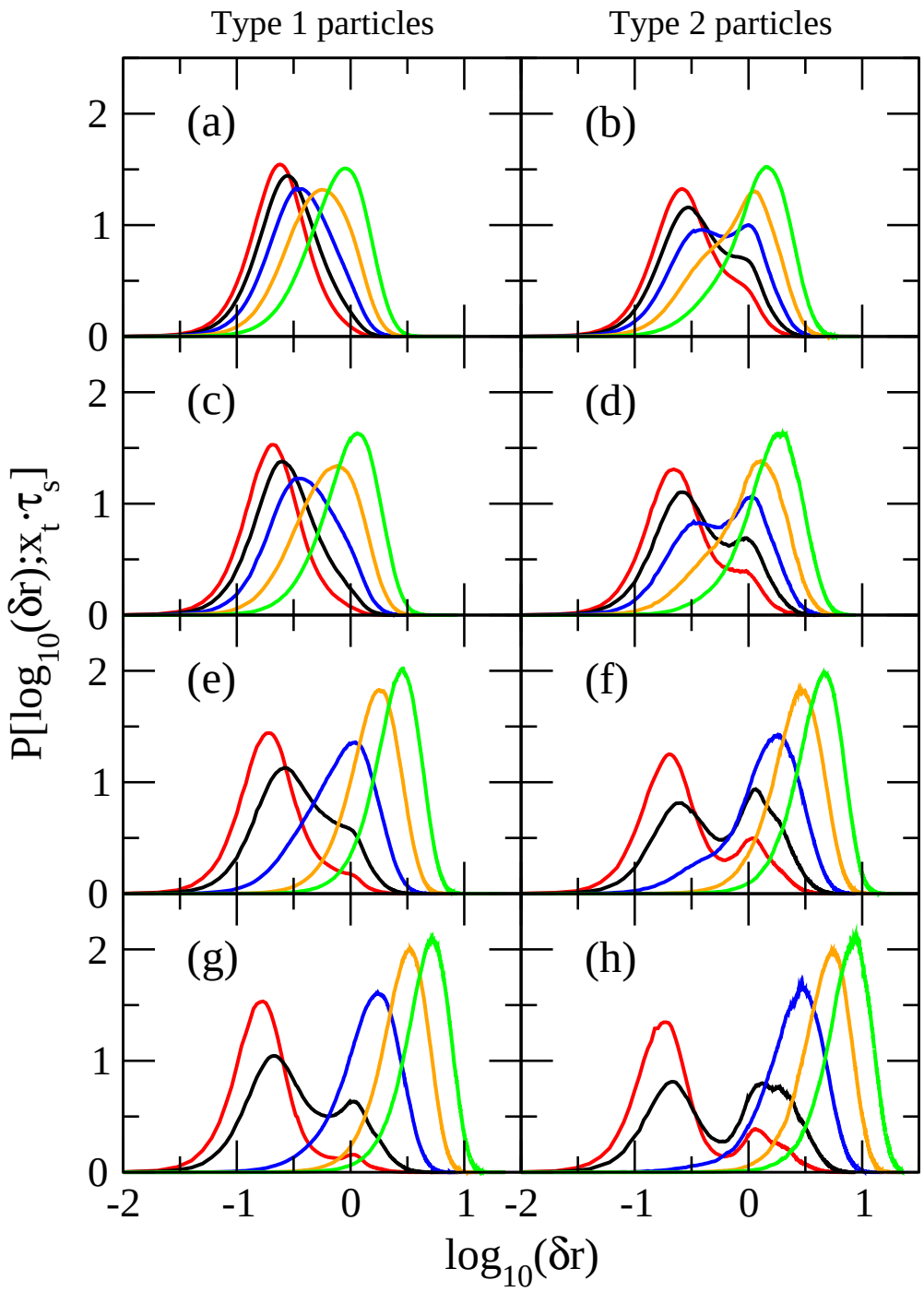

FIGURE 4.8. $P[\log_{10}(\delta r); x_t \cdot \tau_s]$ for the large type 1 particles (left column) and the small type 2 particles (right column) in equilibrium at $T = 0.5$ (a, b), and for the initial cooling rates of 3.33×10^{-n} where $n = 4$ (c, d), 6 (e, f), and 8 (g, h). In each panel, times are shown at x_t times the out of equilibrium relaxation time, τ_s, at a waiting time, t_w, of 0. The colors correspond to $x_t = 0.5$, 1, 2, 4, and 8 for the red, black, blue, orange, and green curves respectively. Note that for the equilibrium curves $\tau_s = \tau_\alpha$.

times. This double-peak means that particles have hopping-like dynamics. We also see, for both types of particles, that as cooling rate slows, the side peak becomes more pronounced and separate from the main peak, which suggests that dynamic heterogeneity is increasing as cooling rate is lowered.

In this system, we calculated the susceptibility, $\chi_4(t)$, as a function of the overlap function, $q_m(t, t_w = 0) = q_m(t)$. Thus we write the susceptibility as

$$\chi_4(t) = \frac{1}{N}\left(\left\langle\left[\sum_m q_m(t)\right]^2\right\rangle - \left\langle\sum_m q_m(t)\right\rangle^2\right). \tag{4.13}$$

In eq. 4.13 $q_m(t)$ is the overlap function measured at $t_w = 0$, and it is given by $q_m(t) = \Theta\left(a - |\mathbf{r}_m(t) - \mathbf{r}_m(0)|\right)$, where Θ is the Heaviside step function. We calculate the four point structure factor for the overlap function, $S_4^{\text{ov}}(q;t)$, using

$$S_4^{\text{ov}}(q;t) = \frac{1}{N}\left\langle\sum_{n,m} q_n(t)q_m(t)e^{i\mathbf{q}\cdot[\mathbf{r}_n(0)-\mathbf{r}_m(0)]}\right\rangle. \tag{4.14}$$

These four point correlations are both measures of the strength of dynamic heterogeneity.

Recall that we can get a length scale of dynamic heterogeneity using the Ornstein-Zernicke fit,

$$\frac{\chi_4}{1+(q\xi_4)^2}, \tag{4.15}$$

on the small q values of $S_4(q;t)$. This procedure for getting ξ_4 is only meant to work on a system in equilibrium. Even if we were to ignore this issue, our simulation size gives us another problem. Due to periodic boundary conditions, we can only calculate $S_4(q;t)$ at $\mathbf{q} = (2\pi l/L, 2\pi m/L, 2\pi n/L)$, where l, m, and n are integers that are greater than or equal

to 0, (though at least one of l, m, or n must be non zero), and L is the length of one side of our simulation box. We found that we did not have enough small q values to fit to the Ornstein-Zernicke fit in the simulations of this chapter. Thus we couldn't get a dynamic correlation length, ξ_4. Recall that we could improve the fit to S_4 by measuring the ensemble independent susceptibility, χ_4, which is the $q \to 0$ limit of S_4. χ_4 would add a point at $q = 0$ to the fit. However, measuring the ensemble independent susceptibility requires trajectories at high and low particle concentration and density, which would require many more runs.

Figure 4.9 shows the dynamic susceptibility for the heating trajectories. In Figure 4.9 the peak height of the susceptibility increases as cooling rate decreases, which indicates an increase in the strength of the dynamic heterogeneity. We note that the width of the peak on the log scale decreases as cooling rate decreases. This trend indicates that the time scale of heterogeneous dynamics divided by the out of equilibrium relaxation time, τ_s, decreases as cooling rate decreases. In fact, the total time where dynamics are heterogeneous increases, but the time of heterogeneous dynamics relative to the relaxation time decreases. Recall that we saw the same trend in the $P[\log_{10}(\delta r); t]$ function of Figure 4.8, where the length of time where dynamics were heterogeneous decreases relative to the out of equilibrium relaxation time.

Figure 4.10 shows that the time of the peak of dynamic susceptibility, τ_p, tracks the relaxation time, τ_s, at $t_w = 0$, for the cooling rates we studied. In equilibrium liquids, τ_p usually tracks τ_α [109, 110]. This typical behavior of the peak makes us feel that it is reasonable to examine $S_4^{\text{ov}}(q; t)$ at τ_p.

Figure 4.11 shows the four-point structure factor $S_4^{\text{ov}}(q; t)$ of eq. 2.17. At the smallest q values, $S_4^{\text{ov}}(q; t)$ is larger at the slower cooling rates. To find the full susceptibility $\chi_4(t)|_{full} =$

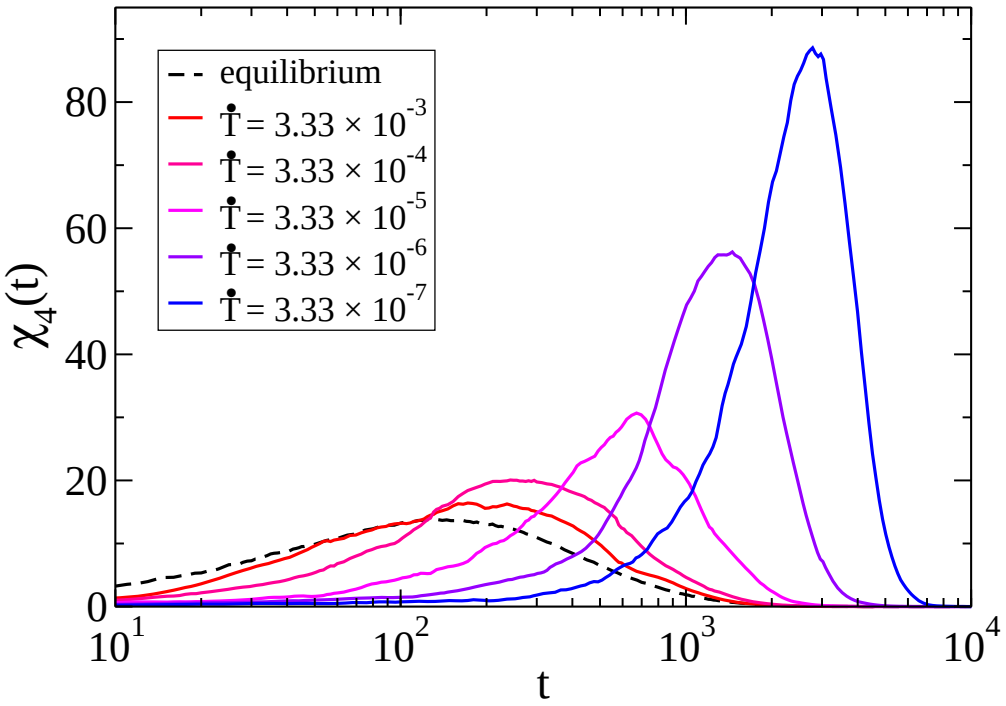

FIGURE 4.9. The solid lines show the dynamic susceptibility, $\chi_4(t)$, versus time for the heating trajectories. The initial cooling rates were 3.33×10^{-n}, where $n = 3, 4, 5, 6, 7$ listed from left to right. The dashed line shows the equilibrium dynamic susceptibility for a temperature of $T = 0.5$.

$\lim_{q\to 0} S_4(q;t)$, we would need to see a plateau in $S_4^{\rm ov}(q;t)$ at small q values. Our system was not large enough to see this behavior, but the trend of $S_4^{\rm ov}(q;t)$ growing at small q values as cooling rate is decreased does indicate that $\chi_4(t)|_{full}$ is growing with decreasing cooling rate and possibly that the length scale of dynamic heterogeneity is also growing.

4.5. MECHANICAL STABILITY

We examined the mechanical stability of our cooled glasses by examining their potential energy and shear modulus. The potential energy provides a very simple way to compare a system prepared in different ways. However, we found that this method of examining the mechanical stability may have problems when comparing to glasses created by vapor deposition. We also examined the shear modulus, which is a direct measure of mechanical stability, and is very useful in a comparison to other simulations.

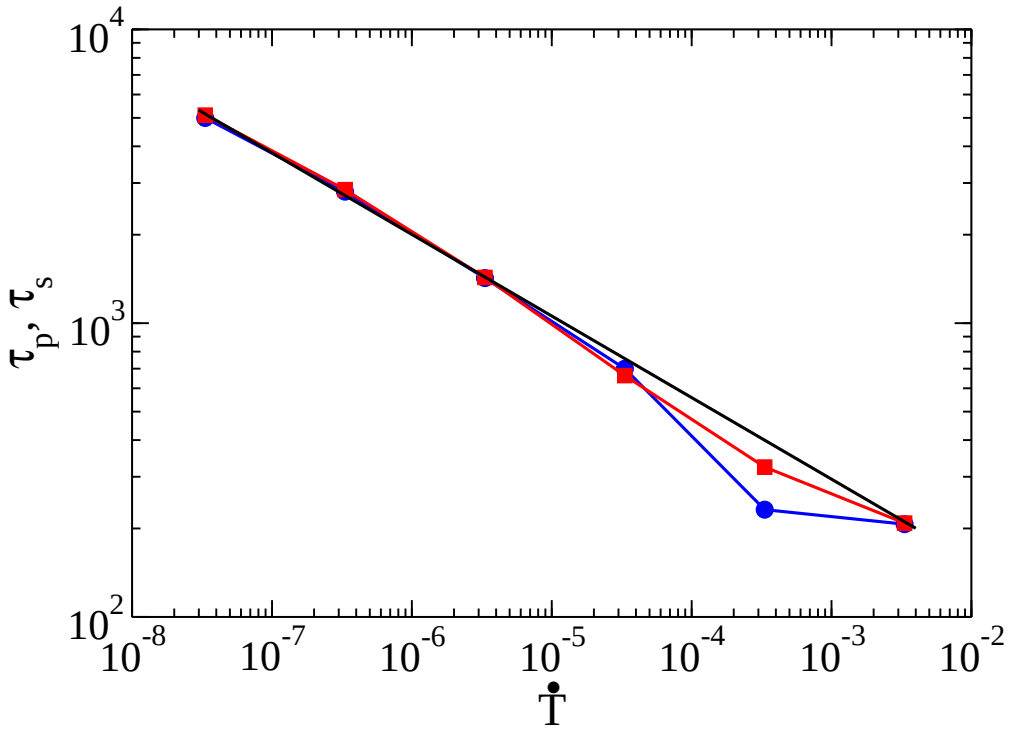

FIGURE 4.10. The red squares show the out of equilibrium relaxation time τ_s at 0 waiting time. The blue circles show the time of the peak, τ_p, of the dynamic susceptibility for the heating trajectories. The black line is a fit to $\tau_s = a\dot{T}^{-1/\zeta}$, where $\zeta = 3.6$.

4.5.1. ENERGY. Figure 4.12 shows the average potential energy per particle $\langle U \rangle$ at $T = 0.3$, versus cooling rate $\dot{T}$. $\langle U \rangle$ decreased with decreasing cooling rate. Similarly, the average inherent structure energy $\langle E_{IS} \rangle$ calculated at $T = 0.3$ decreased with decreasing cooling rate, as is seen in Figure 4.13. $\langle E_{IS} \rangle$ measures the potential energy at the bottom of the potential energy well in which the system was before energy minimization. Section 4.2.1 describes the averaging procedure for $\langle U \rangle$ and $\langle E_{IS} \rangle$. Both these energy measurements indicate that the system explored lower energy configurations more effectively when it was cooled more slowly.

We found the inherent structure energy, which is the energy of the potential energy minimum of the system, using energy minimization. In an energy minimization, the system moves towards lower energies, until it can go no lower. To compute the inherent structure energy we used the FIRE algorithm [119].

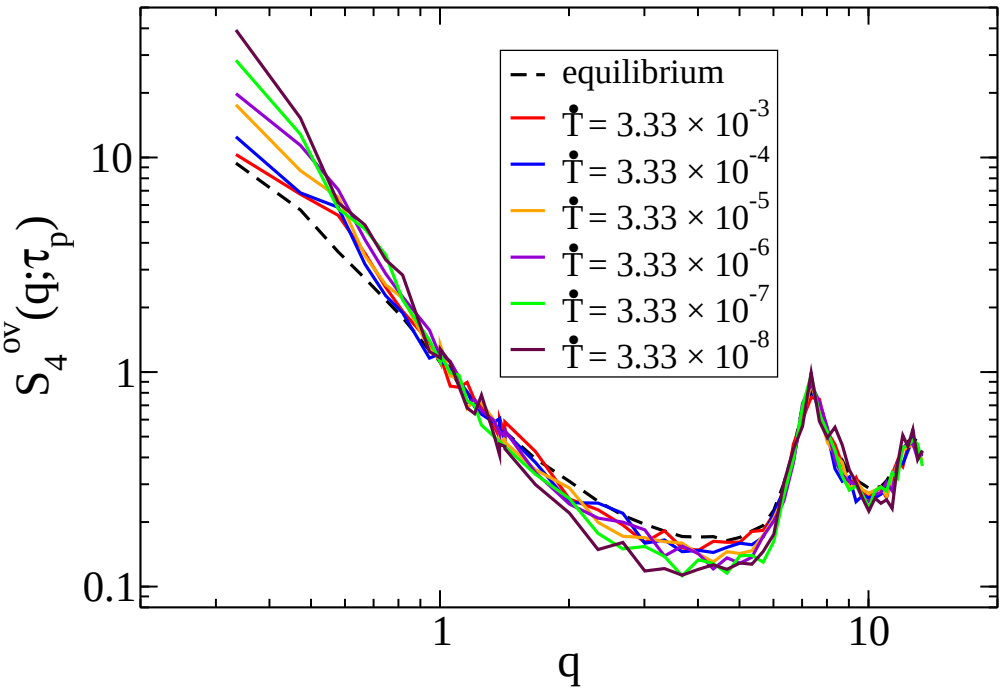

FIGURE 4.11. The four point structure factor $S_4^{\rm ov}(q;\tau_p)$ at wave vectors q, at the time of the peak of the dynamic susceptibility, τ_p. The solid lines are for heating trajectories started from configurations that had been cooled at the rates of 3.33×10^{-n}, where $n = 3, 4, 5, 6, 7, 8$, listed from bottom to top. The dashed line is for the equilibrium run at $T = 0.5$.

The algorithm first uses the specified simulation type, (such as NVE), to calculate position, velocity, and force. It then recalculates velocity so that a component of velocity is in the direction of the force, giving

$$\mathbf{v} \to (1-\alpha)\mathbf{v} + \alpha\hat{\mathbf{F}}|\mathbf{v}|, \tag{4.16}$$

where α is a changing variable initially specified by the simulator, and $\alpha < 1$. $\hat{\mathbf{F}}$ is the unit vector in the direction of the force. The algorithm calculates a term called the power, $P = \mathbf{F} \cdot \mathbf{v}$. If the power is positive and the power has not been negative for more than a given amount of time steps, then the time step is increased and α is decreased. If the power is negative, then the time step is decreased, α is set back to its initial value, and velocity

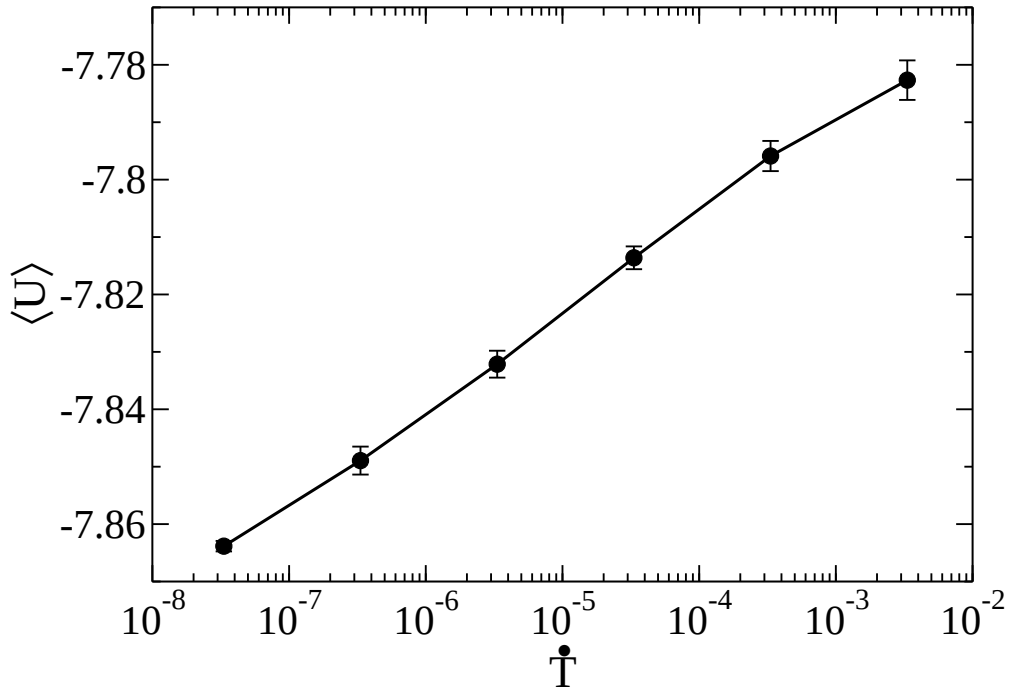

FIGURE 4.12. The average potential energy per particle $\langle U \rangle$ after cooling at the rates of $\dot{T} = 3.33 \times 10^{-n}$, with $n = 8, 7, 6, 5, 4, 3$. The line is a guide for the eye.

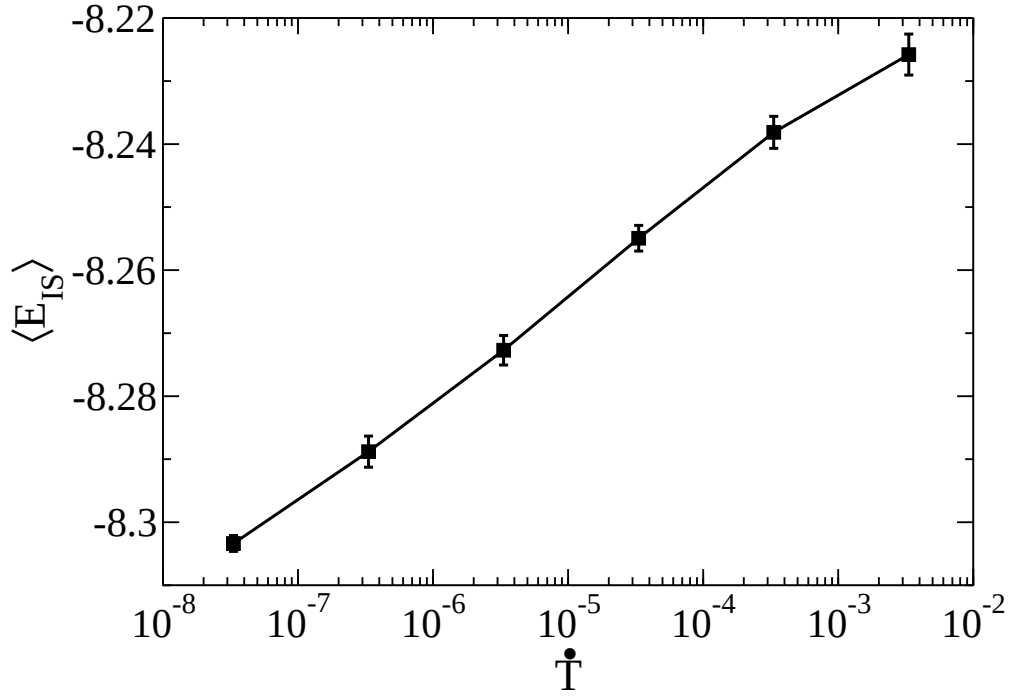

FIGURE 4.13. The average inherent structure energy per particle $\langle E_{IS} \rangle$ at $T = 0.3$ after cooling at the rates of $\dot{T} = 3.33 \times 10^{-n}$, with $n = 8, 7, 6, 5, 4, 3$. The line is a guide for the eye.

is set to zero. The algorithm then repeats the steps, starting from calculation of position, velocity, and force from, returning a non zero velocity. We used the FIRE algorithm to do energy minimizations. We compared our results for inherent structure energy to the results from using other energy minimization algorithms available in LAMMPS, such as conjugate gradient and method of steepest descents. We found that all methods resulted in the same inherent structure energy within error.

Recall that Lyubimov *et al.* [42] modeled vapor deposition of the KA system onto a substrate. They found that a substrate temperature of $T = 0.3$ made the most stable glasses, which had an average potential energy of -7.8 and an average inherent structure energy of -8.35. We note that these values are close to our values of $\langle U \rangle = -7.86$ and $\langle E_{IS} \rangle = -8.30$, from our slowest cooling rate. Our $\langle U \rangle$ is lower than that of the simulated vapor deposited glass [42], while our $\langle E_{IS} \rangle$ is larger than the simulated vapor deposited glass [42]. Energy is sensitive to how the sample was made, anisotropy in the system (due to vapor deposition), and slight differences in the density, as were present in Ref. [42]. Particularly, for the inherent structure energy, their energy minimization allowed the system to densify.

4.5.2. Shear modulus. Elastic moduli measure how stable a system is to being deformed. They are a measure of stress put on the system divided by the strain, which is a measure of how much the system is deformed by the stress. Ultrastable glasses prepared by vapor deposition in experiments [43] and in simulations [46] have larger elastic constants than glasses prepared by ordinary cooling. In experiments, Kearns *et al.* [43] found elastic moduli that were 10% to 15% bigger in vapor deposited glasses of trisnaphthylbenzene (TNB) than in glasses created by cooling, and moduli that were 14% to 19% greater for the vapor deposited glasses of indomethacin (IMC) than in the glasses created by cooling. Using

the KA system, Singh *et al.* [46] measured an elastic modulus that was 18% larger for their simulated vapor deposited glass than their glass created by cooling. We measured one of the elastic moduli, the shear modulus, μ, to examine mechanical stability. One way to understand the shear modulus is to imagine you have a box with height h, with top surface area A [122]. Then imagine that you apply a force F, perpendicular to the top surface normal. The bottom of the box is stuck and doesn't move, but the top of the box moves a distance Δx. Then the shear modulus is

$$\mu = \frac{F/A}{\Delta x/h}. \tag{4.17}$$

The shear modulus is a direct measure of mechanical stability.

In this work, we got the shear modulus, μ, from a method developed by Flenner and Szamel [123]. They showed that the shear modulus can be found using

$$\mu = \lim_{q\to 0}\lim_{t\to\infty} \frac{2k_BT\rho}{q^2 S_4^{\delta r}(q;t)}, \tag{4.18}$$

where $S_4^{\delta r}(q;t)$ is a four point structure factor given by eq. 1 of Ref. [123]. It measures the correlations of the displacements of particles. The four point structure factor, $S_4^{\delta r}(q;t)$, is

$$S_4^{\delta r}(\mathbf{q};t) = \frac{1}{N}\left\langle \sum_{n,m} \delta\mathbf{r}_n^{\perp}(t)\delta\mathbf{r}_m^{\perp}(t)e^{i\mathbf{q}\cdot[\mathbf{r}_n(0)-\mathbf{r}_m(0)]} \right\rangle, \tag{4.19}$$

where $\delta\mathbf{r}_n^{\perp}(t)$ is a component of the displacement of particle n that is perpendicular to $\mathbf{q}$, such that $\delta\mathbf{r}_n^{\perp}(t)\cdot\mathbf{q} = 0$. Note that eq. 4.18 requires that the shear modulus be calculated in the long time limit, but in practice this restriction just means that we must avoid very early times. We found that a time of $t \geq 100$ is sufficient to calculate the shear modulus.

We wanted to average over times when the system was not aging, or else the shear modulus could change as a function of time.

Figure 4.14 shows the mean square displacement of the particles in the glass after it has been cooled to $T = 0.3$, and is being annealed. At early times the mean square displacement, $\langle \delta r^2(t) \rangle$, has a plateau region, and at later times $\langle \delta r^2(t) \rangle$ takes a significant upward turn. When we examined the mean square displacement of a system cooled at the rate of 3.33×10^{-4}, after annealing, the upturn had moved to a later time in the mean square displacement. Thus the system is aging. The procedure developed Flenner and Szamel, for calculating the shear modulus, requires that measurements must be made at a time in the plateau of the mean square displacement. If the mean square displacement is increasing then the system is flowing and the shear modulus would be zero. For glasses prepared at the fastest two cooling rates the mean square displacement is already increasing at $t = 100$. Thus, we were unable to calculate the shear modulus at those cooling rates.

Figure 4.15 shows the four point structure factor $S_4^{\delta r}(\mathbf{q}; t)$ of eq. 4.19 for the four slowest cooling rates. Figure 4.16 shows $(2k_BT\rho)/\left[q^2 S_4^{\delta r}(q;t)\right]$, which is used in eq. 4.18 to calculate the shear modulus, μ. Recall that μ is the small q and long t limit of $(2k_BT\rho)/\left[q^2 S_4^{\delta r}(q;t)\right]$. At small wave vectors, $(2k_BT\rho)/\left[q^2 S_4^{\delta r}(q;t)\right]$ grows with decreasing cooling rate, at the time of $t = 100$.

Figure 4.17 shows $(2k_BT\rho)/[q^2 S_4^{\delta r}(q;t)]$ versus q, at $T = 0.3$ after cooling at the rate of 3.33×10^{-6}, for $t = 100$, 200, and 500. At this cooling rate, these times are all in the mean square displacement plateau, as can be seen in Figure 4.14. The shear modulus should be measured in the long time limit of $(2k_BT\rho)/[q^2 S_4^{\delta r}(q;t)]$, but Flenner and Szamel [123] found that measuring $(2k_BT\rho)/[q^2 S_4^{\delta r}(q;t)]$ over times when the mean square displacement

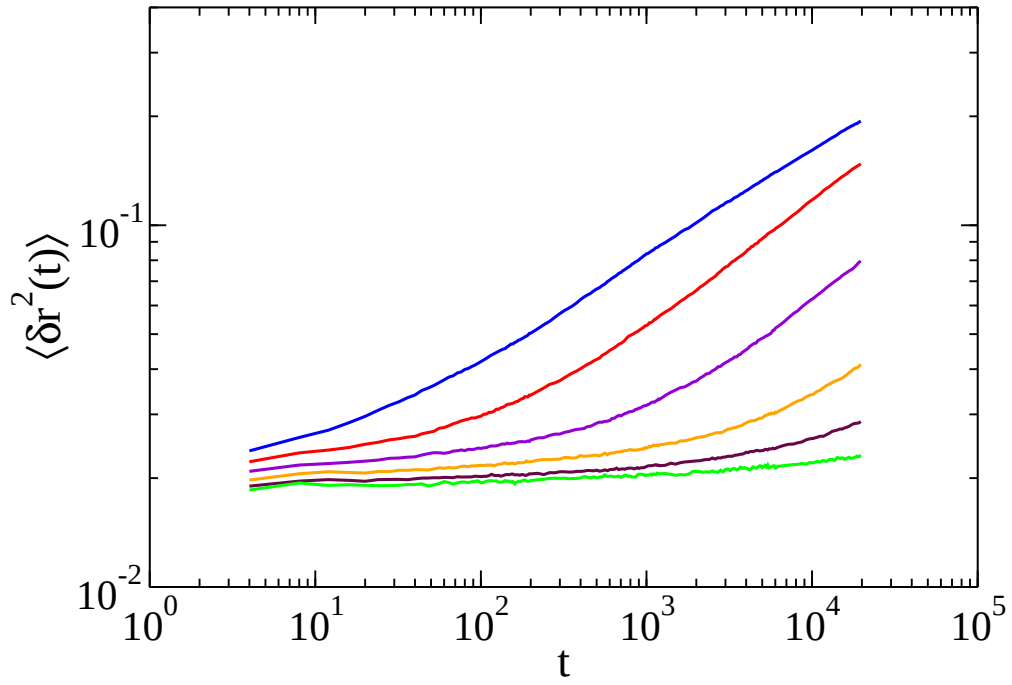

FIGURE 4.14. The mean square displacement run at $T = 0.3$ after cooling. The cooling rates are 3.33×10^{-n} where $n = 3, 4, 5, 6, 7, 8$, from top to bottom.

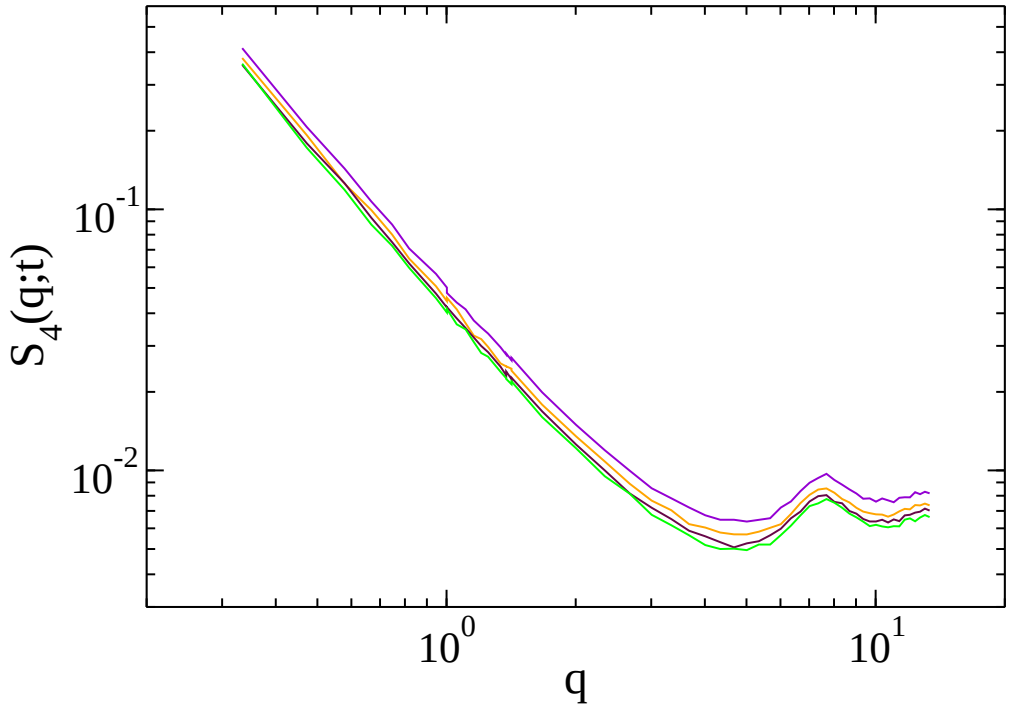

FIGURE 4.15. The four point structure factor, $S_4^{\delta r}(\mathbf{q}; t)$, used in calculating the shear modulus, at $t = 100$. The cooling rates are 3.33×10^{-n} where $n = 5, 6, 7, 8$, from top to bottom.

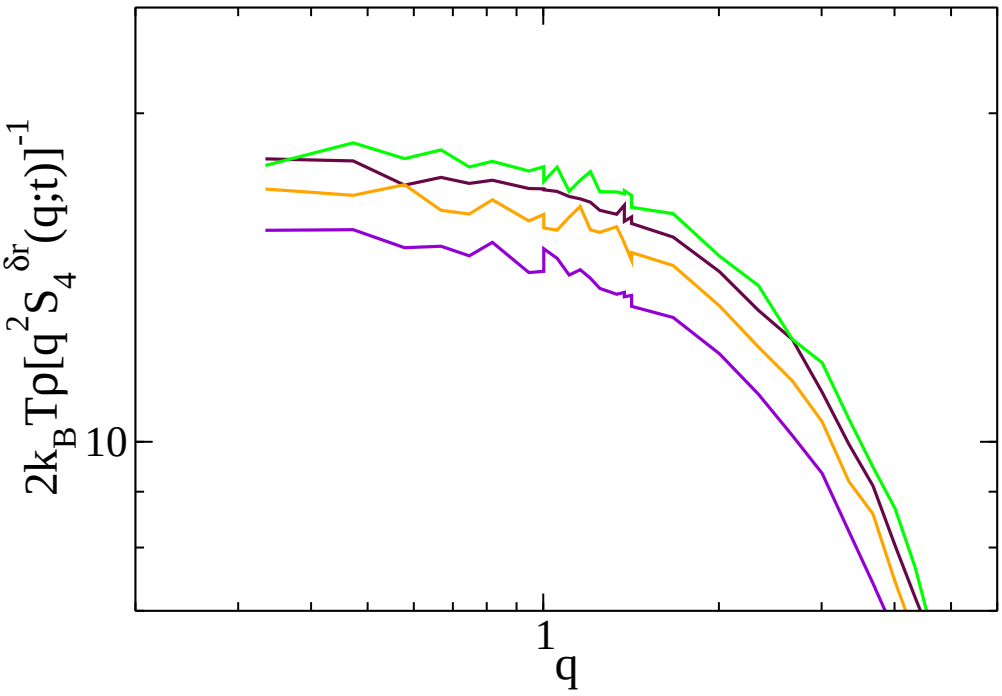

FIGURE 4.16. The wave vector, q, dependence of $(2k_BT\rho)/\left[q^2S_4^{\delta r}(q;t)\right]$ at time $t = 100$ for the $T = 0.3$ glass. Only the four slowest cooling rates are shown. These cooling rates are 3.33×10^{-n} where $n = 5, 6, 7, 8$, listed from bottom to top.

is fairly constant succeeds in getting the shear modulus. We note that we chose times in the plateau of the mean square displacement, and the resulting $(2k_BT\rho)/[q^2S_4^{\delta r}(q;t)]$ curves are all very close together, indicating that μ is fairly constant in the plateau region, for our system. Thus, our averaging procedure described in Section 4.2.3 is legitimate.

We took the average of the low q values of $(2k_BT\rho)/[q^2S_4^{\delta r}(q;t)]$ shown in Figure 4.16 to get the shear modulus, μ. Figure 4.18 shows the shear modulus as a function of cooling rate for the four slowest cooling rates where we could legitimately calculate μ. The rate of increase of the shear modulus scales more slowly as cooling rate, $\dot{T}$, decreases, on the log scale. When we fit $\mu = A\log(\dot{T}) + B$, where A and B are fitting parameters, to the slowest three cooling rates, we found that one order of magnitude decrease in the cooling rate corresponds to a 4.6% increase of the shear modulus. Ashwin *et al.* [124] examined

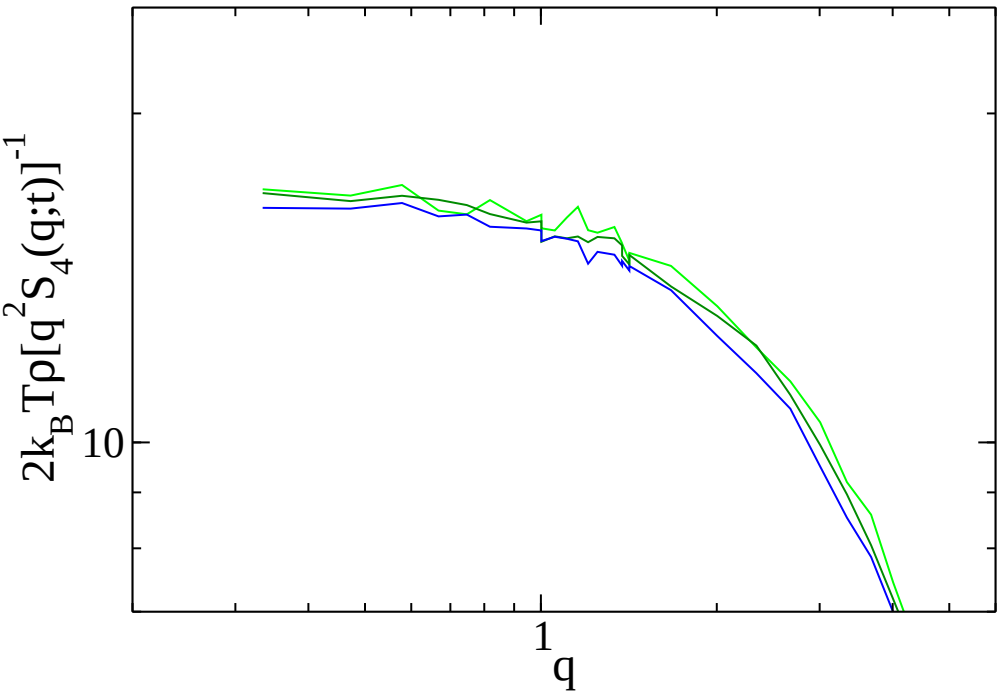

FIGURE 4.17. $(2k_BT\rho)/[q^2S_4^{\delta r}(q;t)]$ versus q at the cooling rate of 3.33×10^{-6}. The three times of 100, 200, and 500, listed from top to bottom (or green to blue), were chosen from the plateau region.

"the shear modulus", (for their two dimensional simulation), after cooling at different rates in a two-dimensional model system. We can not directly compare to their results, as we used different systems, but we did find that over a similar range of cooling rates our shear modulus increased by 15% and theirs increased by 12%.

Kearns *et al.* [43] did experiments where they created ultrastable glasses by vapor deposition and compared them to glasses created by ordinary cooling. They saw that the ultrastable glasses had a 19% (indomethacin) and a 15% (trisnaphthylbenzene) higher shear modulus than the glasses created by cooling. These increases are comparable to the increases Ashwin *et al.* [124] and our group saw when we decreased our cooling rate by three orders of magnitude. Of course, if the times of computer simulations could be converted to real times, they would be much shorter than the experiments can run. For our longest colling run at the

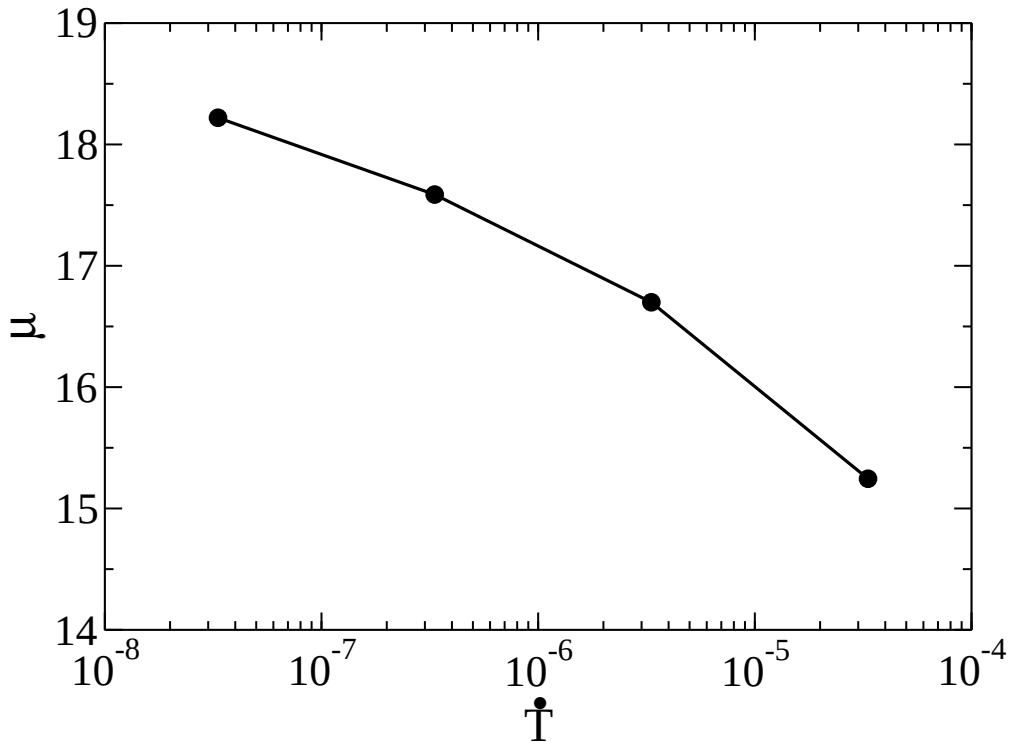

FIGURE 4.18. The shear modulus, μ, versus cooling rate, $\dot{T}$, at $T = 0.3$. Only the four slowest cooling rates are calculated and shown.

cooling rate of $\dot{T} = 3.33 \times 10^{-8}$, we could convert time to that in liquid argon, as mentioned in Section 2.2. For this conversion, our slowest cooling rate run took approximately 3 μs.

CHAPTER 5

Conclusions and Future Work

I summarize and make some conclusions about the work presented in previous chapters, and discuss possible future work. I examine what the work presented in Chapters 2, 3, and 4 has added to the field of supercooled liquids and glasses.

5.1. Universal features of dynamic heterogeneity in fragile glass-formers

We saw universal behavior of dynamic heterogeneity in all the model fragile glass-formers we studied in Chapter 2. In all the systems, below the temperature T_s (or above the volume fraction ϕ_s) where the Stokes-Einstein relation was violated, we were able to collapse the data for a dynamic correlation length plotted as a function of rescaled relaxation time onto a single curve, and we noted that clusters of particles with correlated mobility were compact.

We note that T_s (ϕ_s) is lower (higher) than the onset temperature T_o (volume fraction ϕ_o) for slow dynamics (at least in the systems studied in Chapter 2). At supercooled temperatures (volume fractions) between T_s and T_o (between ϕ_s and ϕ_o), the dynamics may affect the shape of dynamic heterogeneity. We observed the effect of dynamics in Section 2.4.3 for lengths calculated from the four point structure factor $S_4(\mathbf{k}, \mathbf{q}; t)$. We found the dynamic correlation lengths, calculated from $S_4(\mathbf{k}, \mathbf{q}; t)$ were shorter in systems that didn't conserve momentum than in systems where momentum was conserved, at temperatures above T_s (volume fractions below ϕ_s). At temperatures below T_s (volume fractions above ϕ_s), we saw universal features of dynamic heterogeneity.

At the Stokes-Einstein violation temperature T_s (volume fraction ϕ_s) we saw the formation of compact regions of particles with correlated mobility in all our fragile glass-formers.

The study of a system of quasi two-dimensional ellipsoids by Mishra and Ganapathy [99] also found that Stokes-Einstein violation corresponded to the formation of compact clusters of correlated particles. In their two-dimensional experiment on colloidal ellipsoids, they studied the 10% most mobile particles. They counted how many of a particle's nearest neighbors were also part of the set of most mobile particles. If a particle had only 2 mobile nearest neighbors, then it was in a string of particles, and if it had more, then it was in a more compact cluster of particles. They used this strategy to determine compactness, unlike our use of four-point correlation functions, which are difficult to calculate in experiments. Also note that two-dimensional glass-formers, like the one used by Mishra and Ganapathy, have several features that are different than three-dimensional glass-formers [31]. The fragile glass-formers of Chapter 2 had particle clusters that were compact below T_s (above ϕ_s), whereas in the two-dimensional model glass-former of Ref. [31] $\chi_4 \sim \xi_4^{1.5}$ for clusters of particles with small displacements (slow particles). In two dimensions, χ_4 should grow as ξ_4 squared if clusters are compact. The lower exponent value of 1.5 means that regions of dynamic heterogeneity were more ramified than in three dimensions. However, based on the study of Mishra and Ganapathy, Stokes-Einstein violation marks the onset of compact clusters of correlated particles in both two and three dimensions.

We discovered a universal curve for plotting dynamic correlation length as a function of relaxation time, and we compared our result to different glass theories. The data we collected did not reach low enough temperatures to differentiate between predictions of two widely discussed theories, random first order transition theory and dynamic facilitation theory. We would have liked to extend the simulations to lower temperatures (higher volume fractions) to investigate which theory's prediction matches the data best. This extension would take

too long, as the slowest simulations for the harmonic sphere system, the system where we found the largest length, took eighteen weeks. We predict that we would need an order of magnitude increase in relaxation time to get enough data to distinguish between the predictions of the two theories. This increase would result in longer dynamic correlations lengths, which require a larger simulation box, with a volume around eight times bigger. Thus, simulations at larger relaxation times are not reasonable.

Our systems displayed universal features of dynamic heterogeneity regardless of the different potentials in the systems we simulated. We observed universal features of dynamic heterogeneity in model glass-formers with purely repulsive potentials and a glass-former with an attractive and repulsive potential. When using our universal scaling relationships, we found no difference in dynamic heterogeneity between the different systems, at temperatures below T_s (volume fractions above ϕ_s). We were able to compare systems and find universal behavior of dynamic heterogeneity by using our scaling variables. Zhang *et al.* [87] performed two dimensional colloidal experiments. They found that the size and shape of clusters of fast particles depended on the presence of attraction between particles. We note that all our systems were three dimensional, and we examined clusters of slow particles. Our systems had compact clusters below T_s (above ϕ_s).

5.2. Comparison of dynamic heterogeneity in strong and fragile glass-formers

In Chapter 3 we investigated dynamic heterogeneity in a model strong glass-former, comparing it to the fragile glass-formers of Chapter 2. We studied dynamic susceptibility χ_4, a measure of the number of correlated particles, and dynamic correlation length ξ_4, a measure of the spatial extent of regions of correlated particles. The dynamic susceptibility

can be shown to diverge when temperature is decreased using a simple argument. Recall that the full susceptibility $\chi_4(t)$ can't be measured in a finite system where fluctuations are suppressed. The susceptibility we measure in a particular ensemble has correction terms for suppressed fluctuations. The correction term for the suppressed energy fluctuations turns out to be significant. The sum of the other terms that make up the full susceptibility is positive. The energy correction term can be shown to be inversely related to temperature squared in strong glass-formers, and thus it diverges. If this term diverges, then the full susceptibility diverges as well. We examined what happened to the dynamic correlation length when temperature was decreased and its relationship with dynamic susceptibility. In the strong glass system that we studied the glass forms a tetrahedral network, and thus we studied two distances, one for nearest neighbors, $a = 0.2$, and one for tetrahedral order, $a = 0.35$. At the Stokes-Einstein violation temperature T_s, dynamic correlation lengths were different for the different a distances. However for both a there was a crossover in the behavior of dynamic heterogeneity at T_s, a trend which was observed in fragile glass-formers.

We examined the relationship between susceptibility χ_4 and dynamic correlation length ξ_4, as we did for fragile glass-formers. This relationship gave us information on the compactness of clusters of slow particles. We related χ_4 and ξ_4 by $\chi_4 \sim (\xi_4)^z$, and found that the power z grew from less than 2 for temperatures above T_s to greater than 2 when temperature fell below T_s. In the fragile liquids, z was 3 below T_s, meaning that clusters were compact. This also applies for when ϕ is above ϕ_s, and T above T_s goes with ϕ less than ϕ_s. To check when and if clusters become compact in the strong system, we would need to examine lower temperatures. A single simulation run at the lowest temperature took less than two weeks on the CSU Cray. We would probably need to simulate at least an order of

magnitude larger relaxation times to check for compactness. This increase in relaxation time would most likely correspond to larger dynamic correlation lengths, requiring an increase in the simulation size. These increases would lead to simulations that would take well over a year, making such simulations unreasonable.

Similarly to our study on fragile-glass formers, we studied the dependence of the dynamic correlation length ξ_4 on the α relaxation time τ_α or the peak time τ_p of the susceptibility. This relationship, like that of χ_4 to ξ_4, also showed a change at T_s. This change in ξ_4 could be fit, but not with confidence, as ξ_4 had such slow growth as temperature decreased, and thus our range of values were not large enough for a fit. In the fragile glass-formers we found a couple different universal fits to ξ_4 on τ_α. To find fits in the strong glass-former, we would need data at lower temperatures and longer correlation lengths, (perhaps at least double our current longest length). As mentioned above, these larger dynamic correlation lengths are out of the range of our simulations. Also, since the lengths at T_s were small, around one particle diameter, we would not be able to fit to the small change in length at temperatures above T_s.

In Chapter 2 we found a useful way to compare various fragile systems using Stokes-Einstein violation. We then compared a strong glass-former to the fragile glass-formers. We clearly see, from Figure 3.11, that the length scale of dynamic heterogeneity is smaller in our strong glass-former than in the fragile glass-formers. This result does not agree with the trend predicted by dynamic facilitation theory in Section 1.5.3 about the relationship between length and fragility. Recall that dynamic facilitation theory predicts that its dynamic correlation length, ξ_{fac}, should be bigger for stronger systems. We saw the opposite trend with our dynamic correlation length ξ_4.

We expect that the slow growth of dynamic correlation length and perhaps the clusters of correlated particles that were more ramified in strong glasses than in fragile glasses are probably features of strong glass-formers. We would need to study other strong glasses, such as the BKS [104] model of silicon dioxide (SiO_2) or a model of germanium dioxide (GeO_2) [125], to provide evidence for this idea. We could do a study to investigate if strong glasses have universal features of dynamic heterogeneity. We would check if data for the strong system followed the same universal curves as we saw for fragile glasses. Such a study might be difficult, if other strong glass-formers have the same slow growth of dynamic correlation length that we saw in Chapter 3. Also, some of the strong systems are computationally expensive, as is the case for the BKS model and the model of GeO_2 from Ref. [125]. In these models the atoms have charges, and the Coulomb force due to the charges is long ranged. However, if the Stokes-Einstein violation temperature is similarly close to the onset temperature for supercooled dynamics in other strong systems as it was in the strong system studied in Chapter 3, then we might be able to collect enough data to make a reasonable comparison of strong liquids. We would collect data on dynamic heterogeneity in a number of strong glass-formers following the procedure we used for fragile glass-formers in Chapter 2, continuing to to use the Stokes-Einstein violation temperature to rescale data.

We could also approach the study of comparing dynamic heterogeneity to fragility by examining intermediate strength (between strong and fragile) glass-formers, to investigate whether compactness of clusters of correlated particles and the relationship between ξ_4 and τ_α are correlated with strength. The systems we studied in Chapter 2 had different fragilities and they showed universal features of dynamic heterogeneity. Thus, we might expect a jump or quick change from the universal features seen in fragile glasses to the features seen in strong

glasses at a particular system strength. One way to examine this idea is to find or create a potential that has a single parameter that corresponds to fragility. A binary Lennard-Jones system of this type is discussed in Ref. [108]. This system uses a binary Lennard-Jones potential

$$V_{\alpha\beta}(r) = 4\epsilon_{\alpha\beta}\left[\left(\frac{\sigma_{\alpha\beta}}{r}\right)^{12} - \left(\frac{\sigma_{\alpha\beta}}{r}\right)^{6}\right], \tag{5.1}$$

in three dimensions. In eq. 5.1, r is the distance between a pair of particles, and the subscripts α and β refer to particle types 1 or 2. The system has an equal number of type 1 particles as type 2 particles. The parameters of eq. 5.1 are $\sigma_{11} = \epsilon_{11} = \epsilon_{12} = \epsilon_{22} = m_1 = m_2 = 1$, $\sigma_{12} = (\lambda+1)/2$, and $\sigma_{22} = \lambda$. In the potential parameters, λ is an adjustable parameter that Coslovich and Pastore [108] allowed to vary between 0.6 and 1.0, which varies the size ratio between the two particle types. By varying λ in this range, this system can be varied from being stronger than the Kob Andersen (KA) system of Chapter 4 to being more fragile than the KA system. They found that λ controlled what structures formed in a system. Another system is this type is a variation of the model by Coslovich and Pastore, the CP model, which we studied in Chapter 3. Ozawa, Kim, and Miyazaki [126] changed the original CP potential to be

$$V_{\alpha\beta}(r) = \epsilon_{\alpha\beta}\left[\left(\frac{\sigma_{\alpha\beta}}{r}\right)^{12} - C(1-\delta_{\alpha\beta})\left(\frac{\sigma_{\alpha\beta}}{r}\right)^{6}\right], \tag{5.2}$$

where C is a controlled parameter that can range from 1 to 0, and the other parameters are the same as in the original eq. 3.1. Notice that if $C = 1$, the original potential is recovered. When $C = 1$, the system is strong, as we have seen. Ozawa *et al.* found that decreasing C lead to more fragile glasses. When $C = 0$, the potential is that of a soft sphere system [127],

which is a typical fragile glass-former. We would do studies examining dynamic heterogeneity and the Stokes-Einstein violation temperature in the system for a series of different strengths, controlled by a single parameter in the potential. We would use a consistent way to measure strength in all the systems, such as finding the fragility parameter in the VFT fit, eq. 1.6, where relaxation time is a function of temperature. (The VFT fit is an alternative to the Arrhenius fit, eq. 1.5, for fragile-glass formers.) We could find the dependence of χ_4 on ξ_4 and of ξ_4 on τ_α for each fragility. This study would tell us how the transition from the universal features of dynamic heterogeneity seen in fragile glass formers to the features seen in strong glasses occurs.

5.3. Cooling a Kob Andersen system

In Chapter 4 we investigated the kinetic and mechanical stability of glasses obtained by cooling at a constant rate in computer simulations. We studied average dynamics and dynamic heterogeneity as the glasses were quickly heated and then held at a constant temperature. We also examined the mechanical properties of the glasses at a temperature below the glass transition temperature. We have presented methods for analyzing kinetic and mechanical stability. We hope that others creating glasses in various ways will find these methods useful.

We were motivated to make glasses created at a range of cooling rates by previous simulations that created highly stable glasses: systems with a higher probability of inactive states [114], systems with pinned particles [115], an Ising spin model [51], and, in particular, vapor deposited glasses [52, 46, 42]. Vapor deposition was a new simulation technique, and a reliable way to measure its success was needed. Our measures of stability gave high stability glass simulations a way to compare the difference in stability of their glasses and ordinary

glasses created by cooling to the difference in stability of experimental vapor deposited glasses over ordinary glasses.

Using dynamic correlation functions, we observed that glasses created with slower cooling rates took longer to return to liquid equilibrium. We measured this rate of return to equilibrium with the transformation time, t_{trans}, and scaled it by the α relaxation time at the equilibrated liquid temperature of 0.5 to get a stability ratio, $S = t_{trans}/\tau_\alpha$. For our glasses created with the slowest cooling rate, we found a stability ratio of 66. We note that if we were to cool an order of magnitude slower, we would expect to get a stability ratio of 100, according to our fit. One run at this next slowest cooling rate would take almost a year using a single precision HOOMD-blue simulation on a single NVIDIA K20c GPU. We hope that our stability ratio will be a useful comparison for other simulations creating stable glasses, including simulations mimicking vapor deposition and simulations using random pinning.

Based on the results of our study, we found that kinetic stability is the best measure of stability when comparing systems prepared in different manners. We believe that our stability ratio, $S = t_{trans}/\tau_\alpha$, is a very good measure of kinetic stability. It is highly comparable between glasses prepared using the Kob Andersen [27], KA, potential in different ways. Our stability ratio might also be used when comparing to other systems, as it is a ratio of times, not a system dependent time. However, S does depend on the temperature to which the system is heated. Finding an equivalent temperature in another system might be difficult, as we will go into later. The other measures of stability have some issues. The shear modulus can't be calculated in all systems, such as Ising spin systems and a system with pinned particles. Also, the shear modulus requires a large enough system size to be able to average over small wavevectors, q, of a four-point structure factor. Recall that the

smallest q is inversely related to the length of the simulation box. The issues with energy are that it is very sensitive to anisotropy in a system and the system's density.

While the stability ratio S that we measured is very useful in comparing to other studies of the Kob Andersen (KA) system, comparing to other systems is more complicated. S could be useful for comparing different systems as well, though not quite as accurately as we could compare to different simulations of the KA system. The temperatures where supercooling begins and ends are different for systems with different potentials. However, we saw that while S depended on the supercooled temperatures to which we heat our system, the variation was not huge. If other simulators wish to compare their systems to ours, then they should pick a low supercooled temperature that is still reasonable to simulate, such as $T = 0.5$ in th KA system. We note that one order of magnitude difference between initial cooling rates lead to a greater percent difference in S then the percent difference in S between heating to $T = 0.5$ and any of the other heating temperatures we examined at the cooling rate of $\dot{T} = 3.33 \times 10^{-8}$. Thus, if others compare S calculated in a different system to our S values, the comparison will not be exact, but it should show what order of magnitude initial cooling rate the S in the new system corresponds to.

The potential energy proved to be a poor quantity for comparing to the simulated vapor deposited systems. When we compared the energy of our Kob Andersen [27], KA, system to that of the simulated vapor deposited KA system prepared by Lyubimov *et al.* [42], we found that our most stable glasses prepared at the slowest cooling rate had a lower average potential energy than their vapor deposited glasses. On the other hand, our average inherent structure energy was higher than theirs. We would expect that the vapor deposited glass would have lower average potential energy than our glasses, since a lower average potential

energy would indicate greater stability. We expect higher stability in the simulated vapor deposited glasses, since experimenters find that vapor deposited glasses are more stable than glasses creating by cooling. The fact that our potential energy was lower is probably due to the fact that the average potential energy is sensitive to anisotropy in the system, as Lyubimov *et al.* [42] found. The average inherent structure energy was lower in the vapor deposition simulations than in our cooling simulation. This behavior is expected, as inherent structure energy is also a measure of stability, but, like the potential energy, the inherent structure energy also depends on density and anisotropy in composition.

We note that the energy minimization Lyubimov *et al.* [42] used to find the inherent structure energy allowed the thickness of the films to change. In their simulations, this energy minimization procedure resulted in the system shrinking and thus the density increased. This increase of density may have caused the low inherent structure energy that they measured. Although, the density of their energy minimized systems was the density at which we modeled our systems. Having comparable densities may mean that the comparison of our inherent structure energies was valid. We could check how important a factor density is to the energy and inherent structure energy by studying how the stability of the KA system depends on density. We would prepare systems at a range of densities, to see precisely what effect density has on energy and how our new energies compare to their potential energies. We would need to repeat the study we did in Chapter 4 at different densities. In particular we would wish to examine energy and inherent structure energy. These energies don't require any four-point structure factors, so we could use a smaller system size. A smaller system would lead to shorter simulations.

Energy can also be affected by anisotropy in particle concentration. E. Flenner has done preliminary work on vapor deposition in the KA system, in a way that should deal with this anisotropy. The vapor deposition in computer simulations done previously [52, 46, 42] used energy minimization to mimic vapor deposition. Flenner is working on a more realistic simulation of vapor deposition that does not include this step. His simulation will also be different by depositing on a substrate of a stable KA glass, namely, one of the most stable glasses I created by cooling. Previously, researchers [42, 46] deposited their model system onto a substrate with different potential parameters than the system. In the case of Ref. [52], the substrate atoms were different than the deposited molecules. The substrate Flenner used, which is the same material as the deposited glass, should help prevent particle concentration from varying in the deposited glass. This study would create vapor deposited glasses with little or no anisotropy, unlike the glasses created in Refs. [42, 52, 46]. We would be able to compare the glasses created by cooling of Chapter 4 with these new vapor deposited glasses, which should deal with the problem of anisotropy.

When we examined mechanical stability, we found that increases in the shear modulus when cooling rate was slowed were comparable to the increases in the shear modulus seen in experiments between a glass created by cooling and one created by vapor deposition [43]. In Figure 4.18, the shear modulus seems to be flattening out on the linear-log scale as cooling rate is decreased. In experiments on glycerol, Miller and MacPhail [128, 129] found that the shear modulus only increased modestly as a quenched system was aged. Liu *et al.* [130] reported that cooling rate had little to no effect on elastic modulus in a zirconium-based metallic glass. The shear modulus in our glasses had a significant dependence on cooling rate. This difference from experiments may be due to the fact that when simulation times

are translated into real times, experiments are orders of magnitude longer than simulations. Therefore, a comparison with experiments may not be reasonable. We suggest that further exploration is needed in this topic. In our KA system, we would need slower cooling rates to investigate whether the trend of flattening out of the shear modulus continues. Unfortunately, in this system, slower cooling would be very time consuming, as the next slowest order of magnitude in cooling rate would take about a year to simulate.

We could use the glasses we prepared at a range of cooling rates to do a study on melting. Some experiments and simulations have melted vapor deposited glasses, studying how the melting occurred and at what rate. In experiments [131, 132, 47] on highly stable vapor deposited glasses, researchers have observed heterogeneous melting. Films of vapor deposited glasses melted via fronts initiating from the free surface of the glass, which moved inward. Sepúlveda *et al.* [47] observed that for a large enough film thickness the melting was no longer dominated by a growth front, but by the bulk melting. In a vapor deposition simulation, Lyubimov, Ediger, and de Pablo [42] examined the melting of vapor deposited glasses and glasses created by cooling, in the KA system. As in experiments, they noted that the vapor deposited glasses melted heterogeneously starting from the free surface. In their glasses created by ordinary cooling, they observed uniform melting of the glass. We note that the slowest rate with which we cooled KA glasses was 3.33×10^{-8}, while they examined melting in a glass cooled at the rate of 3.33×10^{-5}, which is 1000 times faster than our slowest cooling rate. We could examine melting in our glasses created by cooling at our slowest rate to look for any melting fronts. We would measure the mean square displacement for sheets of particles a set distance from the free surface of the film. A greater mean square displacement in a particular layer indicates more melting at that distance from the surface.

If melting is not observed then we could slice our sample, to investigate whether thinner films of our glass have melting fronts. Sepúlveda *et al.* observed that even for vapor deposited glasses film thickness could get too large for heterogeneous melting. Thus, we could see if there is a sample thickness that produces melting fronts in glasses created by cooling. A study such as this one could help us decide whether vapor deposited glasses are the same as glass created by very slow cooling, or if they are fundamentally different.

5.4. General conclusions

Our exploration of supercooled liquids and glasses suggested the existence of a temperature where there is a possible crossover in dynamics. Regions became more compact and the dependence of dynamic correlation length on relaxation time changed. We saw a crossover in dynamics at the Stokes-Einstein violation temperature, T_s. We also studied the dependence of stability on cooling rate for simulated glasses. Stability increased when cooling rate decreased, as reported through a stability ratio, potential energy, and the shear modulus.

More investigation is needed into the crossover in dynamics in supercooled liquids investigated in Chapters 2 and 3. We are left wondering if the Stokes-Einstein violation temperature T_s is really as important as we thought, since it does not seem to mark the same crossover in dynamics in a strong glass as it does in fragile glasses. It may still mark a universal change in dynamics, just not the one we originally proposed for fragile glass-formers. Our study of a strong glass-former raised more questions than it answered, but it gave us new directions in which to look for ways to compare glass-forming systems. Many theories have predictions about all systems having a crossover in dynamics, particularly a crossover to activated dynamics. We do not claim to have seen such a crossover, but we do observe a definite change in dynamics at T_s.

In our study of glasses created by cooling, we obtained data that others in the field can use for comparisons to their data. Simulations, such as pinned systems [115], systems with a higher probability of inactive states [114], and systems mimicking vapor deposition [52, 46, 42] need to compare the stability of their system to glasses created by cooling. Through our study of stability, we found that not all measures of stability are useful. Indeed some can't be used in certain types of simulations. Hence we described a variety of stability measures. We hope that others will not only compare to our data, but learn about the differences between various measures of stability. Studies using simulation techniques like vapor deposition, pinning particles, and systems with more inactive states will be able to show how much more stable their system is than a glass created by cooling, and allow comparison of this stability to experiments of vapor deposition.

Bibliography

[1] E. Flenner, H. Staley, and G. Szamel, "Universal features of dynamic heterogeneity in supercooled liquids," *Physical Review Letters*, vol. 112, p. 097801(5), 2014.

[2] H. Staley, E. Flenner, and G. Szamel, "Reduced strength and extent of dynamic heterogeneity in a strong glass former as compared to fragile glass formers," *Journal of Chemical Physics*, vol. 143, p. 244501(7), 2015.

[3] H. Staley, E. Flenner, and G. Szamel, "Cooling-rate dependence of kinetic and mechanical stabilities of simulated glasses," *Journal of Chemical Physics*, vol. 142, p. 244508(8), 2015.

[4] L. Berthier and G. Biroli, "Theoretical perspective on the glass transition and amorphous materials," *Reviews of Modern Physics*, vol. 83, pp. 587–645, 2011.

[5] M. D. Ediger and P. Harrowell, "Perspective: Supercooled liquids and glasses," *The Journal of Chemical Physics*, vol. 137, p. 080901(15), 2012.

[6] B. C. Hancock and M. Parks, "What is the true solubility advantage for amorphous pharmaceuticals," *Pharmaceutical Research*, vol. 17, no. 4, pp. 397–404, 2000.

[7] http://liquidmetal.com.

[8] http://www.nrel.gov/ncpv.

[9] C. P. Royall and S. R. Williams, "The role of local structure in dynamical arrest," *Physics Reports*, vol. 560, pp. 1–75, 2015.

[10] J.-P. Hansen and I. R. McDonald, *Theory of Simple Liquids*. Academic Press, 2nd ed., 1990.

[11] Y. Brumer and D. R. Reichman, "Mean-field theory, mode-coupling theory, and the onset temperature in supercooled liquids," *Physical Review E*, vol. 69, p. 041202(5), 2004.

[12] M. Goldstein, "Viscous liquids and the glass transition: A potential energy barrier picture," *The Journal of Chemical Physics*, vol. 51, no. 9, pp. 3728–3739, 1969.

[13] Y. S. Elmatad, D. Chandler, and J. P. Garrahan, "Corresponding states of structural glass formers," *The Journal of Physical Chemistry B*, vol. 113, pp. 5563–5567, 2009.

[14] M. D. Ediger, "Spatially heterogeneous dynamics in supercooled liquids," *Annual Review of Physical Chemistry*, vol. 51, pp. 99–128, 2000.

[15] D. R. Reichman and P. Charbonneau, "Mode-coupling theory," *Journal of Statistical Mechanics: Theory and Experiment*, p. P05013, 2005.

[16] D. Coslovich and G. Pastore, "Dynamics and energy landscape in a tetrahedral network glass-former: direct comparison with models of fragile liquids," *Journal of Physics:Condensed Matter*, vol. 21, p. 285107(13), 2009.

[17] K. Kim and S. Saito, "Multiple length and time scales of dynamic heterogeneities in model glass-forming liquids: A systematic analysis of multi-point and multi-time correlations," *The Journal of Chemical Physics*, vol. 138, p. 12A506(12), 2013.

[18] A. Cavagna, "Supercooled liquids for pedestrians," *Physics Reports*, vol. 476, pp. 51–124, 2009.

[19] C. Rainone, *Following the evolution of metastable glassy states under external perturbations: compression and shear-strain (unpublished)*. PhD thesis, Sapienza Universita di Roma, 2015.

[20] C. A. Angell, "Perspective on the glass transition," *Journal of Physics and Chemistry of Solids*, vol. 49, no. 8, pp. 863–871, 1988.

[21] T. Al-Shemmeri, *Engineering Fluid Mechanics*. Ventus Publishing ApS, 2012.

[22] C. A. Angell, "Formation of glasses from liquids and biopolymers," *Science*, vol. 267, no. 5206, pp. 1924–1935, 1995.

[23] W. Kauzmann, "The nature of the glassy state and the behavior of liquids at low temperatures," *Chemical Reviews*, vol. 43, no. 2, pp. 219–256, 1948.

[24] F. H. Stillinger, "Supercooled liquid, glass transitions, and the Kauzmann paradox," *The Journal of Chemical Physics*, vol. 88, no. 12, pp. 7818–7825, 1988.

[25] R. Richert and C. A. Angell, "Dynamics of glass-forming liquids. V. On the link between molecular dynamics and configurational entropy," *The Journal of Chemical Physics*, vol. 108, no. 21, pp. 9016–9026, 1998.

[26] J. Wuttke, I. Chang, O. G. Randl, F. Fujara, and W. Petry, "Tagged-particle motion in viscous glycerol: Diffusion relaxation crossover," *Physical Review E*, vol. 54, no. 5, pp. 5364–5369, 1996.

[27] W. Kob and H. C. Andersen, "Testing made-coupling theory for a supercooled binary Lennard-Jones mixture: The van Hove correlation function," *Physical Review E*, vol. 51, no. 5, pp. 4626–4641, 1995.

[28] T. A. Weber and F. H. Stillinger, "Local order and structural transitions in amorphous metal-metalloid alloys," *Physical Review B*, vol. 31, no. 4, pp. 1954–1963, 1985.

[29] C. Donati, J. F. Douglas, W. Kob, S. J. Plimpton, P. H. Poole, and S. C. Glotzer, "Stringlike cooperative motion in a supercooled liquid," *Physical Review Letters*, vol. 80, no. 11, pp. 2338–2341, 1998.

[30] M. M. Hurley and P. Harrowell, "Kinetic structure of a two-dimensional liquid," *Physical Review E*, vol. 52, no. 2, pp. 1694–1698, 1995.

[31] E. Flenner and G. Szamel, "Fundamental differences between glassy dynamics in two and three dimensions," *Nature Communications*, vol. 6, p. 7392(6), 2015.

[32] K. Schmidt-Rohr and H. W. Spiess, "Nature of nonexponential loss of correlation above the glass transition investigated by multidimensional nmr," *Physical Review Letters*, vol. 66, no. 23, pp. 3020–3023, 1991.

[33] L. Berthier, G. Biroli, J.-P. Bouchaud, and R. L. Jack, "Overview of different characterisations of dynamic heterogeneity," *arXiv:1009.4765 [cond-mat.stat-mech]*, 2010.

[34] E. R. Weeks, J. C. Crocker, A. C. Levitt, A. Schofield, and D. A. Weitz, "Three-dimensional direct imaging of structural relaxation near the colloidal glass transition," *Science*, vol. 287, no. 5453, pp. 627–631, 2000.

[35] C. Dasgupta, A. V. Indrani, S. Ramaswamy, and M. K. Phani, "Is there a growing correlation length near the glass transition?," *Europhysics Letters*, vol. 15, no. 3, pp. 307–312, 1991.

[36] E. Flenner and G. Szamel, "Anisotropic spatially heterogeneous dynamics on the α and β relaxation time scales studied via a four-point correlation function," *Physical Review E*, vol. 79, p. 051502(9), 2009.

[37] E. Flenner and G. Szamel, "Long-range correlations in glasses and glassy fluids," *Journal of Physics: Condensed Matter*, vol. 27, p. 194125(10), 2015.

[38] M. P. Allen and D. J. Tildesley, *Computer Simulation of Liquids*. Clarendon Press, 1994.

[39] L. Berthier, G. Biroli, J.-P. Bouchaud, L. Cipelletti, D. E. Masri, D. L'Hote, F. Ladieu, and M. Pierno, "Direct experimental evidence of a growing length scale accompanying the glass transition," *Science*, vol. 310, pp. 1797–1800, 2005.

[40] C. Dalle-Ferrier, C. Thibierge, C. Alba-Simionesco, L. Berthier, G. Biroli, J.-P. Bouchaud, F. Ladieu, D. L'Hôte, and G. Tarjus, "Spatial correlations in the dynamics of glassforming liquids: Experimental determination of their temperature dependence," *Physical Review E*, vol. 76, p. 041510(15), 2007.

[41] E. Flenner and G. Szamel, "Dynamic heterogeneity in a glass forming fluid: Susceptibility, structure factor, and correlation length," *Physical Review Letters*, vol. 105, p. 217801(4), 2010.

[42] I. Lyubimov, M. D. Ediger, and J. J. de Pablo, "Model vapor-deposited glasses: Growth front and composition effects," *Journal of Chemical Physics*, vol. 139, p. 144505(7), 2013.

[43] K. L. Kearns, T. Still, G. Fytas, and M. D. Ediger, "High-modulus organic glasses prepared by physical vapor deposition," *Advanced Materials*, vol. 22, pp. 39–42, 2010.

[44] G. Parisi and F. Sciortino, "Flying to the bottom," *Nature Materials*, vol. 12, pp. 94–95, 2013.

[45] S. F. Swallen, K. L. Kearns, M. K. Mapes, Y. S. Kim, R. J. McMahon, M. D. Ediger, T. Wu, L. Yu, and S. Satija, "Organic glasses with exceptional thermodynamic and kinetic stability," *Science*, vol. 315, pp. 353–356, 2007.

[46] S. Singh, M. D. Ediger, and J. J. de Pablo, "Ultrastable glasses from *in silico* vapour deposition," *Nature Materials*, vol. 12, pp. 139–144, 2013.

[47] A. Sepúlveda, M. Tylinski, A. Guiseppi-Elie, R. Richert, and M. Ediger, "Role of fragility in the formation of highly stable organic glasses," *Physical Review Letters*, vol. 113, p. 045901(5), 2014.

[48] L. Zhu, C. W. Brian, S. F. Swallen, P. T. Straus, M. D. Ediger, and L. Yu, "Surface self-diffusion of an organic glass," *Physical Review Letters*, vol. 106, p. 256103(4), 2011.

[49] Z. Shi, P. G. Debenedetti, and F. H. Stillinger, "Properties of model atomic free-standing thin films," *The Journal of Chemical Physics*, vol. 134, p. 114524(7), 2011.

[50] A. Wisitsorasak and P. G. Wolynes, "Fluctuating mobility generation and transport in glasses," *Physical Review E*, vol. 88, p. 022308(5), 2013.

[51] S. Leonard and P. Harrowell, "Macroscopic facilitation of glassy relaxation kinetics: Ultrastable glass films with frontlike thermal response," *The Journal of Chemical Physics*, vol. 133, p. 244502(12), 2010.

[52] S. Singh and J. J. de Pablo, "A molecular view of vapor deposited glasses," *The Journal of Chemical Physics*, vol. 134, p. 194903(7), 2011.

[53] I. Lyubimov, L. Antony, D. M. Walters, D. Rodney, M. D. Ediger, and J. J. de Pablo, "Orientational anisotropy in simulated vapor-deposited molecular glasses," *Journal of Chemical Physics*, vol. 143, p. 094502(8), 2015.

[54] S. S. Dalal and M. D. Ediger, "Influence of substrate temperature on the transformation front velocities that determine thermal stability of vapor-deposited glasses," *The Journal of Physical Chemistry B*, vol. 119, no. 9, pp. 3875–3882, 2015.

[55] Y. Z. Chua, M. Ahrenberg, M. Tylinski, M. D. Ediger, and C. Schick, "How much time is needed to form a kinetically stable glass? AC calorimetric study of vapor-deposited

glasses of ethylcyclohexane," *Journal of Chemical Physics*, vol. 142, p. 054506(11), 2015.

[56] E. Leutheusser, "Dynamical model of the liquid-glass transition," *Physical Review A*, vol. 29, no. 5, pp. 2765–2773, 1984.

[57] U. Bengtzelius, W. Gotze, and A. Sjolander, "Dynamics of supercooled liquids and the glass transition," *Journal of Physics C: Solid State Physics*, vol. 17, pp. 5915–5934, 1984.

[58] W. Gotze, "Recent tests of the mode-coupling theory for glassy dynamics," *Journal of Physics: Condensed Matter*, vol. 11, pp. A1–A45, 1999.

[59] W. Kob, "Lecture notes for Les Houches summer school - Session LXXVII: Slow relaxations and nonequilibrium dynamics in condensed matter," *arXiv:cond-mat/0212344v1 [cond-mat.stat-mech]*, 2002.

[60] W. Kob and H. C. Andersen, "Testing mode-coupling theory for a supercooled binary Lennard-Jones mixture. II. Intermediate scattering function and dynamic susceptibility," *Physical Review E*, vol. 52, no. 4, pp. 4134–4153, 1995.

[61] J. Wuttke, W. Petry, and S. Pouget, "Structural relaxation in viscous glycerol: Coherent neutron scattering," *The Journal of Chemical Physics*, vol. 105, no. 12, pp. 5177–5182, 1996.

[62] G. Szamel, "Mode-coupling theory and beyond: A diagrammatic approach," *Progress of Theoretical and Experimental Physics*, p. 012J01(24), 2013.

[63] L. M. C. Janssen, P. Mayer, and D. R. Reichman, "Relaxation patterns in supercooled liquids from generalized mode-coupling theory," *Physical Review E*, vol. 90, p. 052306(8), 2014.

[64] L. M. C. Janssen and D. R. Reichman, "Microscopic dynamics of supercooled liquids from first principles," *Physical Review Letters*, vol. 115, p. 205701(5), 2015.

[65] T. R. Kirkpatrick and D. Thirumalai, "Dynamics of the structural glass transition and the p-spin-interaction spin-glass model," *Physical Review A*, vol. 58, no. 20, pp. 2091–2094, 1987.

[66] T. R. Kirkpatrick and P. G. Wolynes, "Connections between some kinetic and equilibrium theories of the glass transition," *Physical Review A*, vol. 35, no. 7, pp. 3072–3080, 1987.

[67] T. R. Kirkpatrick, D. Thirumalai, and P. G. Wolynes, "Scaling concepts for the dynamics of viscous liquids near an ideal glassy state," *Physical Review A*, vol. 40, no. 2, pp. 1045–1054, 1989.

[68] T. B. Schroder, S. Sastry, J. C. Dyre, and S. C. Glotzer, "Crossover to potential energy landscape dominated dynamics in a model glass-forming liquid," *The Journal of Chemical Physics*, vol. 112, no. 22, pp. 9834–9840, 2000.

[69] V. Lubchenko and P. G. Wolynes, "Theory of structural glasses and supercooled liquids," *Annual Review of Physical Chemistry*, vol. 58, pp. 235–266, 2007.

[70] J. D. Stevenson, J. Schmalian, and P. G. Wolynes, "The shapes of cooperatively rearranging regions in glass-forming liquids," *Nature Physics*, vol. 2, pp. 268–274, 2006.

[71] X. Xia and P. G. Wolynes, "Fragilities of liquids predicted from the random first order transition theory of glasses," *Proceedings of the National Academy of Sciences of the United States of America*, vol. 97, pp. 2990–2994, 2000.

[72] C. A. Angell and L. M. Torell, "Short time structural relaxation processes in liquids: Comparison of experimental and computer simulation glass transitions on picosecond time scales," *The Journal of Chemical Physics*, vol. 78, pp. 937–945, 1983.

[73] L. M. Torell, D. C. Ziegler, and C. A. Angell, "Short time relaxation processes in liquids from viscosity and light scattering studies in molten kcl 2bicl3," *The Journal of Chemical Physics*, vol. 81, pp. 5053–5058, 1984.

[74] D. Chandler and J. P. Garrahan, "Dynamics on the way to forming glass: Bubbles in space-time," *Annual Review of Physical Chemistry*, vol. 61, pp. 191–217, 2010.

[75] A. S. Keys, L. O. Hedges, J. P. Garrahan, S. C. Glotzer, and D. Chandler, "Excitations are localized and relaxation is hierarchical in glass-forming liquids," *Physical Review X*, vol. 1, p. 021013(15), 2011.

[76] J. P. Garrahan and D. Chandler, "Coarse-grained microscopic model of glass formers," *Proceedings of the National Academy of Sciences of the United States of America*, vol. 100, pp. 9710–9714, 2003.

[77] D. Kivelson, S. A. Kivelson, X. Zhao, Z. Nussinov, and G. Tarjus, "A thermodynamic theory of supercooled liquids," *Physica A*, vol. 219, pp. 27–38, 1995.

[78] G. Wahnstrom, "Molecular-dynamics study of a supercooled two-component lennard-jones system," *Physical Review A*, vol. 44, no. 6, pp. 3752–3764, 1991.

[79] G. M. Hocky, D. Coslovich, A. Ikeda, and D. R. Reichman, "Correlation of local order with particle mobility in supercooled liquids is highly system dependent," *Physical Review Letters*, vol. 113, p. 157801(5), 2014.

[80] M. Grousson, G. Tarjus, and P. Viot, "Comment on "Stripe glasses: Self-generated randomness in a uniformly frustrated system"," *Physical Review Letters*, vol. 86, no. 15, p. 3455, 2001.

[81] M. Grousson, G. Tarjus, and P. Viot, "Evidence for "fragile" glass-forming behavior in the relaxation of coulomb frustrated three-dimensional systems," *Physical Review E*, vol. 65, p. 065103(4), 2002.

[82] F. Sausset, G. Tarjus, and P. Viot, "Tuning the fragility of a glass-forming liquid by curving space," *Physical Review Letters*, vol. 101, p. 155701(4), 2008.

[83] M. Dzugutov, S. I. Simdyankin, and F. H. M. Zetterling, "Decoupling of diffusion from structural relaxation and spatial heterogeneity in a supercooled simple liquid," *Physical Review Letters*, vol. 89, no. 19, p. 195701(4), 2002.

[84] L. Berthier and G. Tarjus, "Nonperturbative effect of attractive forces in viscous liquids," *Physical Review Letters*, vol. 103, p. 170601(4), 2009.

[85] U. R. Pedersen, T. B. Schroder, and J. C. Dyre, "Repulsive reference potential reproducing the dynamics of a liquid with attractions," *Physical Review Letters*, vol. 105, p. 157801(4), 2010.

[86] G. M. Hocky, T. E. Markland, and D. R. Reichman, "Growing point-to-set length scale correlates with growing relaxation times in model supercooled liquids," *Physical Review Letters*, vol. 108, p. 225506(5), 2012.

[87] Z. Zhang, P. J. Yunker, P. Habdas, and A. G. Yodh, "Cooperative rearrangement regions and dynamical heterogeneities in colloidal glasses with attractive versus repulsive interactions," *Physical Review Letters*, vol. 107, p. 208303(5), 2011.

[88] E. Flenner and G. Szamel, "Dynamic heterogeneities above and below the mode-coupling temperature: Evidence of a dynamic crossover," *The Journal of Chemical Physics*, vol. 138, p. 12A523(13), 2013.

[89] L. Berthier and T. A. Witten, "Compressing nearly hard sphere fluids increases glass fragility," *Europhysics Letters*, vol. 86, p. 10001(6), 2009.

[90] U. R. Pedersen, T. B. Schroder, and J. C. Dyre, "Repulsive reference potential reproducing the dynamics of a liquid with attractions," *Physical Review Letters*, vol. 105, p. 157801(4), 2010.

[91] J. D. Weeks, D. Chandler, and H. C. Andersen, "Role of repulsive forces in determining the equilibrium structure of simple liquids," *The Journal of Chemical Physics*, vol. 54, no. 12, pp. 5237–5247, 1971.

[92] D. Chandler, J. D. Weeks, and H. C. Andersen, "Van Der Waals picture of liquids, solids, and phase transformations," *Science*, vol. 220, no. 4599, pp. 787–794, 1983.

[93] E. Flenner, M. Zhang, and G. Szamel, "Analysis of a growing dynamic length scale in a glass-forming binary hard-sphere mixture," *Physical Review E*, vol. 83, p. 051501(15), 2011.

[94] L. Berthier and W. Kob, "The Monte Carlo dynamics of a binary Lennard-Jones glass-forming mixture," *Journal of Physics: Condensed Matter*, vol. 19, p. 205130(10), 2007.

[95] http://lammps.sandia.gov.

[96] S. Plimpton, "Fast parallel algorithms for short-range molecular-dynamics," *Journal of Computational Physics*, vol. 117, pp. 1–19, 1995.

[97] http://codeblue.umich.edu/hoomd-blue.

[98] J. A. Anderson, C. D. Lorenz, and A. Travesset, "General purpose molecular dynamics simulations fully implemented on graphics processing units," *Journal of Computational Physics*, vol. 227, pp. 5342–5359, 2008.

[99] C. K. Mishra and R. Ganapathy, "Shape of dynamical heterogeneities and fractional Stokes-Einstein and Stokes-Einstein-Debye relations in quasi-two-dimensional suspensions of colloidal ellipsoids," *Physical Review Letters*, vol. 114, p. 198302(5), 2015.

[100] G. Brambilla, D. E. Masri, M. Pierno, L. Berthier, L. Cipelletti, G. Petekidis, and A. B. Schofield, "Probing the equilibrium dynamics of colloidal hard spheres above the mode-coupling glass transition," *Physical Review Letters*, vol. 102, p. 085703(4), 2009.

[101] K. Kim and R. Yamamoto, "Apparent finite-size effects in the dynamics of supercooled liquids," *Physical Review E*, vol. 61, no. 1, pp. 41–44, 2000.

[102] L. Berthier, G. Biroli, J.-P. Bouchaud, L. Cipelletti, and W. van Saarloos, *Dynamical Heterogeneities in Glasses, Colloids, and Granular Media*. Oxford University Press, 2011.

[103] K. H. Nagamanasa, S. Gokhale, A. K. Sood, and R. Ganapathy, "Direct measurements of growing amorphous order and non-monotonic dynamic correlations in a colloidal glass-former," *Nature Physics*, vol. 11, pp. 403–408, 2015.

[104] B. W. H. van Beest, G. J. Kramer, and R. A. van Santen, "Force fields for silicas and aluminophosphates based on *ab initio* calculations," *Physical Review Letters*, vol. 64, no. 16, pp. 1955–1958, 1990.

[105] T. Kawasaki, K. Kim, and A. Onuki, "Dynamics in a tetrahedral network glassformer: Vibrations, network rearrangements, and diffusion," *The Journal of Chemical Physics*, vol. 140, p. 184502(12), 2014.

[106] L. Berthier, G. Biroli, D. Coslovich, W. Kob, and C. Toninelli, "Finite-size effects in the dynamics of glass-forming liquids," *Physical Review E*, vol. 86, p. 031502(17), 2012.

[107] T. S. Grigera, A. Cavagna, I. Giardina, and G. Parisi, "Geometric approach to the dynamic glass transition," *Physical Review Letters*, vol. 88, p. 055502(4), 2002.

[108] D. Coslovich and G. Pastore, "Understanding fragility in supercooled Lennard-Jones mixtures. I. Locally preferred structures," *The Journal of Chemical Physics*, vol. 127, p. 124504(13), 2007.

[109] G. Szamel and E. Flenner, "Four-point susceptibility of a glass-forming binary mixture: Brownian dynamics," *Physical Review E*, vol. 74, p. 021507(7), 2006.

[110] C. Toninelli, M. Wyart, L. Berthier, G. Biroli, and J.-P. Bouchaud, "Dynamical susceptibility of glass formers: Contrasting the predictions of theoretical scenarios," *Physical Review E*, vol. 71, p. 041505(20), 2005.

[111] K. D. L. A. Kopff, L. Zhu, R. J. McMahon, L. Yu, R. Richert, and M. D. Ediger, "Molecular packing in highly stable glasses of vapor-deposited tris-naphthylbenzene isomers," *Journal of Chemical Physics*, vol. 136, p. 094505(11), 2012.

[112] K. R. Whitaker, D. J. Scifo, M. D. Ediger, M. Ahrenberg, and C. Schick, "Highly stable glasses of *cis*-decalin and *cis/trans*-decalin mixtures," *The Journal of Physical Chemistry B*, vol. 117, pp. 12724–12733, 2013.

[113] E. Leon-Gutierrez, A. Sepúlveda, G. Garcia, M. T. Clavaguera-Mora, and J. Rodríguez-Viejo, "Stability of thin film glasses of tolune and ethylbenzene formed by vapor deposition: an *in situ* nanocalorimetric study," *Physical Chemistry Chemical Physics*, vol. 12, pp. 14693–14698, 2010.

[114] R. L. Jack, L. O. Hedges, J. P. Garrahan, and D. Chandler, "Preparation and relaxation of very stable glassy states of a simulated liquid," *Physical Review Letters*, vol. 107, p. 275702(5), 2011.

[115] G. M. Hocky, L. Berthier, and D. R. Reichman, "Equilibrium ultrastable glasses produced by random pinning," *The Journal of Chemical Physics*, vol. 141, p. 224503(8), 2014.

[116] W. Brown, P. Wang, S. Plimpton, and A. Tharrington, "Implementing molecular dynamics on hybrid high performance computers - short range forces," *Computer Physics Communications*, vol. 182, pp. 898–911, 2011.

[117] W. Brown, A. Komlmeyer, S. Plimpton, and A. Tharrington, "Implementing molecular dynamics on hybrid high performance computers - particle-particle particle-mesh," *Computer Physics Communications*, vol. 183, pp. 449–459, 2012.

[118] F. H. Stillinger, "A topographic view of supercooled liquids and glass formation," *Science*, vol. 267, no. 5206, pp. 1935–1939, 1995.

[119] E. Bitzek, P. Koskinen, F. Gahler, M. Moseler, and P. Gumbsch, "Structural relaxation made simple," *Physical Review Letters*, vol. 97, p. 170201(4), 2006.

[120] P. J. Steinhardt, D. R. Nelson, and M. Ronchetti, "Bond-orientational order in liquids and glasses," *Physical Review B*, vol. 28, no. 2, pp. 784–805, 1983.

[121] E. Flenner and G. Szamel, "Relaxation in a glassy binary mixture: Comparison of the mode-coupling theory to a Brownian dynamics simulation," *Physical Review E*, vol. 72, p. 031508(15), 2005.

[122] G. de With, *Structure, Deformation, and Integrity of Materials*, vol. 1. Wiley-VCH, 2006.

[123] E. Flenner and G. Szamel, "Long-range spatial correlations of particle displacements and the emergence of elasticity," *Physical Review Letters*, vol. 114, p. 025501(5), 2015.

[124] A. J., E. Bouchbinder, and I. Procaccia, "Cooling-rate dependence of the shear modulus of amorphous solids," *Physical Review E*, vol. 87, p. 042310(5), 2013.

[125] R. D. Oeffner and S. R. Elliott, "Interatomic potential for germanium dioxide empirically fitted to an *ab initio* energy surface," *Physical Review B*, vol. 58, no. 22, pp. 14791–14803, 1998.

[126] M. Ozawa, K. Kim, and K. Miyazaki, "Tuning pairwise potential can control the fragility of glass-forming liquids: From tetrahedral network to isotropic soft sphere models," *arXiv:1602.00829v1 [cond-mat.soft]*, 2016.

[127] B. Bernu, J. P. Hansen, Y. Hiwatari, and G. Pastore, "Soft-sphere model for the glass transition in binary alloys: Pair structure and self diffusion," *Physical Review A*, vol. 36, no. 10, pp. 4891–4903, 1987.

[128] R. S. Miller and R. A. MacPhail, "Physical aging in supercooled glycerol: Evidence for heterogeneous dynamics?," *The Journal of Physical Chemistry B*, vol. 101, pp. 8635–8641, 1997.

[129] R. S. Miller and R. A. MacPhail, "Ultraslow nonequilibrium dynamics in supercooled glycerol by stimulated brillouin gain spectroscopy," *Journal of Chemical Physics*, vol. 106, pp. 3393–3401, 1997.

[130] Z. Y. Liu, Y. Yang, S. Guo, X. J. Liu, J. Lu, Y. H. Liu, and C. T. Liu, "Cooling rate effect on Young's modulus and hardness of a Zr-based metallic glass," *Journal of Alloys and Compounds*, vol. 509, pp. 3269–3273, 2011.

[131] S. F. Swallen, K. Traynor, R. J. McMahon, M. D. Ediger, and T. E. Mates, "Stable glass transformation to supercooled liquid via surface-initiated growth front," *Physical Review Letters*, vol. 102, p. 065503(4), 2009.

[132] A. Sepulveda, S. F. Swallen, L. A. Kopff, R. J. McMahon, and M. D. Ediger, "Stable glasses of indomethacin and α,α,β-tris-naphthylbenzene transform into ordinary supercooled liquids," *Journal of Chemical Physics*, vol. 137, p. 204508(9), 2012.